UNIVERSIDADE FEDERAL DO PARÁ
INSTITUTO DE GEOCIÊNCIAS
PROGRAMA DE PÓS-GRADUAÇÃO EM GEOLOGIA E GEOQUÍMICA

TESE DE DOUTORADO Nº 97

DESENVOLVIMENTO DA VEGETAÇÃO E MORFOLOGIA DA FOZ DO AMAZONAS-PA E RIO DOCE-ES DURANTE O QUATERNÁRIO TARDIO

Tese apresentada por:

MARLON CARLOS FRANÇA
Orientador: Prof. Dr. Marcelo Cancela Lisboa Cohen (UFPA)
Coorientador: Prof. Dr. Luiz Carlos Ruiz Pessenda (CENA/USP)

BELÉM

2013

Universidade Federal do Pará
Instituto de Geociências
Programa de Pós-Graduação em Geologia e Geoquímica

DESENVOLVIMENTO DA VEGETAÇÃO E MORFOLOGIA DA FOZ DO AMAZONAS-PA E RIO DOCE-ES DURANTE O QUATERNÁRIO TARDIO

TESE APRESENTADA POR

MARLON CARLOS FRANÇA

Como requisito parcial à obtenção do Grau de Doutor em Ciências na Área de GEOLOGIA

Data da aprovação: 05/11/2013

Banca Examinadora:

Prof. Dr. Marcelo Cancela Lisboa Cohen
(Orientador – UFPA)

Profª. Dra. Maria Inês Feijó Ramos
(Membro – MPEG/PA)
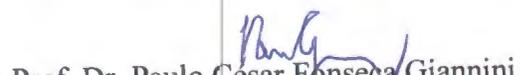
Prof. Dr. Paulo César Fonseca Giannini
(Membro – IG/USP)

Prof. Dr. Mário Luiz Gomes Soares
(Membro – UERJ)

Profª. Dra. Susy Eli Marques Gouveia
(Membro – UFPA)

Dedico este trabalho aos meus pais Franco e Lene, aos meus irmãos Fabrycio, Brandon, Christopher e Glayson (in memoriam), à minha amada esposa Renata França e meus amados filhos Maria Clara e Yuri.

AGRADECIMENTOS

Agradeço novamente de forma especial à minha família, que tanto amo, por todo apoio e carinho durante a construção deste trabalho. À minha amada esposa Renata de Castro Ribeiro França, meus filhos Maria Clara e Yuri, meus pais Franco França e Valdilene Alves, meus irmãos Fabrycio França, Glayson França (*in memoriam*) Brandon França e Christopher França, minha sogra Carmem S. R. do Carmo e meu sogro Paulo da Cruz Castro.

Muito obrigado!

RESUMO

Este trabalho compara as mudanças morfológicas e vegetacionais ocorridas ao longo da zona costeira da Ilha de Marajó, litoral amazônico, e da planície costeira do Rio Doce, sudeste do Brasil, durante o Holoceno e Pleistoceno tardio/Holoceno, respectivamente, com foco especificamente sobre a resposta dos manguezais para as flutuações do nível do mar e mudanças climáticas, já identificadas em vários estudos ao longo da costa brasileira. Esta abordagem integra datações por radiocarbono, descrição de características sedimentares, dados de pólen, e indicadores geoquímicos orgânicos (δ^{13}C, δ^{15}N e C/N). Na planície costeira do Rio Doce entre ~47.500 e 29.400 anos cal AP, um sistema deltaico foi desenvolvido em resposta principalmente à diminuição do nível do mar. O aumento do nível do mar pós-glacial causou uma incursão marinha com invasão da zona costeira, favorecendo a evolução de um sistema estuarino/lagunar com planícies lamosas ocupadas por manguezais entre pelo menos ~7400 e ~5100 anos cal AP. Considerando a Ilha de Marajó durante o Holoceno inicial e médio (entre ~7500 e ~3200 anos cal AP) a área de manguezal aumentou nas planícies de maré lamosas com acúmulo de matéria orgânica estuarina/marinha. Provavelmente, isso foi resultado da incursão marinha causada pela elevação do nível do mar pós-glacial associada a uma subsidência tectônica da região. As condições de seca na região amazônica durante o Holoceneo inicial e médio provocou um aumento da salinidade no estuário, que contribuiu para a expansão do manguezal. Portanto, o efeito de subida do nível relativo do mar foi determinante para o estabelecimento dos manguezais na sua atual posição nas regiões norte e sudeste do Brasil. Entretanto, durante o Holoceno tardio (~3050-1880 anos cal AP) os manguezais em ambas as regiões retrairam para pequenas áreas, com algumas delas substituídas por vegetação de água doce. Isso foi causado pelo aumento da vazão dos rios associada a um período mais úmido registrado na região amazônica, enquanto que na planície costeira do Rio Doce, os manguezais encolheram em resposta a um aumento da entrada de sedimento fluvial associado a uma queda no nível relativo do mar.

Palavras-chave: Manguezais. Palinologia. Análise de fácies. Carbono e Nitrogênio. Região amazônica. Sudeste do Brasil.

ABSTRACT

This work compares the vegetation and morphological changes occurred along the littoral of the Marajó Island, Amazonian littoral, and the coastal plain of the Rio Doce, southeastern Brazil, during the Holocene and late Pleistocene/Holocene, respectively, focused specifically on the response of mangroves to sea-level fluctuations and climate change, which have been identified in several studies along the Brazilian coast. This integrated approach combined radiocarbon dating, description of sedimentary features, pollen data, and organic geochemical indicators ($\delta^{13}C$, $\delta^{15}N$ and C/N). On coastal plain of the Doce River between ~47,500 and ~29,400 cal yr BP, a deltaic system was developed in response mainly to sea-level fall. The post-glacial sea-level rise caused a marine incursion with invasion of embayed coast and broad valleys, and it favored the evolution of a lagoonal/estuary system with wide tidal mud flats occupied by mangroves between at least ~7400 and ~5100 cal yr BP. Considering the Marajó Island during the early and middle Holocene (~7500 and ~3200 cal yr BP) mangrove area increased over tidal mud flats with accumulation of estuarine/marine organic matter. It was a consequence of the marine incursion caused by post-glacial sea-level rise, further driven by tectonic subsidence. Dry conditions in the Amazon region during this time led to a rise is tidal water salinity and contributed to mangrove expansion. Therefore the effect of relative sea-level (RSL) rise was determinant to the mangrove establishment in the southeastern and northern region. During the late Holocene (~3050 – 1880 cal yr BP) the mangroves in both regions were retracted to a small area, with some areas replaced by freshwater vegetation. This was caused by the increase in river discharge associated to a wet period recorded in the Amazon region, and considering the coastal plain of the Doce River (southeastern Brazil), the mangroves shrank in response to an increase in fluvial sediment input associated to a sea-level fall.

Keywords: Mangrove, Palynology, Facies analysis, Carbon and Nitrogen isotopes, Amazon region, Southeastern Brazil.

LISTA DE ILUSTRAÇÕES

1 CHAPTER I: VEGETATION AND MORPHOLOGY CHANGES IN MOUTH OF THE AMAZON-PA AND DOCE-ES RIVER DURING THE LATE QUATERNARY

Figure 1 – A) South America with studies areas at the Brazilian littoral. B) Location of the study area and sampling site at the northern Brazil coast, northeastern Marajó Island, with sea water salinity, Amazon River plume and North Brazil Current-NBC (Santos et al., 2008). C) Sampling site at the Southeastern Brazil, State of Espirito Santo, Miocene Barreiras Formation and coastal plain of the Doce River, RGB Landsat composition – SRTM, with a topographical profile obtained from SRTM digital elevation data illustrating a large area slightly more depressed on coastal plain of the Doce River. D) Contact between arboreal vegetation and herbaceous vegetation at the coastal plain of the Doce River. E) Mangrove and herbaceous vegetation. F) Mangrove vegetation.

Figure 2 – Model of the Amazonian mangrove development during the Holocene in the: Macapá (2a and 2e); Marajó Island (2b and 2f) and eastern Marajó Island (2c and 2g).

Figure 3 – Model for coastal plain evolution of the Doce River during the late Pleitocene to Holocene.

2 CHAPTER II: THE LAST MANGROVES OF MARAJÓ ISLAND – EASTERN AMAZON: IIMPACT OF CLIMATE AND/OR RELATIVE SEA-LEVEL CHANGES

Figure 1 – Location of the study area: a) seawater salinity, Amazon River plume and North Brazil Current (Santos et al., 2008), b)Marajó Island; c) source coastal plain; d) vegetation units; e) sampling site on Soure coastal plain; f)mangrove and sand plain; g) degraded mangrove.

Figure 2 – Sediment profile with sedimentary features and ecological groups from cores R-1, R-2 and R-3.

Figure 3 – Sediment profile with sedimentary feature and ecological groups from cores R-4 and R-5.

Figure 4 – Pollen record from core R-1 with percentages of the most frequent pollen taxa and sample age.

Figure 5 – Pollen record from core R-2 with percentages of the most frequent pollen taxa and sample age.

Figure 6 – Pollen record from core R-3 with percentages of the most frequent pollen taxa and sample age.

Figure 7 – Pollen record from core R-4 with percentages of the most frequent

3 CHAPTER III: AN INTER-PROXY APPROACH TO ASSESSING THE DEVELOPMENT OF THE AMAZONIAN MANGROVE, DURING THE HOLOCENE

4 CHAPTER IV: LANDSCAPE EVOLUTION DURING THE LATE QUATERNARY AT THE DOCE RIVER MOUTH, ESPÍRITO SANTO STATE, SOUTHEASTERN BRAZIL

5 CHAPTER V: MANGROVE VEGETATION CHANGES ON HOLOCENE TERRACES OF THE DOCE RIVER, SOUTHEASTERN BRAZIL

SUMÁRIO

Introduction

Study area

Present climate and vegetation

Materials and methods

Field work and sample processing

Pollen and spore analyses

Radiocarbon dating

Results

Radiocarbon dates and sedimentation rates

Facies description and pollen association

Mangrove/herbaceous flat facies association

Mangrove flat facies association

Lagoon facies association

Foreshore facies association

Lake facies association

Discussion

Pollen signal and vegetation changes in Marajó Island during the Holocene (central and eastern coastal zone)

Mangrove dynamics during the last decades in the eastern coastal zone of Marajó Island

Conclusions

3 CHAPTER III: AN INTER-PROXY APPROACH TO ASSESSING THE DEVELOPMENT OF THE AMAZONIAN MANGROVE, DURING THE HOLOCENE
* Paper accepted on Vegetation History and Archaeobotany

Abstract

Introduction

Study site

Geological and geomorphological setting

Regional climate and oceanographic characteristics

Modern vegetation

Materials and methods

Sampling

4 CHAPTER IV: LANDSCAPE EVOLUTION DURING THE LATE QUATERNARY AT THE DOCE RIVER MOUTH, ESPÍRITO SANTO STATE, SOUTHEASTERN BRAZIL
* Paper accepted on Palaeogeography, Palaeoclimatology, Palaeoecology

Methods

Remote sensing

Sampling processing and facies description

Pollen and spore analysis

Isotopic and chemical analysis

Radiocarbon dating

Results

Radiocarbon dates and sedimentation rates

Facies description

Delta plain and Estuary central basin/lagoon-bay (A)

Facies Association A1- Beach ridge complex

Facies Association A2- Lake

Facies Association A3-Fluvial channel

Facies Association A4-Tidal channel

Facies Association A5- Marshes

Facies Association A6- Estuary central basin/lagoon-bay

Deltaic system (B)

Facies Association B1-Delta Plain

Facies Association B2-Delta Front

Facies Association B3-Prodelta

Palaeoenvironmental Interpretation

Climate and sea-level changes during the late Quaternary

Sea-level changes and fluvial sediment supply

Conclusion

5 CHAPTER V: MANGROVE VEGETATION CHANGES ON HOLOCENE TERRACES OF THE DOCE RIVER, SOUTHEASTERN BRAZIL
* Paper published on Catena 110 (2013) 59-69
http://www.sciencedirect.com/science/article/pii/S0341816213001501

Abstract

Introduction

Modern settings

Study area and geological setting

Climate

Vegetation

Materials and methods

Field work and sampling processing

Facies description

Palynological analysis

Isotopic and chemical analysis

Radiocarbon dating

Results

Radiocarbon date and sedimentation rates

Facies, pollen description and isotopes values from sediment core

Facies association A (foreshore)

Facies association B (lagoon)

Facies association C (lake)

Facies association D (herbaceous plain)

Interpretation and discussion

Early Holocene: foreshore to lagoon

Middle-Late Holocene: Lagoon/lake transition to herbaceous flat

Holocene sea-level changes, climate and vegetation dynamics

Conclusion

REFERENCES

CHAPTER I:

VEGETATION AND MORPHOLOGY CHANGES IN MOUTH OF THE AMAZON-PA AND DOCE-ES RIVER DURING THE LATE QUATERNARY

Introduction

Climate change and Atlantic sea-level oscillation have produced an impact on sedimentary dynamics and displacements of coastal ecosystems along the Brazilian littoral during the late Quaternary (Suguio et al., 1985; Dominguez et al., 1992; Ledru et al., 1996; Angulo and Lessa, 1997; Behling et al., 1998; Grimm et al., 2001; Bezerra et al., 2003; Martin et al., 2003; Cohen et al., 2005a,b; Angulo et al., 2006; Vedel et al., 2006; Behling et al., 2007; Sawakuchi et al., 2008; Lara and Cohen, 2009; Zular et al., 2013, Guimarães et al., 2012, 2013; Buso Junior et al., 2013 – *in press*; França et al., 2012; 2013a,b – *in press*). The region is largely controlled by complex interactions involving gradients of tidal oscillation, river discharge, littoral currents, sediment and nutrient supply and winds (Dominguez, 2006; Schaeffer-Novelli et al., 2000; Cohen et al., 2005a,b; Amaral et al., 2006; Cohen et al., 2009; Dillenburg et al., 2009; Sanders et al., 2010, 2012; Pessenda et al., 2012; Smith et al., 2012; Guimarães et al., 2012).

Regarding the mangroves, they occur broadly on the Brazilian coast (Schaeffer-Novelli et al., 2000), and they have reacted clearly to climate change and sea-level fluctuations, as they respond to environmental factors such as water salinity, nutrients and input of sediment and freshwater (Krauss et al., 2008; Stevens et al., 2006; Stuart et al., 2007). The evolutionary development of these forests is controlled by land-ocean interaction, and their expansion is determined by topography, sediment geochemistry (Alongi, 2002), as well as current energy conditions (Woodroffe, 1982). This ecosystem is highly adaptive, with plants tolerant of extreme environmental conditions such as high salinity, anoxia and constant water inundation (Vannucci, 2001). This adaptability has allowed mangroves to withstand environmental change throughout the Holocene (Monacci et al., 2009), and become a marker of great importance for scientific analysis of coastal change (Blasco et al., 1996).

The mangroves in the northern Brazilian littoral were present along the current coastline since the early Holocene (Behling, 2001; Cohen et al., 2005a,b; 2012; Smith et al., 2011; França et al., 2012). This ecosystem expanded along the coastal plain of the Doce River during the early-middle Holocene (Buso Junior et al., 2013 – *in press*; França et al., 2013a – *in press*). Currently the mangroves have presented a limited distribution in the northern Brazilian littoral influenced by Amazon River and along the southeastern Brazilian coastline (Amaral et al., 2006; Cohen et al., 2012; Pessenda et al., 2012).

Previous studies of pollen, biogeochemistry and sedimentary records along the Brazilian coast have demonstrated that proxy analysis can provide important information about coastal vegetation history (e.g. Grindrod et al., 2002; Amaral et al., 2006; Pessenda et

al., 2008; Cohen et al., 2009; Smith et al., 2011; França et al., 2012; Guimarães et al., 2012; França et al., 2013b – *in press*). In this context, the goal of this study was to compare the impact of sea-level fluctuations, and sediment/freshwater supply changes in mangrove areas and morphological dynamics influenced by Amazon and Doce River during the late Quaternary. This was carried out by the integration of multi-proxy data, including pollen, sedimentary features, $\delta^{13}C$, $\delta^{15}N$, C/N and radiocarbon-date from twelve cores sampled along the northern (Chapters II and III) and southeastern Brazilian coast (Chapters IV and V).

Study area

The study sites are located on Marajó Island (northern Brazil), at the mouth of the Amazon River, and in the coastal plain of the Doce River (southeastern Brazil) (Figure 1). Currently, the Marajó Island's coastal vegetation is dominated by a regime of semidiurnal meso- and macro-tides (tidal range of 2 to 4 m and 4 to 6 m, respectively) with variations during the spring tide between 3.6 and 4.7 m (DHN, 2003), and influenced by Amazon River discharge of approx. 170,000 m^3 s^{-1} (ANA, 2003). Consequently, the river discharge and hydrodynamic conditions allow a strong reduction of tidal water salinity along the adjacent coast (Vinzon et al., 2008; Rosario et al., 2009) with salinity values between 7 and 30‰.

The second area located on the southeastern Brazilian littoral, State of Espírito Santo, is between Conceição da Barra and Barra do Riacho. The coastal plain of the Doce River has a maximum width of about 40 km and length of about 150 km (Suguio et al., 1982; Bittencourt et al., 2007). This coastal region is influenced by the Atlantic ocean with semidiurnal micro-tides (tidal range < 2 m), tidal water salinity between 9 and 34‰ and two main rivers, the Doce River, with maximum and minimum outflow of 1900 and 400 m^3 s^{-1}, and the São Mateus River with discharge about 11 m^3 s^{-1} (Bernini et al., 2006; Freitas et al., 2010).
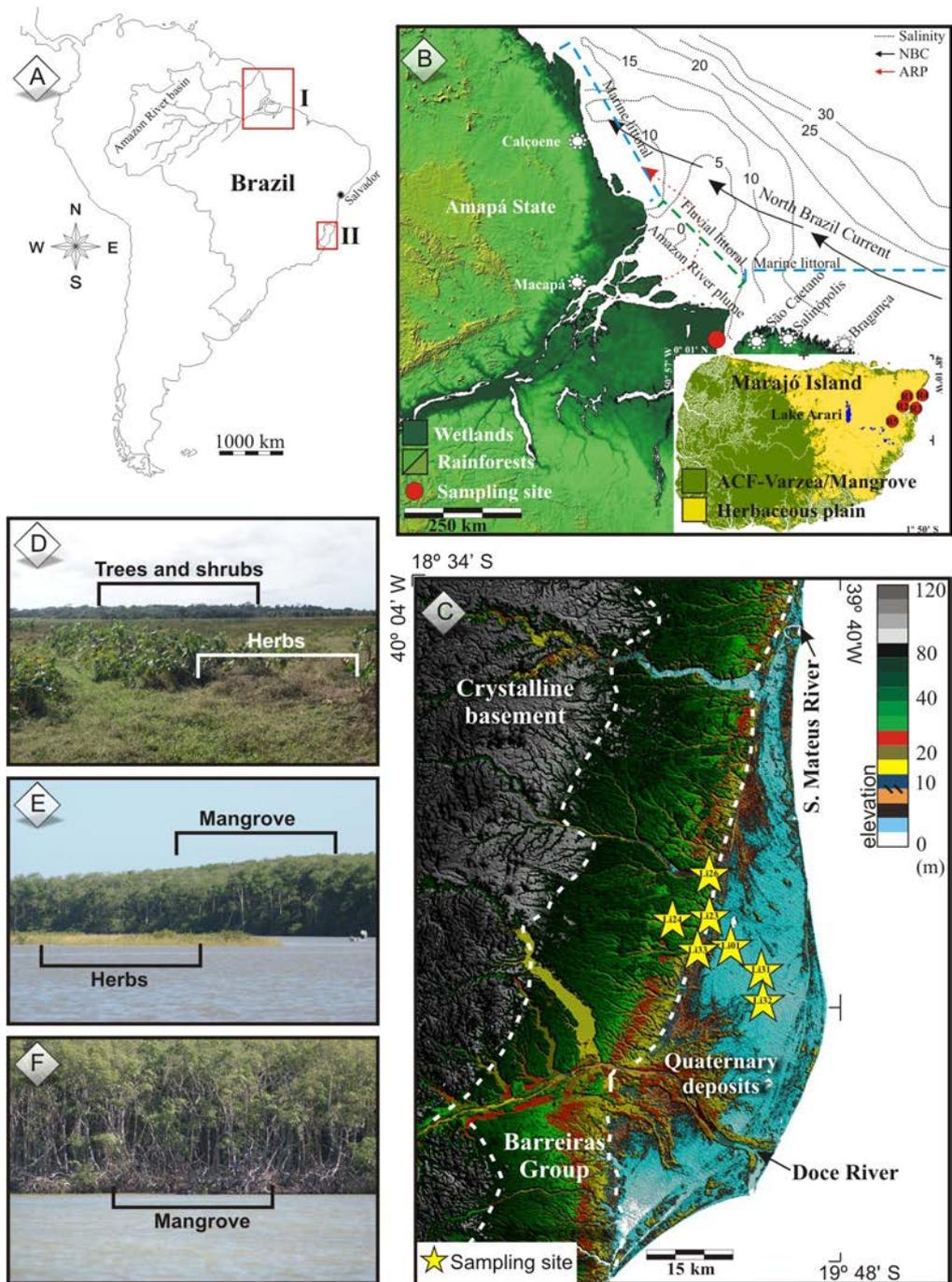
Figure 1 – A) South America with studies areas at the Brazilian littoral. B) Location of the study area and sampling site at the northern Brazil coast, northeastern Marajó Island, with sea water salinity, Amazon River plume and North Brazil Current-NBC (Santos et al., 2008). C) Sampling site at the Southeastern Brazil, State of Espirito Santo, Miocene Barreiras Formation and coastal plain of the Doce River, with a topographical profile obtained from SRTM digital elevation data illustrating a large area slightly more depressed on coastal plain of the Doce River. D) Contact between arboreal vegetation and herbaceous vegetation at the coastal plain of the Doce River. E) Mangrove and herbaceous vegetation in the coastal plain of the Doce River F) Mangrove vegetation in the Marajó island.

Geological Setting

Marajó Island – Northern Brazil

The coastal plain of Soure is located on the Pará platform of northern Brazil. It pertains to a large area of crystalline and Palaeozoic sedimentary basement that remained tectonically stable relative to adjacent Cretaceous and Cenozoic sedimentary basins (Rossetti et al., 2008). The coastal plateau of northern Brazil is formed by the Barreiras Formation. These deposits occur from northern to southeastern Brazil and are of Miocene age (Arai, 1997).

Except for a narrow belt where the Barreiras Formation occurs, the eastern portion of the island is characterized by lowlands with altitudes averaging 4-6 m above the modern sea-level (Rossetti et al., 2007, 2008) and is dominated by Holocene sedimentation, which is topographically slightly lower than the western side (Behling et al., 2004; Rossetti et al., 2007; Lara and Cohen, 2009). Along the eastern portion, the Barreiras Formation is represented by sandstones and mudstones followed by post-Barreiras deposits (Rossetti et al., 2008).

Marajó Island has a river system consisting of numerous small, straight and meandering channels and ponds that are either permanent or ephemeral (Bemerguy, 1981). The flat surface of the eastern part of the island has been deeply incised by a drainage system during the Pleistocene and Holocene.

Coastal plain of the Doce River – Southeastern Brazil

The study site is located in the coastal plain between two large rivers, Doce and São Mateus, northern Espírito Santo – Brazil, running along a nearly N-S section between Conceição da Barra and Barra do Riacho (Suguio et al., 1982; Bittencourt et al., 2007). The Holocene sedimentary history in this sector is strongly controlled by RSL changes, fluvial supply and longshore transport. The formation of a barrier island/lagoonal system began about 7000 yr BP (Suguio et al., 1982; Martin et al., 1996; Martin et al., 2003).

The study area is composed of a Miocene age plateau of Barreiras Formation continental deposits, whose surface is slightly sloping to the ocean. The site is characterized by the presence of many wide valleys with flat bottoms, resulting from Quaternary deposition of silty sediments (Martin et al., 1996). The study area is part of a larger area of tectonically stable Precambrian crystalline rocks. Four geomorphological units are recognized in the area: (1) a mountainous province, made up of Precambrian rocks, with a multidirectional rectangular dendritic drainage net; (2) a tableland area composed of Barreiras Formation

constituted by sandstones, conglomerates and mudstones attributed mainly to Neogene fluvial and alluvial fan deposits, but possibly including deposits originating from a coastal overlap associated with Neogene marine transgressions (Arai, 2006; Dominguez et al., 2009). The drainage catchment slopes gently down towards the sea; and (3) a coastal plain area, with fluvial, transitional and shallow marine sediments, which were deposited during RSL changes (Martin et al., 1987) and (4) an inner continental shelf area (Asmus et al. 1971).

Climate

Climate along the northern coast of Brazil is tropical (warm and humid), with annual precipitation averaging 2300 mm (Lima et al., 2005). The rainy season occurs between the months of December and May, with a drier period between June and November. Average temperatures range between 25º and 29º C (Marengo et al., 1993, 2001; Nobre and Shukla, 1996; Fu et al., 2001; Liebmann and Marengo, 2001). Southeastern Brazil is characterized by a warm and humid tropical climate with annual precipitation averaging 1400 mm (Peixoto and Gentry, 1990). Precipitation generally occurs in the summer with a dry fall-winter season. The rainy season occurs between the months of November and January with a drier period between May and September. The average temperature ranges between 20º and 26º C (Carvalho et al., 2004).

Vegetation

Modern vegetation on Marajó Island consists of herbaceous flats, natural open areas that are dominated by Cyperaceae and Poaceae, "várzea" vegetation (swampland seasonally and permanently inundated by freshwater) is composed of wetlands trees such as *Euterpe oleraceae* and *Hevea guianensis*, while the "terra firme" vegetation, represented by the Amazon Coastal Forest (ACF) unit, is characterized by *Cedrela odorata*, *Hymenaea courbaril* and *Manilkara huberi* (Behling et at., 2004; Cohen et al., 2008; Smith et al., 2011, 2012). "Restinga" (shrub and herb vegetation that occurs on sand plains and on dunes close to the shore line) is dominated by Anacardiaceae and Malpighiaceae. Mangroves (tree heights reaching ~20 m) are classified as *Rhizophora* sp. dominated with a presence of *Avicennia* sp. and *Laguncularia* sp. (Cohen et al., 2008).

The coastal plain of the Doce River is characterized by forest pioneering freshwater species such as *Hypolytrum* sp., *Panicum* sp and also brackish/marine water species such as *Polygala cyparissias*, *Remiria maritima*, *Typha* sp., *Cyperus* sp., *Montrichardia* sp., *Tapirira guianensis* and *Symphonia globulifera*. Tropical rainforest type vegetation is also present in

this region, where the most representative plant families are Annonaceae, Fabaceae, Myrtaceae, Sapotaceae, Bignoniaceae, Lauraceae, Hippocrateaceae, Euphorbiaceae, and Apocynaceae (Peixoto and Gentry, 1990). The mangrove ecosystem is characterized by *Rhizophora* sp., *Laguncularia* sp. and *Avicennia* sp., which are currently restricted to the northern and southern littoral part of the coastal plain (Bernini et al., 2006).

Materials and methods

Fields work and sample processing

For this study twelve sediment cores were analysed from areas occupied by different vegetation units (Table 1): "várzea" (R-1), mangroves (R-2 and R-4), mangrove and herbaceous vegetation (R-3), lacustrine herbaceous plain (R-5), herbaceous plain (LI-01, LI-23, LI-26, LI-31, LI-32 and LI-33) and mixture between forest and herbaceous plain (LI-24). Three sediment cores were collected in northern Brazil (R-1, R-2 and R-3) using a Russian sampler (Cohen, 2003) and two sediment cores were taken with a vibracorer using an aluminium tube (R-4 and R-5). Considering the coastal plain of the Doce River, one sediment core was sampled (LI-32) using a Russian sampler and to the others was used a percussion drilling Robotic Key System (RKS), model COBRA MK1 (COBRA Directional Drilling Ltd., Darlington, U.K.).

The cores were X-rayed in order to identify sedimentary structures. Samples were collected for grain size analysis in the Laboratory of Chemical Oceanography/UFPA. Grain size was determined by laser diffraction using a Laser Particle Size SHIMADZU SALD 2101. The sediment grain size distributions were determined following the methods of Wentworth (1922) and the graphics were elaborated using the SYSGRAN software (Camargo, 1999), with sand (2-0.0625 mm), silt (62.5-3.9 µm) and clay fractions (3.9-0.12 µm). Facies analysis included descriptions of color (MunsellColor, 2009), lithology, texture and structure (Harper 1984; Walker, 1992). The sedimentary facies were codified according to Miall (1978).

Table 1 – Sites, vegetation types, sampling method, coordinate and location.

Code site	Unit vegetation	Sampling method	Coordinates	Location
R-1	Mangrove/*várzea*	RSC	S00º40'26''/W48º29'37''	Marajó Island
R-2	Mangrove	RSC	S00º40'23''/W48º29'38''	Marajó Island
R-3	Mangrove/herbaceous	RSC	S00º40'25''/W48º29'35''	Marajó Island
R-4	Mangrove	VBC	S00º39'37''/W48º29'3.3''	Marajó Island
R-5	Herbaceous plain	VBC	S00º55'41''/W48º39'47''	Marajó Island
LI-01	Herbaceous plain	RKS	S19º10'53''/W39º51'55''	Doce River
LI-23	Herbaceous plain	RKS	S19º08'58''/W39º53'29''	Doce River
LI-24	Forest/herbaceous plain	RKS	S19º9'8.5''/W39º55'47''	Doce River
LI-26	Herbaceous plain	RKS	S19º07'4''/W39º52'57''	Doce River
LI-31	Herbaceous plain	RKS	S19º11'16''/W39º49'33''	Doce River
LI-32	Herbaceous plain	RSC	S19º11'36''/W39º48'2''	Doce River
LI-33	Herbaceous plain	RKS	S19º10'19''/W39º53'10''	Doce River

RSC. Russian Sampler; VBC. Vibracorer; RKS. Percussion drilling

Palynological analysis

The sediment cores were sub-sampled with 372 total samples at different downcore intervals. 1 cm^3 of sediment was taken for palynological analysis. All samples were prepared using standard analytical techniques for pollen including acetolysis (Faegri and Iversen, 1989). Sample residues were placed in Eppendorf microtubes and kept in a glycerol gelatin medium. Reference morphological descriptions (Roubik and Moreno, 1991; Behling, 1993; Herrera and Urrego, 1996; Colinvaux et al., 1999) were consulted for identification of pollen grains and spores. A minimum of 300 pollen grains were counted in each sample. Software packages TILIA and TILIAGRAPH were used to calculate and plot pollen diagrams (Grimm, 1990). The pollen diagrams were statistically subdivided into zones of pollen and spore assemblages using a square-root transformation of the percentage data, followed by stratigraphically constrained cluster analysis (Grimm, 1987).

δ^{13}C, δ^{15}N and C/N

A total of 1043 samples (6-50 mg) were collected from the cores for geochemical analyses (e.g. Pessenda et al., 2010). δ^{13}C, δ^{15}N and elemental C and N (C/N) concentrations were analyzed at the Stable Isotopes Laboratory of Center for Nuclear Energy in Agriculture (CENA), University of São Paulo (USP), using a Continuous Flow Isotopic Ratio Mass Spectrometer (CF-IRMS). Organic carbon and nitrogen results (C/N ratio) are expressed as percentages of dry weight. The isotope ratios results (δ^{13}C and δ^{15}N) are expressed in delta

per mil notation with an analytical precision greater than 0.2‰, with respect to the VPDB standard and atmospheric air, respectively.

The relationship between δ^{13}C, δ^{15}N and C/N was used to provide information about the origin of organic matter preserved in the coastal environment (Fry et al., 1977; Peterson and Howarth, 1987; Schidlowski et al., 1983; Meyers, 1997, 2003; Wilson et al., 2005; Lamb et al., 2006).

The δ^{13}C values have different mean value between terrestrial plants, freshwater and marine sources (Meyers, 1997). Some classes of plants also have different sources of CO_2 (air vs. water) or different carbon isotopic fractionations (C_3 vs. C_4 photosynthetic pathways). Atmospheric nitrogen has a δ^{15}N value of zero, and terrestrial plants tends to have δ^{15}N values close to 0‰, whereas *Spartina* sp. has δ^{15}N values around +6‰, and near shore plankton have values of around +6 to +10‰ (Wada 1980; Macko et al., 1984; Altabet and McCarthy, 1985).

Radiocarbon dating

Twenty nine bulk samples of ~10g each were used for radiocarbon dating (Table 2). Samples were checked and physically cleaned (no roots) under the stereo microscope. The residual material for each sample was then extracted with 2% HCl at 60°C for 4 hours, washed with distilled water until neutral pH was reached, at 50 ºC and dried (Pessenda et al., 2010, 2012). The organic matter from the sediment was analyzed by Accelerator Mass Spectrometry (AMS) at the Center for Applied Isotope Studies (Athens, Georgia, USA) and LACUFF (Fluminense Federal University). Radiocarbon ages are reported in years before AD 1950 (yr BP) normalized to δ^{13}C of –25‰VPDB and in cal yr BP, 2σ (Reimer et al., 2009) and use the median of the range for discussing our and other authors data in the text.

Table 2 – Sediment cores with sampling site, depth, $\delta^{13}C$, ^{14}C conventional and calibrated ages (using Calib 6.0; Reimer et al., 2009) from Marajó Island (Amazon region) and coastal plain of the Doce River (Southeastern Brazil).

Cody site and lab. number	Sampling site	Depth (m)	^{14}C ages (yr B.P.)	CALIB - 2σ (cal yr B.P.)	Median (cal yr B.P.)	$\delta^{13}C$ (‰)
R-1						
UGAMS4924	Marajó	1.47-1.50	540 ± 25	560-520	540	-27.8
R-2						
UGAMS4925	Marajó	1.47-1.50	1260 ± 30	1160-1120	1150	-28.2
R-3						
UGAMS4927	Marajó	1.07-1.10	40 ± 25	70-30	50	-28.5
UGAMS4926	Marajó	1.47-1.50	690 ± 25	680-640	660	-28.8
R-4						
UGAMS5318	Marajó	2.09-2.11	1510 ± 25	1420-1340	1380	-26.4
UGAMS4933	Marajó	2.18-2.20	1760 ± 30	1740-1570	1655	-26.6
R-5						
UGAMS4928	Marajó	0.22-0.24	1920 ± 30	1950-1820	1880	-25.3
UGAMS8209	Marajó	0.78-0.83	5730 ± 30	6640-6580	6610	-30.2
UGAMS4929	Marajó	1.42-1.46	5840 ± 30	6740-6600	6670	-27.0
UGAMS8207	Marajó	1.85-1.94	6150 ± 30	7160-6960	7060	-29.1
UGAMS4930	Marajó	2.48-2.51	6600 ± 30	7530-7440	7500	-27.1
LI-01						
UGAMS10565	D. River	1.65-1.75	6710 ± 30	7556-7622	7600	-
UGAMS10566	D. River	3.70-3.75	24,610 ± 70	29,226-29,678	29,500	-
LACUFF13018	D. River	6.20-6.30	33,358 ± 948	36,105-40,014	38,000	-
UGAMS11693	D. River	8.80-8.86	31,220 ± 100	35,162-36,321	35,700	-
LACUFF00038	D. River	11.5-11.7	44,232 ± 812	45,775-49,391	47,500	-
LI-24						
UGAMS10567	D. River	0.80-0.90	Modern	Modern	Modern	-
UGAMS10568	D. River	2.70-2.80	1480 ± 25	1310-1400	1355	-32.5
UGAMS10569	D. River	4.80-4.90	4500 ± 25	5210-5290	5250	-29.8
UGAMS10570	D. River	6.73-6.77	6330 ± 30	7170-7230	7200	-29.6
UGAMS10571	D. River	9.40-9.50	6560 ± 30	7545-7555	7550	-29.6
LI-31						
UGAMS10572	D. River	1.05-1.10	4320 ± 25	4840-4893	4860	-
UGAMS10573	D. River	4.95-5.00	3600 ± 20	3845-3933	3890	-
UGAMS10574	D. River	6.55-6.65	25,970 ± 80	30,465-31,022	30,700	-
LI-32						
LACUFF13019	D. River	0.67-0.72	2877 ± 79	3246-2840	3043	-
LACUFF12039	D. River	1.40-1.45	6237 ± 66	7278-6955	7116	-
UGAMS11695	D. River	3.40-3.45	6330 ± 30	7318-7172	7245	-27.6
UGAMS11694	D. River	4.30-4.35	6380 ± 30	7339-7259	7300	-27.5
LACUFF12040	D. River	5.45-5.50	7186 ± 54	8161-7933	8047	-

Results and discussions

Marajó Island – Northern Brazil

The cores from Marajó Island consist of dark gray and light brown muddy and sandy silt sediments. Grain size increases towards the top of the core (see Chapter II). The $\delta^{13}C$ isotopic results exhibit values from –29.34‰ to –22.07‰ (mean= –26.55‰), which indicate the dominance of C_3 plants (–32‰ to –21‰; Deines, 1980; Boutton, 1996). The $\delta^{15}N$ record shows values between –0.61‰ and +6.04‰ (mean= +2.46‰), which suggests a mixture of terrestrial plants (~0‰) and aquatic matter (+6 to +10‰) as observed by Wada (1980), Macko et al. (1984) and Altabet and McCarthy (1985). The C/N values showed considerable variation between 3.55 and 45.67 (mean= 22.04), which also indicate a mixture of organic matter from vascular plants and algae (<10 algae dominance and >12 vascular plants; Meyers, 1994; Tyson, 1995) (França et al., 2013b – *in press*; see Chapter III).

The texture analysis and description of sedimentary structures of the materials collected in the tidal flat, together with pollen records, grain size, isotopic ($\delta^{13}C$ and $\delta^{15}N$) and C/N values, allowed five facies associations to be defined: mangrove flat, lake, foreshore, lagoon and mangrove/mixed flat on the eastern coast of the island during at least the last 7500 cal yr BP.

The results indicate a tidal mud flat colonized by mangroves with estuarine organic matter between ~7500 and ~3200 cal yr BP. During the late Holocene this led to a gradual migration of mangroves from the central region to the northeastern littoral zone of the island, and, consequently, its isolation since at least ~1150 cal yr BP. This likely results from lower tidal water salinity caused by a relatively wet period that resulted in greater river discharge during the late Holocene. The northeastern area of the island exhibits relatively greater tidal water salinity, due to the southeast-northwest trending littoral current which brings brackish waters from more marine influenced areas. It has provided a refuge for the mangroves of Marajó Island (França et al., 2012, see chapter II).

Over the last century, the increase in flow energy evidenced by upward mud/sand transitions also contributes to mangrove retraction, as recorded in the upper part of core R-3 (see Chapter II). This is mainly due to landward sand migration, which covers the mudflat and asphyxiates the mangrove. The increase in flow energy and exposure to tidal influence may have been driven by the RSL rise, either associated with global fluctuations or tectonic subsidence, and/or by the increase in river water discharge. These processes can modify the size of the area occupied by mangroves (França et al., 2012; see chapter II).

The mangrove dynamic during the Holocene has also been recorded by Cohen et al. (2005a,b, 2009; 2012), Guimarães et al. (2012), Smith et al. (2012) and França et al. (in press) at the northern Brazilian coast, related to RSL change and or/ river water discharge (Figure 2).
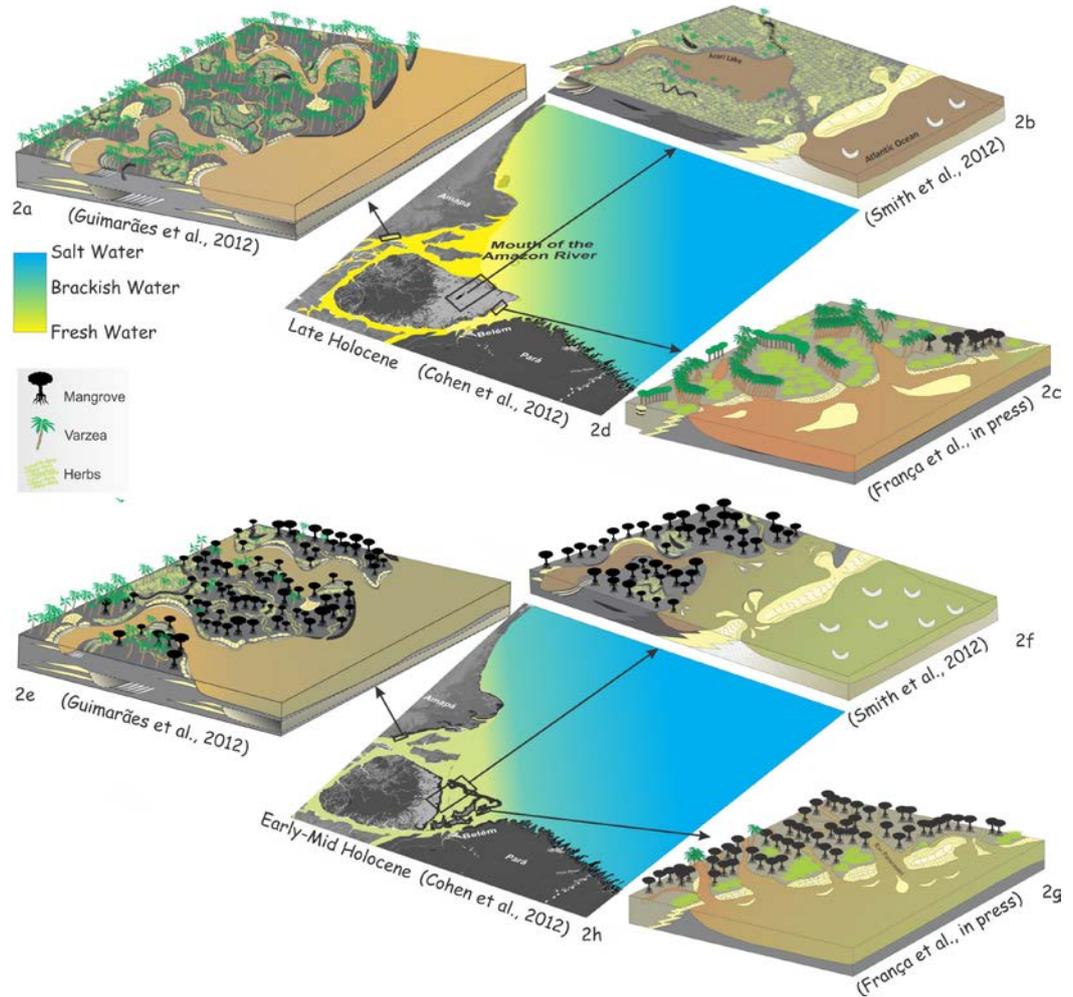
Figure 2 – Model of the Amazonian mangrove development during the Holocene in the: Macapá (2a and 2e); Marajó Island (2b and 2f) and eastern Marajó Island (2c and 2g).

Geomorphology changes in the coastal plain of the Doce River during the late Pleistocene and Holocene

The observed succession of facies association Delta Plain, Estuary Central Basin/Lagoon-bay (mangrove/herbaceous flat) and Deltaic System might be a product of driving forces regulated by cyclic mechanism leading to a delta, estuary and following to a delta plain environment. The Holocene evolution had been controlled by relative sea-level changes, fluvial sediment transport and longshore transport. The build up of its Holocene part began with the formation of a estuary/lagoonal system (Figure 3 and chapter IV).

Probably, the changes in this depositional environment were driven by the equilibrium between the sea-level changes and fluvial sediment supply during the late Pleistocene and Holocene. Probably, this depositional architecture of the late Pleistocene coastal system evolving from a prodelta to a delta front, followed by the delta plain in response to relative sea-level fall between ~47,500 and ~29,400 cal yr B.P.

The deltaic system deposits were recorded during the eustatic sea-level fall between ~47,500 and ~29,400 cal yr B.P. The sediment accumulated during the LGM and the late Pleistocene/Holocene transition was not characterized. Probably, from ~ 30,000 cal yr B.P. to ~7500 cal yr B.P., a sedimentary hiatus occurred, related to an erosive event associated to the rapid post glacial sea-level rise.

The estuary with mangroves was formed during the sea-level rise of the Holocene (~7550 to ~5250 cal yr BP). These environments were formed during the early and middle Holocene as a response of an eustatic sea-level rise that resulted in significant changes in the coastal geomorphology. During the early Holocene, the arboreal and herbaceous vegetation dominated the coastal plain, and the equilibrium between the relative sea-level and fluvial sediment supply created conditions to the development of an estuarine system with fluvial and tidal channels, lagoons and tidal flats colonized by mangroves.

The upward succession composed by the transition estuarine complex with mangrove into the coastal plain colonized by marshes suggests a decrease of marine influence and form the regressive part of the cycle after the post glacial sea-level rise. Thus, the upper sequence of the LI-24 (marshes and fluvial channel, chapter IV) should have been accumulated following a relative sea-level fall or a high fluvial sediment supply during the middle and late Holocene. Considering the increase in the sand input by fluvial channels, the fluvial sediment was reworked by wave and caused the sandy ridges with replacement of mangroves by arboreal and herbaceous vegetation according to a marine regression (see chapter IV and V).
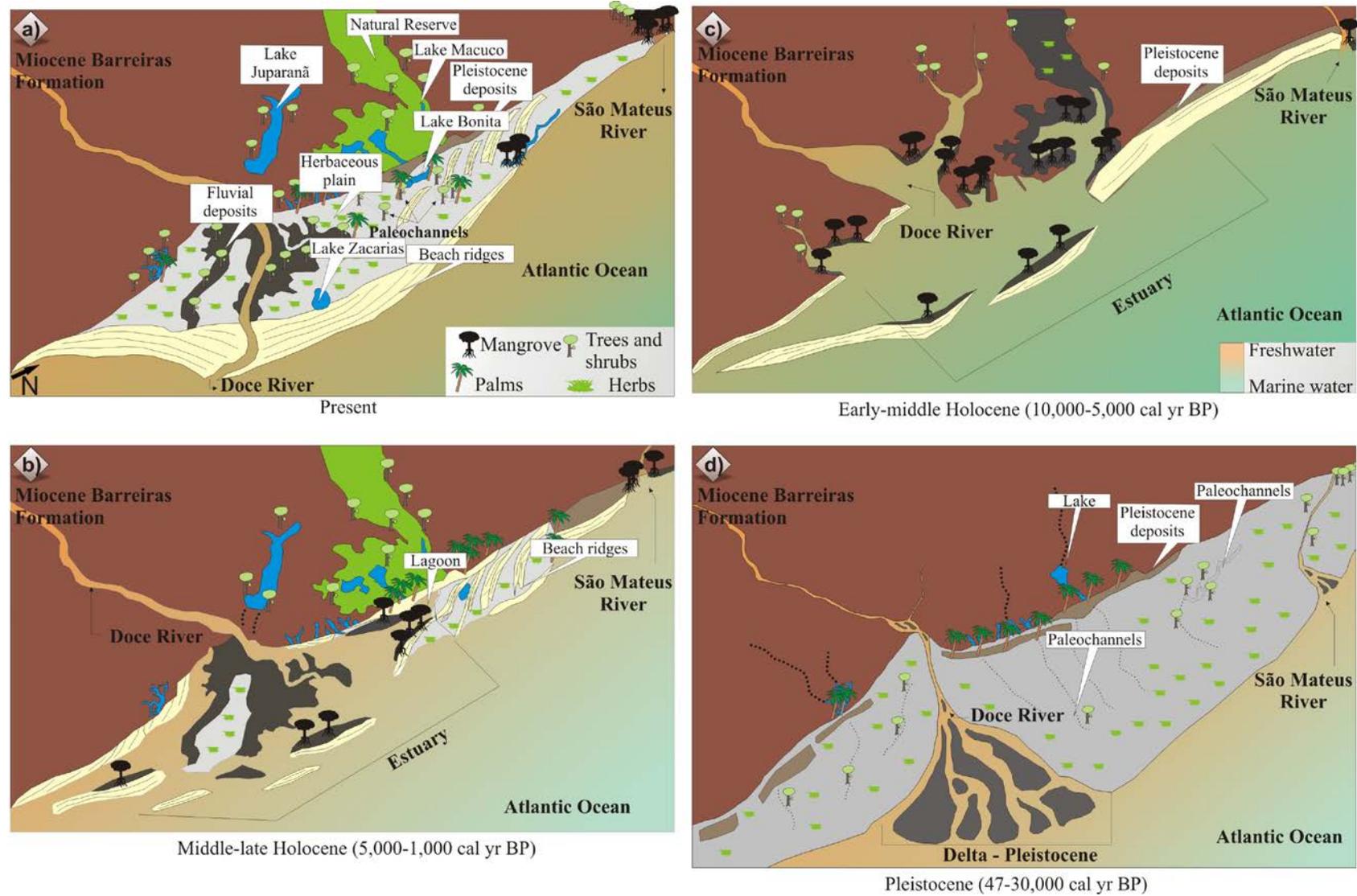
Figure 3 – Model for coastal plain evolution of the Doce River during the late Pleitocene to Holocene.

Mangrove vegetation changes during the Holocene

During the Holocene, the post-glacial sea-level rise and changes in river water discharge have been considered the main driving forces behind the expansion/contraction of mangroves in northern Brazil (Cohen et al., 2008; Lara and Cohen, 2009; França et al., 2012; Guimarães et al., 2012; Smith et al., 2012). The data from Marajó Island indicates a tidal mud flat colonized by mangroves with an influence of estuarine organic matter and terrigenous input between at least ~7500 and ~3200 cal yr BP (chapters II and III). This is likely due to the relatively higher marine influence caused by post-glacial sea-level rise, and the dry period experienced by the Amazon region during the early and middle Holocene (Pessenda et al., 2001; Behling and Hooghiemstra, 2000; Freitas et al., 2001; Sifeddine et al. 2001; Weng et al., 2002; Bush et al., 2007). As rainfall controls the volume of the Amazon River (Eisma et al., 1991; Maslin and Burns, 2000; Latrubesse and Fanzinelli, 2002), lower precipitation resulted in severely reduced freshwater discharge (Amarasekera et al., 1997; Toledo and Bush, 2007, 2008). This led to a greater influence of saline marine water and mangrove expansion in the northern Brazil (Cohen et al., 2012).

During the late Holocene occurred a decrease in mangrove vegetation area in the Marajó Island. Likely it was caused by an increase in river discharge, which resulted in a relatively low tidal water salinity during that time (França et al., 2012; see chapter II and III).

In contrast, the dynamics of these forests in southeastern Brazil have been controlled mainly by sediment supply associated to sea-level fluctuations. The post-glacial sea-level rise caused change in the coastal environment along southeastern Brazil (Giannini et al., 2007; Guedes et al., 2011; Pessenda et al., 2012), which resulted in the formation of numerous lagoons and estuarine systems around 7800 cal yr BP (Martin et al., 1996; Sallun et al., 2012) colonized by mangrove and herbaceous vegetation (Buso Junior et al., *in press*). Sea-level oscillations have apparently been more intense and recognizable in this region. During the early and middle Holocene several studies on the Brazilian coastal zone indicate significant climatic changes and RSL fluctuations (Suguio et al., 1985; Dominguez et al., 1992; Angulo and Lessa, 1997; Bezerra et al., 2003; Martin et al., 2003; Cohen et al., 2005a,b; Angulo et al., 2006; Vedel et al., 2006; Lara and Cohen, 2009). The Salvador sea-level curve (northeastern Brazil), reconstructed by Martin et al. (2003) extends back to around 7800 cal yr BP, when the mean sea level exceeded the current level for the first time in the Holocene. This period coincided with a dryer period in the Amazonian hydrographic region (Van der Hammem, 1974; Absy et al., 1991; Desjardins et al., 1996; Behling and Costa, 2000; Ledru, 2001; Pessenda et al., 2001). Between ~8050 and ~5200 cal yr BP, our data from coastal plain of the

Doce River indicate a predominance of muddy sediments supply and that C_4 plants are present, with greater influence from C_3 plants and estuarine water. During the middle to late Holocene, an increase in the contribution of sandy sediments and terrestrial organic matter occurred with C_4 plants influence (chapters IV and V), probably associated with a RSL fall, resulting in a retraction of mangroves and expansion of herbaceous vegetation, trees and shrubs.

During the late Holocene, there was a decrease in the extent of mangrove vegetation in Marajó Island and in the coastal plain of the Doce River, mainly caused by increase of freshwater discharge and sandy sediment supply associated to RSL fall, respectively. Mangrove environments are now isolated in areas with some marine influence and suitable mud sediment supply. Regarding the coastal plain of the Doce River, the data indicate that the input of freshwater organic matter and terrigenous material during the late Holocene was higher than the early and middle Holocene. This transition from marine to freshwater influence, likely is due to the combined action of RSL fall and sedimentary supply during the late Holocene. Furthermore, tectonic activities may have caused RSL changes in both studied sectors with a potential impact on mangrove distribution (Rossetti et al., 2007; Miranda et al., 2009; Rossetti et al., 2012).

Conclusions

The delta plain of the Doce River presents a stratigraphic sequence with development of a deltaic system to estuarine and to continental terraces produced by the interplay of relative sea-level changes and sediment river discharge. The regressive deposits reveal highstand systems tracts and forced/normal regressive systems tracts in cycles developed according to the rate of relative sea-level changes combined with local sediment supply.

Therefore, the equilibrium between the relative sea-level and fluvial sediment supply allowed the development of a deltaic system in response mainly to sea-level fall during at least ~47,500 and ~29,400 cal yr B.P (chapter IV). After the post-glacial sea-level rise, an estuarine complex was developed with wide tidal mud flats occupied by mangroves during the early and middle Holocene both in the mouth of the Amazon (chapter II and III) and Doce River (chapter V).

Considering the Holocene vegetation history of northern Brazil, the data from Marajó Island indicate a tidal mud flat colonized by mangroves with influence of estuarine organic matter between at least ~7500 and ~3200 cal yr BP (chapter III). This is likely due to the relatively higher marine influence and dryer conditions during this period. During the late

Holocene, there was a decrease in the extent of mangrove vegetation in Marajó Island and in the coastal plain of the Doce River, mainly caused by increase of freshwater discharge and sandy sediment supply associated to RSL fall, respectively. Mangrove environments are now isolated in areas with some marine influence and suitable mud sediment supply. Regarding the southeastern Brazil, the data indicate that the input of freshwater organic matter and terrigenous material during the late Holocene was higher than the early and middle Holocene. This transition from marine to freshwater influence, likely is due to the combined action of RSL fall and sedimentary supply during the late Holocene. In the Marajó Island, during the late Holocene, there was a return to more continental conditions, heavily influenced by freshwater with mangroves isolated to a small area (100-700 m width) in the northeastern part of the island (chapter III).

Over the last century, the increase in flow energy evidenced by upward mud/sand transitions also contributes to mangrove retraction in the Marajó Island (see chapter II). This is mainly due to landward sand migration, which covers the mudflat and asphyxiates the mangrove. The increase in flow energy and exposure to tidal influence may have been driven by the RSL rise, either associated with global fluctuations or tectonic subsidence, and/or by the increase in river water discharge. These processes can modify the size of the area occupied by mangroves (chapter II).

CHAPTER II:

THE LAST MANGROVES OF MARAJÓ ISLAND – EASTERN AMAZON: IMPACT OF CLIMATE AND/OR RELATIVE SEA-LEVEL CHANGES

Abstract

   The dynamics, over the last 7,500 years, of a mangrove at Marajó Island in northern Brazil were studied by pollen and sedimentary facies analyses using sediment cores. This island, located at the mouth of the Amazon River, is influenced by riverine inflow combined with tidal fluctuations of the equatorial Atlantic Ocean. Herbaceous vegetation intermingled with rainforest dominates the central area of the island, while *várzea* is the main vegetation type along the littoral. In particular, the modern northeastern coastal zone is covered by a mosaic of dense rainforest, herbaceous vegetation, mangroves, *várzea* , and *restinga*. The integration of pollen data and facies descriptions indicates a tidal mud flat colonized by mangroves in the interior of Marajó Island between ~ 7,500 cal yr BP and ~ 3,200 cal yr BP. During the late Holocene, mangroves retracted to a small area (100-700 m in width) along the northeastern coastal plain. Mangrove expansion during the early and mid Holocene was likely caused by the post-glacial sea-level rise which, combined with tectonic subsidence, led to a rise in tidal water salinity. Salinity must have further increased due to low river discharge resulting from increased aridity during the early and mid Holocene. The shrinking of the area covered by mangrove vegetation during the late Holocene was likely caused by the increase in river discharge during the late Holocene, which has maintained relatively low tidal water salinity in Marajó Island. Tidal water salinity is relatively higher in the northeastern part of the island than in others, due to the southeast-northwest trending current along the littoral. The mixing of marine and riverine freshwater inflows has provided a refuge for mangroves in this area. The increase in flow energy during the last century is related to landward sand migration, which explains the current retraction of mangroves. These changes may indicate an increased exposure to tidal influence driven by the relative sea-level rise, either associated with global fluctuations or tectonic subsidence, and/or by an increase in river water discharge.

Keywords: Amazon coast; climate; Holocene; palynology; sea level; vegetation

Introduction

Mangroves are highly susceptible to climatic changes and sea-level oscillations (e.g., Fromard et al., 2004; Versteegh et al., 2004; Alongi, 2008; Berger et al., 2008). They have been almost continuously exposed to disturbance as a result of fluctuations in sea-level over the last 11,000 years (Gornitz, 1991; Blasco et al., 1996; Sun and Li, 1999; Behling et al., 2001; Lamb et al., 2006; Alongi, 2008; Berger et al., 2008; Cohen et al., 2008; Gilman et al., 2008). During the Holocene, the post-glacial sea-level rise and changes in river water discharge have been considered the main driving forces behind the expansion/contraction of mangroves in northern Brazil (Cohen et al., 2008; Lara and Cohen, 2009; Guimarães et al., 2010; Smith et al., 2012). However, important changes in coastal morphology have been recorded in this region as a result of tectonic reactivations, which could have modified the relative sea-level (RSL), with a potential impact on mangrove distribution (Rossetti et al., 2007; Miranda et al., 2009; Rossetti et al., 2012).

An empirical model based on an ecohydrological approach, which allows the integration of hydrographical, topographical and physicochemical information with vegetation characteristics of mangroves and marshes, indicates that changes in pore water salinity affect vegetation boundaries (Cohen and Lara, 2003; Lara and Cohen, 2006). In addition to studies in northern Brazil, the relationship between mangrove distribution and sediment geochemistry has been widely studied in other coastal regions (Hesse, 1961; Baltzer, 1970; Walsh, 1974; Baltzer, 1975; Snedaker, 1982; Lacerda et al., 1995; McKee, 1995; Pezeshki et al., 1997; Clark et al., 1998; Youssef and Saenger, 1999; Matthijs et al., 1999; Alongi et al., 1998, 1999, 2000).

Generally, mangroves are distributed parallel to the coast with some species dominating areas more exposed to the sea, and others occurring landward at higher elevations (Snedaker, 1982). This zonation is a response of mangrove species mainly to tidal inundation frequency, nutrient availability, and porewater salinity in the intertidal zone (Hutchings and Saenger, 1987).

Mangroves of the littoral of northern Brazil follow well-known patterns (Behling et al., 2001; Cohen et al., 2005a), where salinity results in the exclusion of freshwater species (Snedaker, 1978) and leads to characteristic patterns of species zonation and predictable types of community structure (Menezes et al., 2003). Mangroves are more tolerant to soil salinity than is *várzea* forest (Gonçalves-Alvim et al., 2001) and sediment salinity is mostly controlled by flooding frequency (Cohen and Lara, 2003) and estuarine gradients (Lara and Cohen, 2006).

Changes in mangrove distribution may also reflect changes in variables that control coastal geomorphology (e.g. Blasco et al., 1996; Fromard et al., 2004; Lara and Cohen, 2009). The development of mangroves is regulated by continent-ocean interactions and their expansion is determined by the topography relative to sea-level (Gornitz, 1991; Cohen and Lara, 2003) and flow energy (Chapman, 1976; Woodroffe, 1989), where mangroves preferentially occupy mud surfaces. Thus, a relative rise in sea-level may result in mangroves migrating inland due to changes in flow energy and tidal inundation frequency. Similarly, vegetation on elevated mudflats is subject to boundary adjustments, since mangroves can migrate to higher locations and invade these areas (Cohen and Lara, 2003).

The potential of each variable to influence mangrove establishment will depend on the environmental characteristics of the given littoral. Climate and hydrology are the main factors controlling the modern distribution of geobotanical units along the coast of the Amazon (Cohen et al., 2008, 2009). According to these authors, mangroves and saltmarshes dominate the marine-influenced littoral when tidal water salinity lies between 30 and 7‰ to the southeastern coastline, and *várzea* and herbaceous vegetation dominate freshwater-influenced coasts with tidal water salinity below 7‰ in the northwest. The littoral of Marajó Island, at the mouth of the Amazon River, is part of the fluvial sector (Figure 1a) (Cohen et al., 2008; Smith et al., 2011, 2012).

The mangroves of Marajó Island are currently restricted to a relatively narrow section of the northeastern area of the island (Cohen et al., 2008; Smith et al., 2012). This mangrove has developed continuously since at least 2,700 cal yr BP (Behling et al., 2004). According to pollen records from hinterland (Lake Arari), the area covered by mangrove vegetation was wider between ~7,250 and ~2,300 cal yr BP (Smith et al., 2011).

The purpose of this work was to study the environmental history of the northeastern part of Marajó Island, and discuss the processes that caused the contraction of the mangrove during the Holocene. We focus on vegetation development, the location of boundaries between mangrove and dry herbaceous vegetation, and areas where changes in sensitive vegetation related to RSL and tidal water salinities can be expected. This approach is based on the integration of pollen and facies analyses of five sediment cores, collected at distinct locations presently covered by mangrove, *várzea* and herbaceous vegetation.

Study area

The study site is located on the island of Marajó in northern Brazil, which covers approximately 39,000 km^2 (Cohen et al., 2008). The island is located at the mouth of the

Amazon River (Figure 1). Sediment cores were taken on the coastal plain of the town of Soure and from a lake surrounded by a herbaceous plain, and cores were denominated R-1, R-2, R-3, R-4 and R-5 (Table 1).

The study area covers the central-eastern part of the coastal plain. Its topographical range is less than 5 m and it extends inland to the maximum of the intertidal zone, which borders the coastal plateau (França and Sousa Filho, 2006).
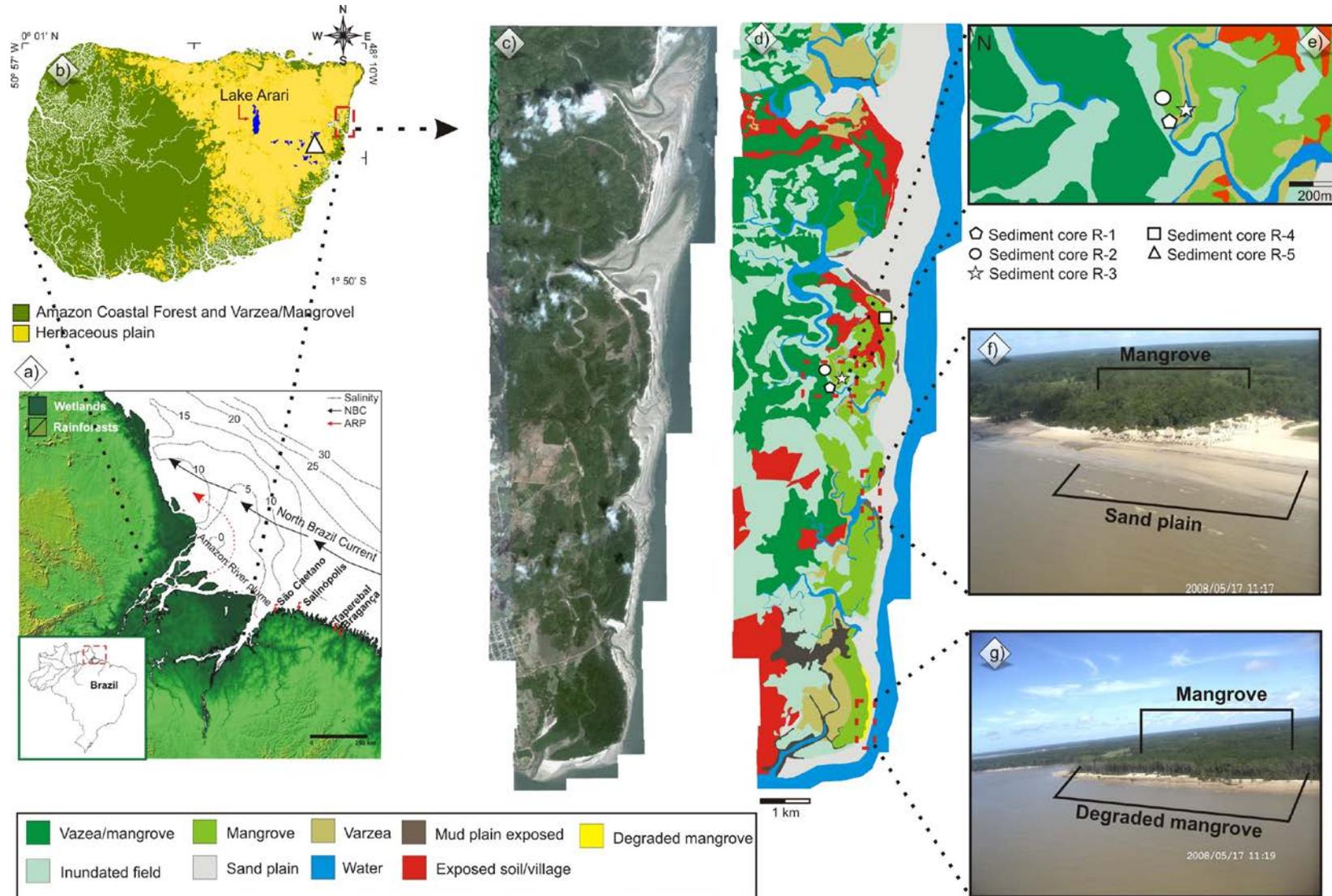
Figure 1 – Location of the study area: a) Sea water salinity, Amazon River plume and North Brazil Current (Santos et al., 2008), b) Marajó Island; c) Soure coastal plain; d) vegetation units; e) sampling site on Soure coastal plain; f) mangrove and sand plain; g) degraded mangrove.

Table 1 – Study site, vegetation types, sampling method and geographic coordinates in the coastal plain of Soure– eastern Marajó Island.

Cody site	Unit vegetation and main taxa	Sampling method	Coordinates
R-1	Mangrove/varzea transition – characterised by *Rhizophora mangle* and others taxa: Arecaceae (*Euterpe oleracea*; *Mauritia flexuosa*); Araceae (*Montrichardia arborescens*); Aizoaceae (*Sesuvium*); Acanthaceae (*Avicennia germinans*); Cyperaceae; Heliconiaceae; Musaceae; Myrtaceae (*Psidium guajava*); Poaceae (Olyra); Pteridaceae (*Acrostichum auereum*)	Russian Sampler	S 00º40'26.3 / W 048º29'37.2"
R-2	Mangrove – characterised by *Rhizophora mangle*	Russian Sampler	S 00º40'23.1 / W 048º29'38.8"
R-3	Herbaceous and restinga vegetation – characterised by Arecaceae (*Euterpe oleracea*; *Mauritia flexuosa*); Birzonimia; Cyperaceae; Poaceae (Olyra); Malpiguiaceae	Russian Sampler	S 00º40'25.2" / W 48º29'35.7"
R-4	Mangrove – characterised by *Rhizophora mangle*	Vibracorer	S 00º39'37" / W 048º29'3.3"
R-5	Herbaceous flat – characterised by Convovulaceae; Rubiaceae; Cyperaceae and Poaceae	Vibracorer	S 00º55'41" / W 048º39'47"

Geological and geomorphological setting

The coastal plain of Soure is located on the Pará platform of northern Brazil. It pertains to a large area of crystalline and Palaeozoic sedimentary basement that remained tectonically stable relative to adjacent Cretaceous and Cenozoic sedimentary basins (Rossetti et al., 2008). The coastal plateau of northern Brazil is formed by the Barreiras Formation. These deposits occur from northern to southeastern Brazil and are of Miocene age (Arai, 1997).

Except for a narrow belt where the Barreiras Formation occurs, the eastern portion of the island is characterized by lowlands with altitudes averaging 4-6 m above the modern sea-level (Rossetti et al., 2007, 2008) and is dominated by Holocene sedimentation (Behling et al., 2004), which is topographically slightly lower than the western side (Behling et al., 2004; Rossetti et al., 2007; Lara and Cohen, 2009). Along the eastern portion, the Barreiras Formation is represented by sandstones and mudstones followed by post-Barreiras deposits (Rossetti et al., 2008).

Marajó Island has a river system consisting of numerous small, straight and meandering channels and ponds that are either permanent or ephemeral (Bemerguy, 1981). The flat surface of the eastern part of the island has been deeply incised by a drainage system during the Pleistocene and Holocene.

Present climate and vegetation

The region is characterized by a warm and humid tropical climate with annual precipitation averaging 2,300 mm (Lima et al., 2005). The rainy season extends between December and May, with average temperatures ranging between 25 and 29ºC. The region is dominated by a regime of meso- and macrotides (tidal range of 2 to 4 m and 4 to 6 m, respectively) with variation during the spring tide between 3.6 and 4.7 m (DHN, 2003).

In contrast to most regions of Amazonia, where dense forest dominates, northeastern Marajó Island is covered with open vegetation. *Restinga* vegetation is represented by shrubs and herbs (e.g., *Anacardium*, *Byrsonima*, *Annona*, *Acacia*) that occur on sand plains and dunes near the shoreline. Mangrove is represented by *Rhizophora* and *Avicennia* (tree heights reaching ~20 m). The herbaceous plain consists of naturally open areas dominated by Cyperaceae and Poaceae that widely colonize the eastern side of Marajó Island. *Várzea* (swamp seasonally and permanently inundated by freshwater, featuring wetland trees such as *Euterpe oleracea* and *Hevea guianensis*) and Amazon coastal forest (ACF) (composed of terrestrial trees such as *Cedrela odorata*, *Hymenaea courbaril* and *Manilkara huberi*) occur on the western side (Cohen et al., 2008). Narrow and elongated belts of dense ombrophilous forest are also present along riverbanks (Rossetti et al., 2008). Detailed information on the most characteristic taxa of each vegetation unit is found in Smith et al. (2011).

Materials and methods

Field work and sample processing

LANDSAT images acquired in 2010 were obtained from INPE (National Space Research Institute, Brazil). A three-color band composition (RGB 543) image was created and processed using the SPRING 3.6.03 system to discriminate geobotanical units (Cohen and Lara, 2003). Aerial photography, visual observation, photographic documentation, and GPS measurements were used to determine typical plant species and characterize the main vegetation units.

Three sediment cores (R-1, R-2 and R-3) were collected during the summer season (Nov. 2008), using a Russian sampler (Cohen, 2003), and two other cores were taken with a

vibracorer using aluminum tubes (R-4 and R-5). Cores were taken from an area occupied by different vegetation units: mangroves (R4 and R2), *várzea* (R-1), mangrove and herbaceous vegetation (R-3), and a lacustrine herbaceous plain (R-5) (Table 1).

The cores were submitted to X-ray to identify sedimentary structures. Samples were collected for grain size analysis at the Chemical Oceanography Laboratory of the Federal University of Pará (UFPA). This analysis made use of a laser particle size analyzer (SHIMADZU SALD 2101), and graphics were obtained using the Sysgran Program (Camargo, 1999). Grain size distribution followed Wentworth (1922), with separation of sand (2 - 0.0625 mm), silt (62.5-3.9 µm) and clay (3.9-0.12 µm) fractions. Facies analysis included descriptions of color (Munsell Color, 2009), lithology, texture and structure (Harper, 1984; Walker, 1992). The sedimentary facies were codified according to Miall (1978).

Pollen and spore analyses

For pollen analysis, 1 cm^3 samples were taken at 2.5 cm intervals along sediment cores R-1, R-2 and R-3 (each 150 cm deep). From sediment cores R-4 and R-5, 24 and 36 samples were collected, respectively. Prior to processing, one tablet of exotic *Lycopodium* spores was added to each sediment sample to allow the calculation of pollen concentration (grains cm^{-3}) and pollen influx rates (grains cm^{-2} yr^{-1}). All samples were prepared using standard analytical techniques for pollen including acetolysis (Faegri and Iversen, 1989). Sample residues were placed in Eppendorf microtubes and kept in a glycerol gelatin medium.

Reference morphological descriptions (Roubik and Moreno, 1991; Behling, 1993; Herrera and Urrego, 1996) were consulted for identification of pollen grains and spores. A minimum of 300 pollen grains were counted in each sample. The pollen sum excludes fern spores, algae and micro-foraminifers. Pollen and spore data are presented in diagrams as percentages of the pollen sum. Taxa were grouped into mangrove, herbaceous plain elements, *restinga*, palms, and Amazon coastal forest. Software packages TILIA and TILIAGRAF were used to calculate and plot pollen diagrams. The pollen diagrams were statistically subdivided into zones of pollen and spore assemblages using a square-root transformation of the percentage data, followed by stratigraphically constrained cluster analysis (Grimm, 1987).

Radiocarbon dating

Based on stratigraphic discontinuities suggesting changes in the tidal inundation regime, fourteen bulk samples (10 g each) were selected. In order to avoid natural contamination (e.g. Goh, 2006), the sediment samples were checked and physically cleaned

under the microscope. The organic matter was submitted to chemical treatment to remove any younger organic fractions (fulvic and/ or humic acids) and carbonates. This treatment consisted of extracting residual material with 2% HCl at 60°C during 4 h, washing with distilled water until neutral pH, followed by drying at 50 ºC. A detailed description of the chemical treatment for sediment samples can be found in Pessenda et al. (1991, 1996).

A chronological framework for the sedimentary sequence was provided by conventional and accelerator mass spectrometer (AMS) radiocarbon dating. Samples were analyzed at the University of Georgia's Center for Applied Isotope Studies (UGAMS). Radiocarbon ages are reported as ^{14}C yr (1σ) BP normalized to a δ^{13}C of -25‰ VPDB and calibrated years as cal yr (2σ) BP using CALIB 6.0 (Stuvier et al., 1998; Reimer et al., 2004, 2009). In the text we use the median of the range for our and other authors' data.

Results

Radiocarbon dates and sedimentation rates

Radiocarbon dates for cores R-1 to R-5 are shown in Table 2. Sedimentation rates are between 0.1 and 10 mm yr^{-1} (Figures 2 and 3). Although the rates are non linear between the dated points, they are within the vertical accretion range of 0.1 to 10 mm yr^{-1} of mangrove forests as reported by other authors (e.g. Bird, 1980; Spenceley, 1982; Cahoon and Lynch, 1997; Behling et al., 2004; Cohen et al., 2005a, 2008, 2009; Vedel et al., 2006; Guimarães et al., 2010).

Table 2 – Sediment samples selected for Radiocarbon dating and results (R-1, R-2, R-3, R-4 and R-5).

Cody site	Laboratory number	Depth (cm)	Radiocarbon ages (yr BP)	CALIB age - 2σ (cal yr BP)	Median of age range (cal yr BP)	$\delta^{13}C$ (‰)
R-1	UGAMS4924	147-150	540 ± 25	560-520	540	-27,8
R-2	UGAMS4925	147-150	1260 ± 30	1160-1120	1140	-28,2
R-3	UGAMS4927	107-110	40 ± 25	70-30	50	-28,5
R-3	UGAMS4926	147-150	690 ± 25	680-640	660	-28,8
R-4	UGAMS4931	2-4	Modern	-	-	-29,3
R-4	UGAMS5316	44-46	Modern	-	-	-27,7
R-4	UGAMS5317	65-69	620 ± 25	620-560	590	-27,5
R-4	UGAMS4932	190-192	1530 ± 30	1520-1460	1490	-26,1
R-4	UGAMS5318	209-211	1510 ± 25	1420-1340	1380	-26,4
R-4	UGAMS4933	218-220	1760 ± 30	1740-1570	1655	-26,6
R-5	UGAMS4928	22-24	1920 ± 30	1950-1820	1885	-25,3
R-5	UGAMS8209	78-83	5730 ± 30	6640-6580	6610	-30,2
R-5	UGAMS4929	142-146	5840 ± 30	6740-6600	6670	-27,0
R-5	UGAMS5319	158-160	6750 ± 30	7670-7580	7625	-26,5
R-5	UGAMS8207	185-194	6150 ± 30	7160-6960	7060	-29,1
R-5	UGAMS8208	234-240	5860 ± 30	6780-6770	6775	-29,3
R-5	UGAMS4930	248-251	6600 ± 30	7530-7440	7485	-27,1
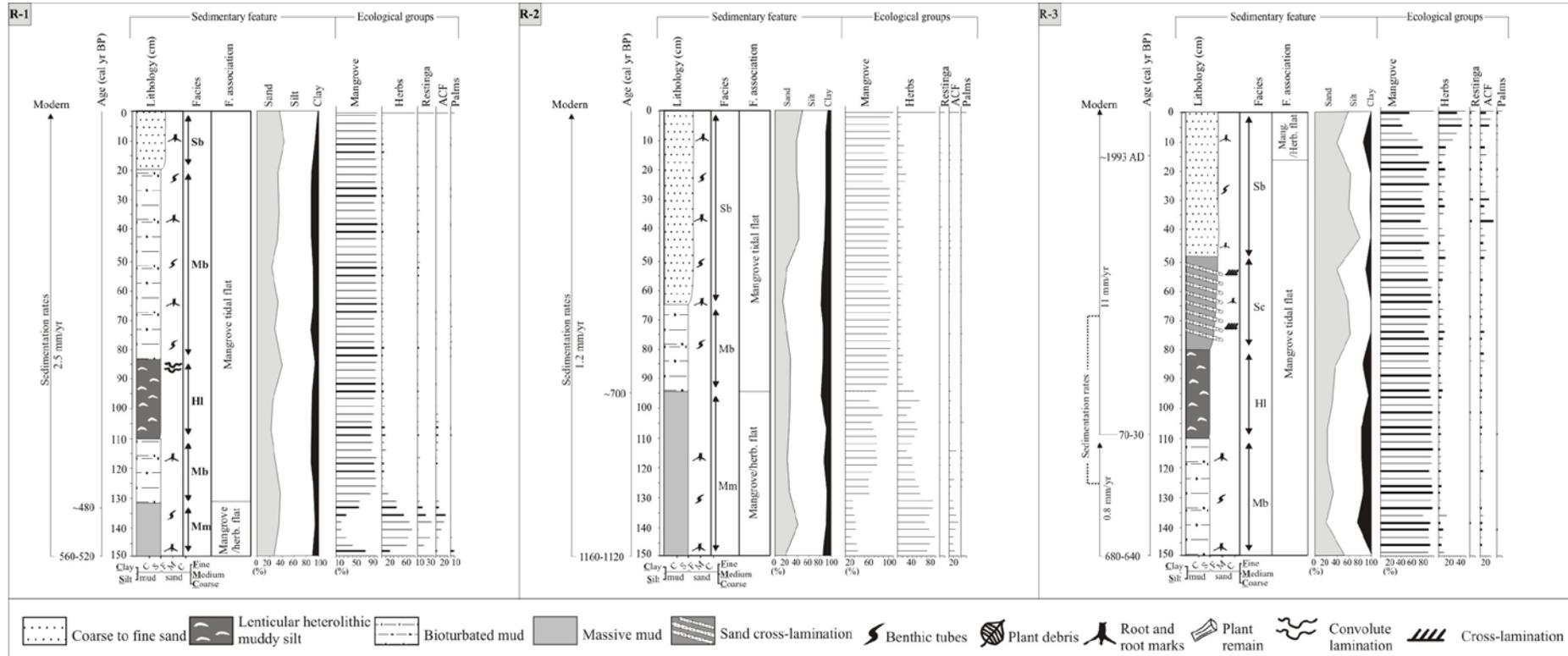
Figure 2 – Sediment profile with sedimentary features and ecological groups from cores R-1, R-2 and R-3.
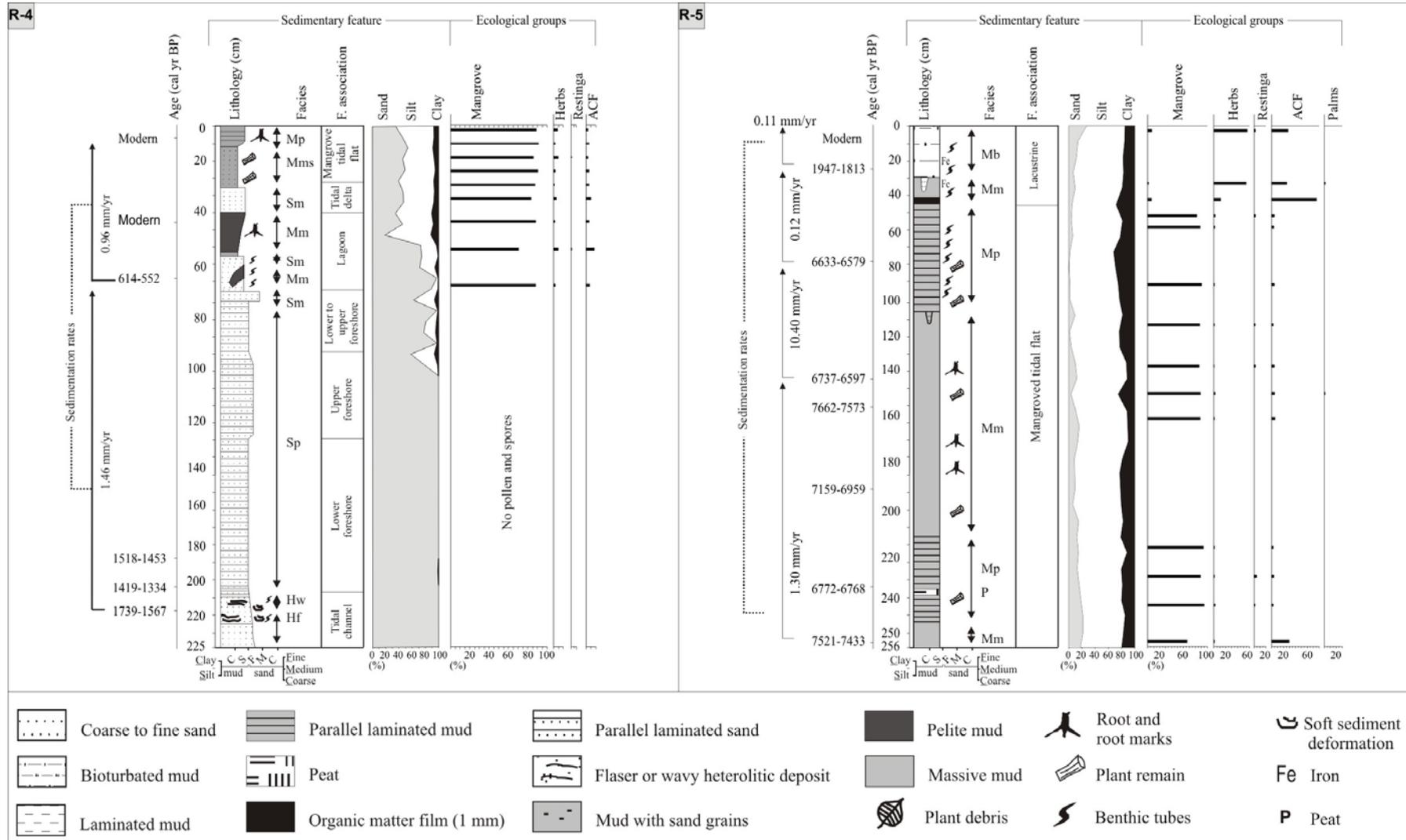
Figure 3 – Sediment profile with sedimentary feature and ecological groups from cores R-4 and R-5.

Facies description and pollen association

       The cores present dark gray and light brown muddy and sandy silt with an upward increase in grain size. These deposits are massive, parallel laminated or heterolithic-bedded. The texture and description of sedimentary structures allowed the identification of eleven sedimentary facies (Table 3).

Table 3 – Lithofacies description of cores R-1, R-2, R-3, R-4 and R-5, from the Soure coastal plain, eastern margin Marajó Island.

Facies	Description	Sedimentary process
Bioturbated mud (Mb)	Brownish black and brown mud with many roots and root marks, dwelling structure and diffuse fine sand following the root traces and benthic tubes.	Diffused mixture of sediments and alternating colors by intense bioturbation and diagenic process, repectively.
Lenticular heterolitic (Hl)	Dark brown mud with single and connected flat lenses of bright brown, rippled fine to very fine sand.	Low energy flows with mud deposition from suspension, but with periodic sand inflows through migration of isolated ripples.
Cross laminated sand (Sc)	Brownish gray, well sorted, fine to medium sand with current ripple cross-lamination.	Migration of small ripples formed during low energy, either unidirectional or combined (unidirectional and oscillatory) flows.
Bioturbated sand (Sb)	Pale olive silty sand with light gray mottles, many roots, roots traces in growth position and dwelling structures.	Sediment homogenization and mottling by biological activity and diagenic process, repectively.
Parallel laminated mud (Mp)	Plastic, gray to black mud with parallel lamination and muds with thin, continuous streaks of gray to olive, silty to very fine grained sand.	Deposition of mud from suspension under very low flow energy.
Massive mud (Mm)	Plastic, massive mud, gray to dark gray and green, with many roots and root marks	The absence of structures in muddy indicates low flow energy during the sediment accumulation.

Mud/sand grains (Mms)	Gray and greenish gray, mud deposits with fine grained sand.	The absence of structures suggests the transported material by traction during the sediment deposition. This structure and the relative grain size increase may be produced by suspension or sedimentary dispersion through pulse of adjacent environmental and flow energy (tidal).
Massive sand (Sm)	Ligth yellow, moderately sorted, fine-grained massive sand. Mud intraclasts are either diperse or locally form conglomeratic lags.	The massive nature of these deposits might have been produced during drilling. Therefore, the most likely is that these deposits were, at least in great part stratified.
Parallel-laminated sand (Sp)	Fine-to-medium grained sand with parallel lamination or stratification. Local association with mud drape.	High (upper plane bed) energy flows. Parallel laminated sands with mud interbedding are related to low energy flows, before the stage of ripple development.
Heterolithic deposits wavy (Hw)	Greenish gray, mud layers interbedded with fine-to-medium-grained sand forming *wavy* structures.	Equal periods of mud and sand deposition from suspension and bed-load transport, respectively.
Flaser heterolithic deposit (Hf)	Gray mud layers interbedded with fine-to-medium-grained sand forming *flaser* structures.	Fluctuating low and relatively higher flow energies, with a balance between mud deposition from suspensions and sand deposition either from suspension or migrating ripples.

A cluster analysis of pollen assemblages allowed the definition of pollen zones for each sediment core. The pollen diagrams show pollen types (Figures 4, 5, 6, 7 and 8) and the proportions represented by the different ecological groups (Figures 2 and 3). Pollen concentration and pollen influx values ranged from 5,000 to 100,000 grains cm^{-3} and from 100 to 8,000 grains cm^{-2} yr^{-1}, respectively.

The sediment and pollen analyses allowed the identification of five facies associations, described below.
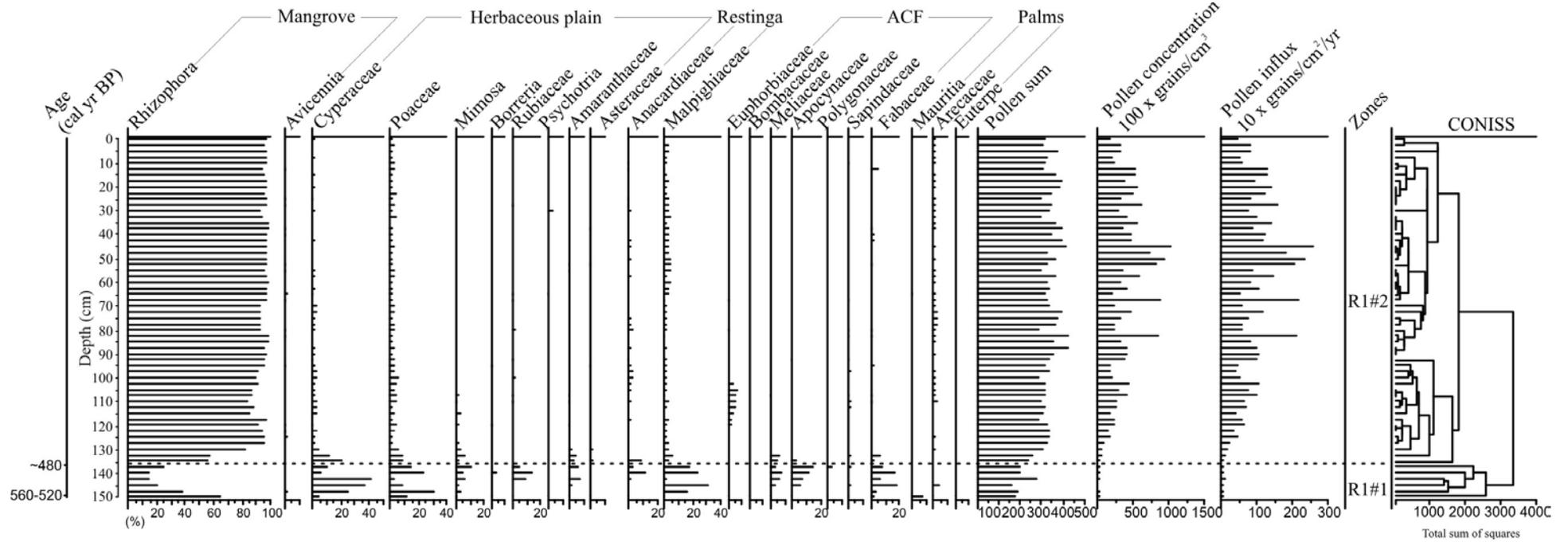
Figure 4 – Pollen record from core R-1 with percentages of the most frequent pollen taxa and sample age.
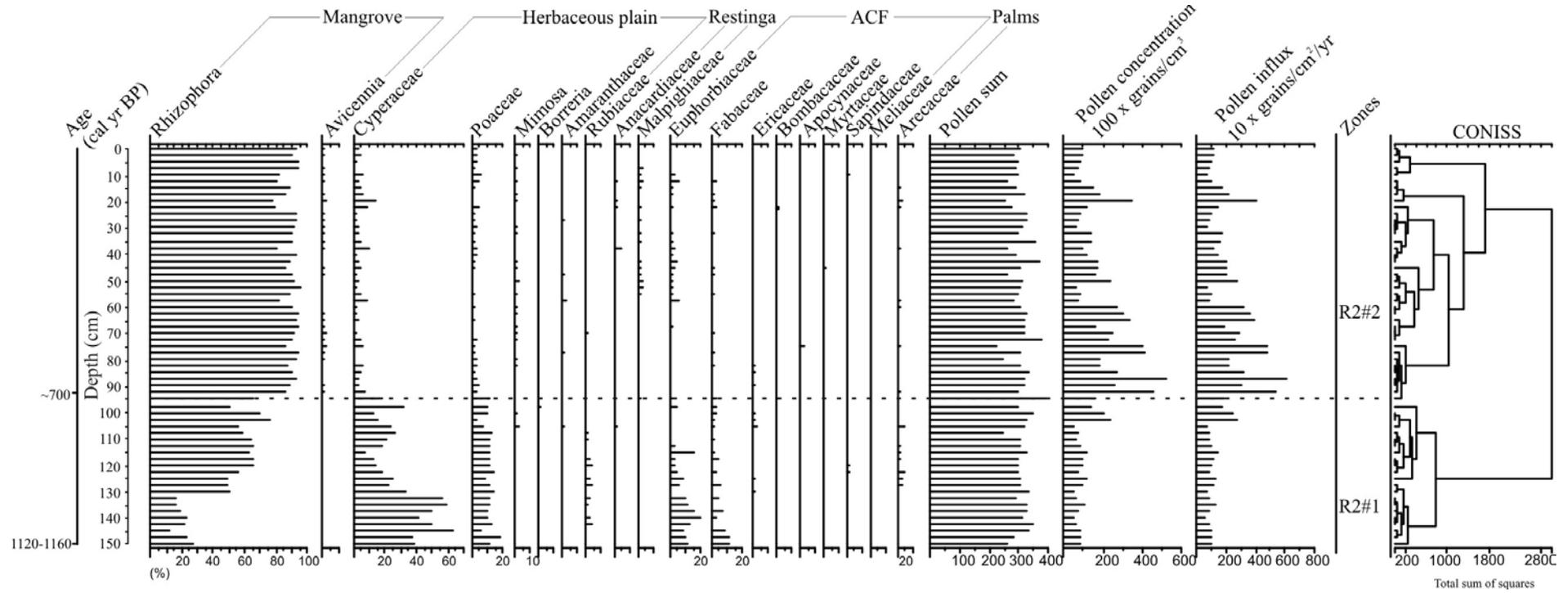
Figure 5 – Pollen record from core R-2 with percentages of the most frequent pollen taxa and sample age.
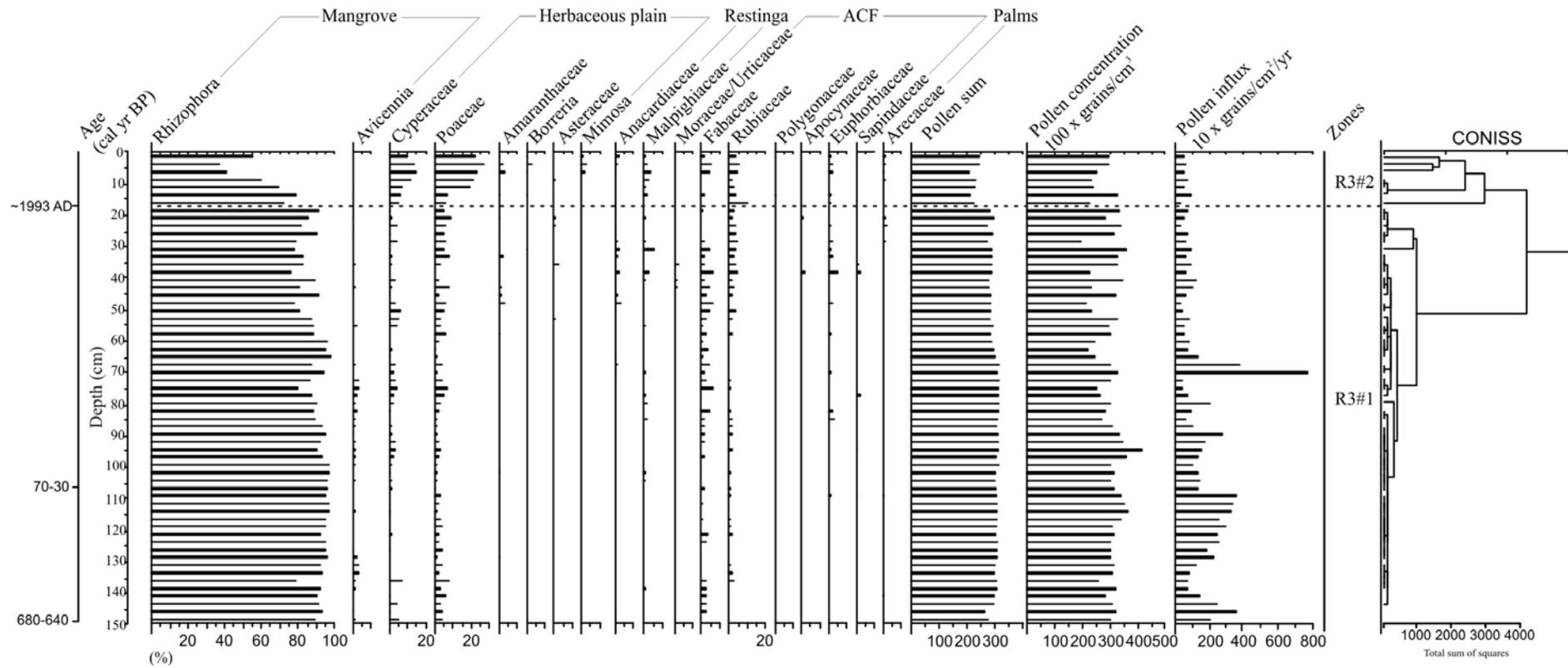
Figure 6 – Pollen record from core R-3 with percentages of the most frequent pollen taxa and sample age.
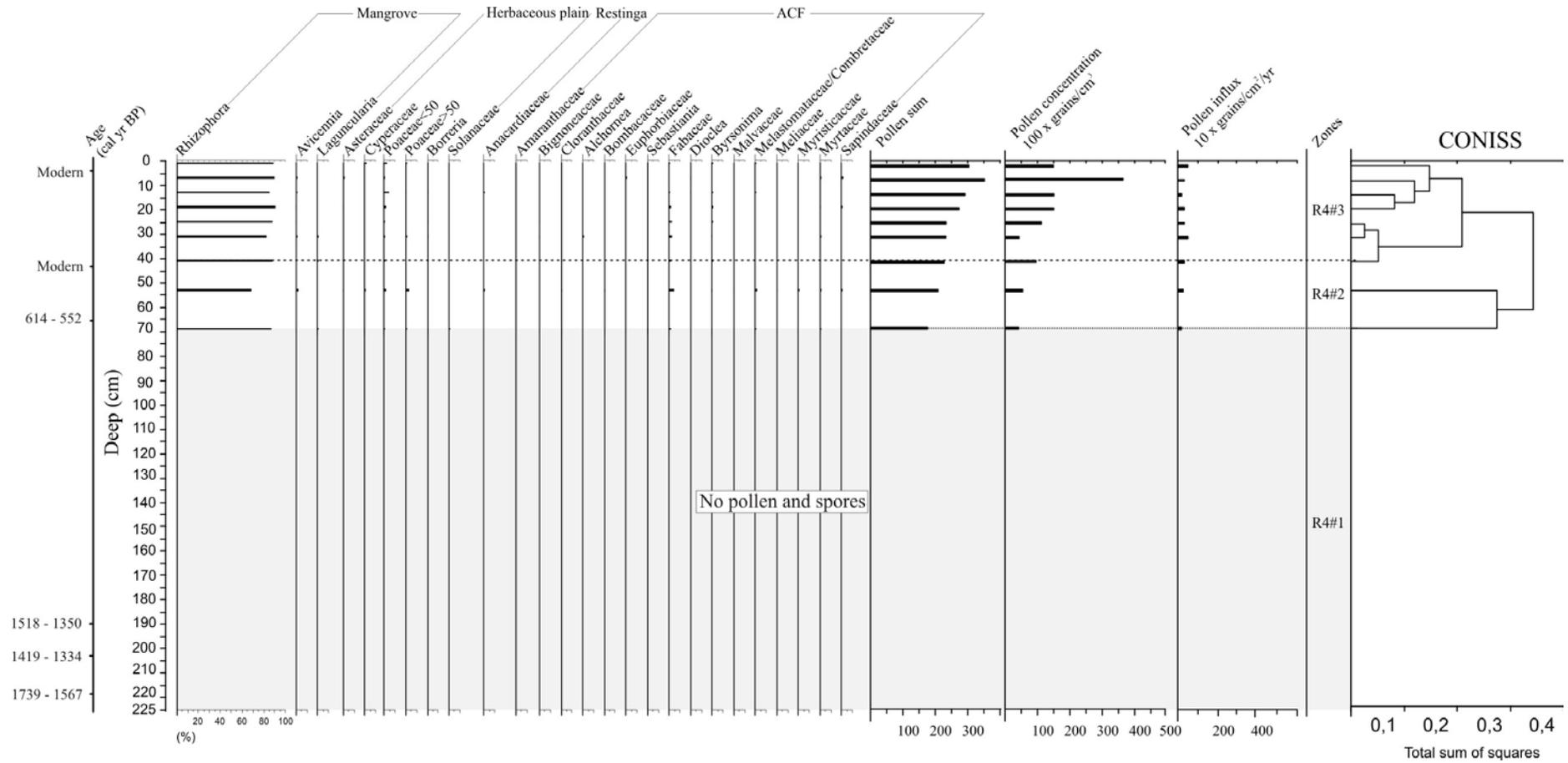
Figure 7 – Pollen record from core R-4 with percentages of the most frequent pollen taxa and sample age.
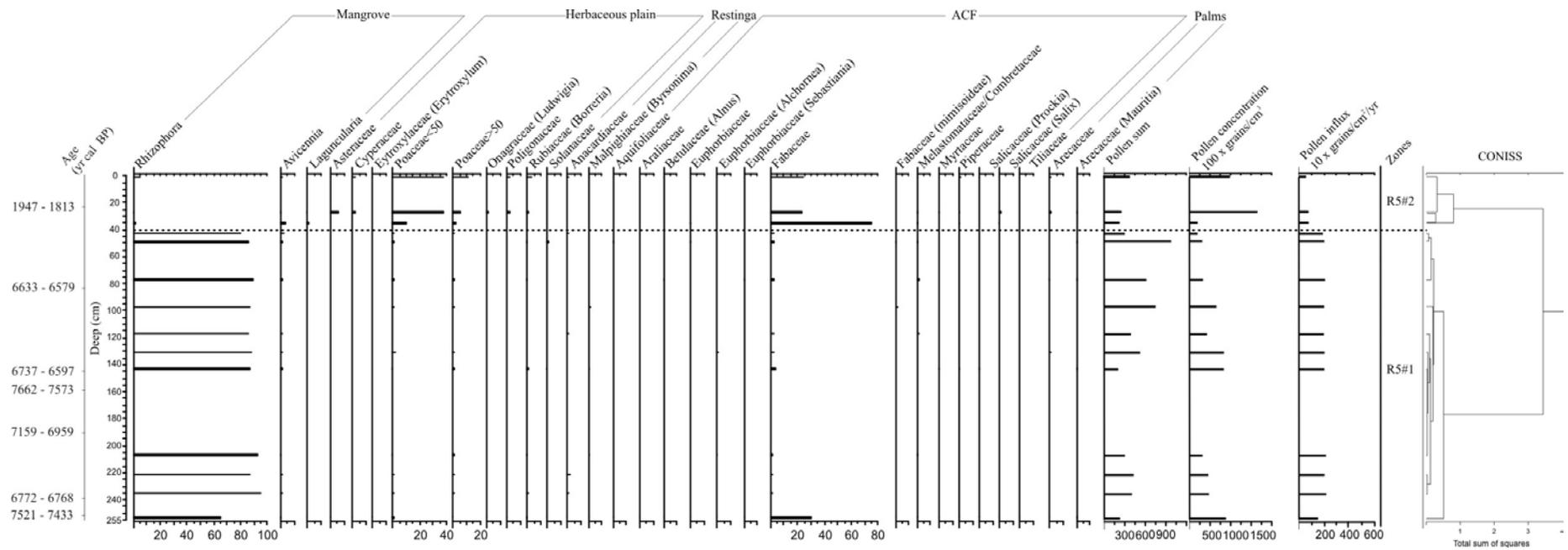
Figure 8 – Pollen record from core R-5 with percentages of the most frequent pollen taxa and sample age.

Mangrove/herbaceous flat facies association

The mangrove/herbaceous flat occurs along the interval 150-135, 150-95 and 15-0 cm in R-1, R-2 and R-3, respectively (Figure 2).This unit consists mostly of massive mud (facies Mm) with plant debris, and bioturbated coarse- to fine-grained sand (facies Sb).

The pollen assemblages of this association correspond to zone R1#1 (Figure 4), R2#1 (Figure 5) and R3#2 (Figure 6). Zone R1#1 (560-520 cal yr BP until ~ 480 cal yr BP) is characterized by pollen of *Rhizophora* (15-65%), Cyperaceae (5-40%), Poaceae (2-30%), Fabaceae (2-20%), Mimosaceae (2-10%), Borreria (~5%), Rubiaceae (5-15%) and Amaranthaceae (2-7%).

Zone R2#1 (1,160-1,120 cal yr BP until ~700 cal yr BP) is characterized by pollen of *Rhizophora* (10-75%), Cyperaceae (10-70%), Poaceae (5-20%), Fabaceae (2-10%) and Rubiaceae (1-5%). The presence of pollen from the Amazon coastal forest can be observed in this zone, represented by Euphorbiaceae (5-20%). Zone R3#2 (1993 AD until present) is characterized mainly by a decrease in *Rhizophora* (35-80%) and increase in Poaceae (10-25%) and Cyperaceae (5-15%) pollen.

Mangrove flat facies association

Cores R-1 and R-2 show the mangrove tidal flat along the intervals 135-0 and 95-0 cm, while this association occurs at depth interval 150-15 cm in R-3, 40-0 cm in R-4, and between 255 and 15 cm in R-5 (Figures 2 and 3). The deposit consists of mud with flat lenses of rippled sand (facies Hl). Bioturbated mud (facies Mb), bioturbated sand (facies Sb), massive sand (Sm) and cross laminated fine-grained sand (facies Sc) are also present in this association. In addition, core R-1 displays mud with convolute lamination, which may contain roots, root channels and dwelling structures produced by benthic fauna.

The pollen assemblages of this association correspond to zone R1#2 (~480 cal yr BP – modern, Figure 4), zone R2#2 (~700 cal yr BP – modern, Figure 5) and to zone R3#1 (~660 cal yr BP – ~1993 AD, Figure 6) in its entirety. This association also occurs in zone R4#3 (~600 cal yr BP – modern, Figure 7), and zone R5#1 (~7,500 cal yr BP – ~3,200 cal yr BP, Figure 8) and is characterized by the predominance of mangrove pollen, mainly represented by *Rhizophora* (40-95%). Pollen of herbaceous plain vegetation of the Cyperaceae, Poaceae, Fabaceae, Mimosaceae, *Borreria*, Rubiaceae, Amaranthaceae and Asteraceae occur at very low percentages (<30%).

Lagoon facies association

This association is mainly represented by massive mud (facies Mm) and massive sand (facies Sm), with mangrove pollen along zone R4#2 (70-40 cm). These deposits contain root and root marks, benthic tubes, mud and very fine silt to medium sand. The presence of mangrove is marked by *Rhizophora* (65-90%) and *Avicennia* (5%) pollen.

Foreshore facies association

This association occurs in core R-4 (225-70 cm), about > 1,650 to 580 cal yr B.P., corresponding to zone R4#1. It consists of parallel-laminated, fine- to medium-grained sand (facies Sp). Roots, root marks and benthic tubes are present locally. Bedding is marked by heavy minerals and/or clay films (Figure 3). The base is characterized by very fine- to medium-grained sand, and either heterolithic wavy deposits (facies Hw) and flaser heterolithic deposits (Hf). In addition, plants debris and oxidized iron blades are present. These deposits did not contain pollen grains.

Lake facies association

This association occurs only in core R-5 (R5#2), between 55 and 0 cm (Figures 3 and 8). It is characterized by massive mud (facies Mm) and bioturbated mud (Mb). Benthic tubes, oxidized iron concretions, plant debris and root marks were present. These deposits are marked by greater amounts of pollen which is characteristics of ACF (3-75%), herbs (2-55%), aquatic vegetation (0-10%) and ferns (1-5%), and accompanied by a decrease in mangrove pollen (85-0%).

Discussion

Pollen signal and vegetation changes in Marajó Island during the Holocene (central and eastern coastal zone)

There often exists two pollen components in sediment—pollen from ''local'' vegetation, and background pollen from ''regional'' vegetation (Janssen, 1966, 1973; Andersen, 1967, 1970; Sugita, 1994). Pollen records of lacustrine sediment cores include pollen sourced from vegetation surrounding the lake, considering that winds blow from various directions. Thus, the proportion of the pollen signal provided by each vegetation type is distance-weighted (e.g. Davis, 2000). Some empirical studies have reported pollen transport in rivers (e.g. Brush and Brush, 1972; Solomon et al., 1982). Flume experiments suggest that pollen grains will settle out into sediment when water velocity is lower than 0.3 m s^{-1}, and therefore grains can remain in suspension and be transported long distances

when water velocity is greater than 0.3 m s^{-1} (Brush and Brush, 1972). According to Xu et al. (2012), the pollen found in lakes originates from three components: an aerial component mainly carried by wind, a fluvial catchment component transported by rivers and a third waterborne component transported by surface wash. Overall, vegetational composition within the "aerial catchment" differs from that of the hydrological catchment.

Influx rates of modern pollen from the Bragança Peninsula, located 150 km east of the study area, indicate that *Rhizophora* is a very prolific pollen producer within mangroves, while *Avicennia* and *Laguncularia* produce lesser amounts. Pollen influx rates of *Rhizophora* and *Avicennia* in the *Rhizophora/Avicennia* dominated forest area are approximately 14,500 and 450 grains cm^{-2} yr^{-1}, respectively. Pollen traps in the herbaceous plain site, which are located at least 1 – 2 km away from the nearest *Rhizophora* trees and 100 m away from the nearest *Avicennia*, document an average of 410 *Rhizophora* grains cm^{-2} yr^{-1} and an average of 8 *Avicennia* grains cm^{-2} yr^{-1}. This indicates that a certain amount of *Rhizophora* pollen grains can be transported by wind, while wind transportation of *Avicennia* pollen is very low (Behling et al., 2001).

Core R-5, sampled from a lake and currently dominated by herbaceous vegetation (Figure 1), indicates change in vegetation patterns. This change likely extends at least to the drainage basin area and is expected to be reflected in pollen records of the lacustrine sediments. Pollen contributions from different vegetation type in the surrounding landscape are also expected to decrease with increasing distance from the lake. For this reason the pollen record of core R-5, at least between depths of 0 and 55 cm, is likely more representative of vegetation dynamics of eastern Marajó Island than those records from cores R-1, R-2, R-3 and R-4, collected from tidal flats.

The results obtained from pollen and sedimentological analyses suggest vegetation changes during the last seven thousand years. The sedimentary deposits consisting of mud/sand alternations formed under oscillating flow energy contain three pollen groups. Vegetation shifts most likely occurred under the influence of fluctuating flow velocity asymmetry in tidal flats. Data suggest a tidal mud flat colonized by mangroves in the central region of the island between ~7,500 cal yr BP and ~3,200 cal yr BP, as recorded in core R-5 (Figures 3 and 8), and other cores from Lake Arari on Marajó Island during the early and mid Holocene (Smith et al., 2011, 2012).

During the late Holocene in the hinterland of Marajó Island, mangroves were largely replaced by herbaceous vegetation. Mangroves occurred on tidal flats on the northeastern

coast of the island (i.e, core R-2) at least since ~1,150 cal yr BP, and continued to be recorded in cores R-1, R-4 and R-3 at 540, 580 and 660 cal yr BP, respectively.

The migration of mangroves recorded in core R-4 (Figure 7) may be a natural response to coast progradation, following stabilization and mud accumulation. Progradation could have also affected other areas of the Marajó coastline, where *várzea* became established instead of mangrove (Cohen et al., 2008 and Smith et al., 2011).

Therefore, mangrove vegetation at the mouth of the Amazon River retreated to a narrow area of northeastern Marajo Island. An increment in river discharge near Marajó Island during the late Holocene constitutes a hypothesis for this isolation (Guimarães et al., 2012; Smith et al., 2012). This process could be responsible for the modern decrease in tidal water salinity along the littoral (0–6 ‰, Santos et al., 2008). It is noteworthy that tidal water salinity is greater in this northeastern area than elsewhere on the island, and this is related to the southeast-northwest trending current along the littoral. This current displaces brackish waters from the marine influenced littoral (Figure 1a).

Greater tidal water salinity during the early and mid Holocene could be attributed to the episode of Atlantic sea-level rise recorded in other parts of South America (e.g., Suguio et al., 1985; Tomazelli, 1990; Rull et al.,1999; Hesp et al., 2007; Angulo et al., 2008). This event could have also produced a marine incursion along the Pará littoral, where the RSL stabilized at its current level between 7,000 and 5,000 yr BP (e.g. Cohen et al., 2005a; Vedel et al., 2006). A transgressive phase occurred on Marajó Island in the early to mid-late Holocene. Subsequently, there was a return to the more continental conditions that prevail today in the study area (Rossetti et al., 2008). This history of RSL fluctuations on Marajó Island seems to have been affected by tectonic activity during the Late Pleistocene and Holocene (Rossetti et al., 2008; Rossetti, et al., 2012). Hence, transgression was favored during increased subsidence, when space was created to accommodate new sediments.

Tectonic stability seems to have prevailed during the mid to late Holocene, leading to coastal progradation that culminated with more continental conditions prevailing on the island.

The post-glacial sea-level rise, likely combined with tectonic subsidence, may have increased tidal water salinity. Salinity might have further increased due to low river discharge resulting from increased aridity during the early and mid Holocene. If river systems are considered to be integrators of rainfall over large areas (Amarasekera et al., 1997), variations in the discharge of the Amazon River during the Holocene may be a consequence of changes in rainfall rates, as recorded in many different regions of the Amazon Basin (e.g. Bush and

Colinvaux, 1988; Absy et al., 1991; Sifeddine et al., 1994; Desjardins et al., 1996; Gouveia et al., 1997; Pessenda et al., 1998a,b, 2001; Behling and Hooghiemstra, 2000; Freitas et al., 2001; Sifeddine et al. 2001; Weng et al., 2002; Bush et al., 2007; Guimarães et al., 2012).

Mangrove dynamics during the last decades in the eastern coastal zone of Marajó Island

Mangroves preferentially occupy mudflats. Mangrove retreat along the coastline may be caused by landward sand migration, which covers the mudflat and asphyxiates the vegetation (Cohen and Lara, 2003). During the last one hundred years, the increase inflow energy on mangroves (Furukawa and Wolanski, 1996) evidenced at Marajó Island by the upward mud into sand (Figures 1f and 1g) may also contribute to mangrove retraction, as recorded in the upper section of core R-3 (Figure 6).

The disappearance of mangrove vegetation along the Marajó coastline has been mostly caused by erosion and landward sand migration above mangrove mud sediments (Figure 1g). At present, this region is exposed to wave action and tidal currents in Marajó Bay, which apparently have caused the retreat of the coastline, and consequently a reduction in the area covered by mangrove vegetation.

 This process is also evidenced along the Pará littoral. The marine influenced littoral in the central area of peninsulas also shows a transition between herbaceous vegetation and mangrove forest, with mangrove migration toward the topographically highest herbaceous areas most likely in response to the modern RSL rise (Cohen and Lara 2003; Cohen et al., 2009).

Greater exposure to tidal influence may have been driven by RSL rise and/or by greater river water discharge. As previously mentioned, the RSL rise in this area may be related to tectonics and it may reduce areas favorable for mangrove development (Blasco et al. 1996) leading to the migration of this ecosystem to topographically more elevated terrains (Cohen and Lara, 2003, Cohen et al., 2005a).

Climate fluctuations (Molodkov and Bolikhovskaya, 2002) which impacted rainfall (e.g. Absy et al., 1991; Pessenda et al., 1998a,b, 2001, 2004; Behling and Costa, 2000; Freitas, et al., 2001; Maslin and Bruns, 2000) could also have caused changes in river flow and estuarine salinity gradients (Lara and Cohen, 2006). This can also affect the RSL (Mörner, 1996, 1999).

The area covered by herbaceous vegetation, located in topographically higher areas, suffered a reduction during the last decades (Cohen and Lara, 2003) and centuries (Cohen et al., 2005a,b). This indicates an increase in the RSL, which has caused erosion and deposition

of sand over mud deposits. This trend was also observed on the Taperebal (12 km north of Bragança) (Vedel et al., 2006). The effects of RSL rise were also observed in cores taken from São Caetano de Odivelas and Salinópolis (Cohen et al., 2009) in the northeastern coast of Pará, in the eastern Amazon region.

Conclusions

The integration of pollen data and facies descriptions of five sediment cores indicates a tidal mud flat colonized by mangroves in the interior of Marajó Island between ~7,500 cal yr BP and ~3,200 cal yr BP. During the late Holocene, mangroves became isolated and grew on a small area (100-700 m width) of the northeastern part of the island. This likely results from lower tidal water salinity caused by a wet period that resulted in greater river discharge during the late Holocene. The northeastern area of the island exhibits relatively greater tidal water salinity, due to the southeast-northwest trending littoral current which brings brackish waters from more marine influenced areas. It has provided a refuge for the mangroves of Marajó Island.

Over the last century, the increase in flow energy evidenced by upward mud/sand transitions also contributes to mangrove retraction, as recorded in the upper part of core R-3. This is mainly due to landward sand migration, which covers the mudflat and asphyxiates the mangrove. The increase in flow energy and exposure to tidal influence may have been driven by the RSL rise, either associated with global fluctuations or tectonic subsidence, and/or by the increase in river water discharge. These processes can modify the size of the area occupied by mangroves.

As demonstrated by this work, using a combination of proxies is efficient for palaeoenvironmental reconstruction, where mangrove retraction during the late Holocene shows the high degree of sensitivity of this ecosystem to the sequence of environmental variables discussed here.

CHAPTER III:

AN INTER-PROXY APPROACH TO ASSESSING THE DEVELOPMENT OF THE AMAZONIAN MANGROVE, DURING THE HOLOCENE

Abstract

The mangrove dynamic on Marajó Island at the mouth of the Amazon River during the past ~7500 cal yr BP was studied using multiple proxies, including sedimentary facies, pollen, $\delta^{13}C$, $\delta^{15}N$ and C/N ratio, temporally synchronized with fifteen sediment samples to ^{14}C dating. The results allowed to propose a palaeogeographical development with changes in vegetation, hydrology and organic matter dynamics. Today, the island's interior is occupied by *várzea*/herbaceous vegetation (freshwater vegetation), but during the early-middle Holocene mangroves with accumulation of estuarine organic matter had colonized the tidal mud flats. This was caused by post-glacial sea-level rise, which combined with tectonic subsidence, produced a marine transgression. It is likely that the relatively higher marine influence at the studied area was favored by reduced Amazon River discharge, caused by a dry period occurred during the early and middle Holocene. During the late Holocene, there was a reduction of mangrove vegetation and the contribution of freshwater organic matter to the area was higher than early and middle Holocene. This suggests a decrease in marine influence during the late Holocene that led to a gradual migration of mangroves from the central region to the northeastern littoral zone of island, and, consequently, its isolation since at least ~1150 cal yr BP. This is probably a result from lower tidal water salinity caused by a wet period that resulted in greater river discharge during the late Holocene. This work details chronologically and spatially the contraction of mangrove forest from northeastern Marajó Island under the influence of Amazon climatic changes that allows to propose a model with successive phases of sediment accumulation and vegetation change according to marine-freshwater influence gradient. As demonstrated by this work, using a combination of proxies is efficient for establish a relationship between the changes in estuarine salinity gradient and depositional environment/vegetation.

Keywords: Amazon coastal area; Holocene; isotopes; sea-level; vegetation; climate change

Introduction

Mangrove distributions are considered indicators of coastal changes (Blasco et al., 1996) and have fluctuated throughout geological and human history. The area covered by mangrove is influenced by complex interactions involving gradients of tidal flooding frequency, nutrient availability and soil salt concentration across the intertidal area (Hutchings and Saenger, 1987; Wolanski et al., 1990). The geomorphic setting of mangrove systems also comprises a range of inter-related factors such as substrate types, coastal processes, sediment, and freshwater delivery. All of these factors influence the occurrence and survivorship of mangroves (Semeniuk, 1994).

Investigations along the littoral zone of the Brazilian Amazon using sedimentological, palynological and isotope data have revealed evidence of expansion/contraction of mangroves during the Holocene (Cohen et al., 2008; Lara and Cohen, 2009; Cohen et al., 2009; Guimarães et al., 2010, 2012; Smith et al., 2011, 2012). Those mangrove variations have been attributed to the combination of post-glacial sea-level rise (Suguio et al., 1985; Tomazelli, 1990; Angulo and Suguio, 1995; Martin et al., 1996; Angulo and Lessa, 1997; Angulo et al., 1999; Rull et al., 1999; Hesp et al., 2007; Angulo et al., 2008), tectonic subsidence (Miranda et al., 2009; Castro et al., 2010; Rossetti et al., 2012) and changes in the Amazon River discharge as consequence of variations in rainfall (e.g. Bush and Colinvaux, 1988; Absy et al., 1991; Sifeddine et al., 1994; Desjardins et al., 1996; Gouveia et al., 1997; Pessenda et al., 1998a, 2001; Behling and Hooghiemstra, 2000; Freitas et al., 2001; Sifeddine et al. 2001; Weng et al., 2002; Bush et al., 2007).

The mangroves of northern Brazil began to develop along their current position during the early and middle-Holocene (Behling et al., 2001; Behling and Costa, 2001; Cohen et al., 2005a, Vedel et al., 2006), due to the stabilization of relative sea-level (RSL) after the post-glacial sea-level rise that invaded the embayed coast and broad valleys (Cohen et al., 2005a; Souza-Filho et al., 2006). Currently, the coastal zone influenced by the Amazon River (fluvial sector – northwestern coastline) is occupied by *várzea*/herbaceous vegetation (freshwater vegetation). However, pollen data indicate that marine influence and mangrove vegetation (brackish water vegetation) were more expressive than they are today on Marajó Island (Smith et al., 2011, 2012; França et al., 2012), as well as on Macapá coast (Guimarães et al., 2012) between >8800 and ~2300 cal yr BP and >5500 and ~5200 cal yr BP, respectively.

During the late Holocene, it is likely that the replacement of brackish/marine water by freshwater vegetation at the mouth of Amazon River was caused by a wetter climate,

which generated a river discharge increase (Bush and Colinvaux, 1988; Absy et al., 1991; Desjardins et al., 1996; Pessenda et al., 1998a,b; Freitas et al., 2001). A higher river discharger has maintained low tidal water salinity surrounding of Marajó Island (0–6 ‰, Santos et al., 2008), while the marine influenced littoral zone presents a relatively higher tidal water salinity than the sector near the Amazon River (Figure 1a, Cohen et al., 2012).

Previously, Smith et al. (2011) and França et al. (2012) indicated a mangrove contraction in the Marajó Island during the Holocene. The main objective of this investigation is to establish a relationship between the changes in estuarine salinity gradient from Amazon River and the mangrove dynamics of Marajó Island-Northern Brazil. Then, this work presents the integration of $\delta^{13}C$, $\delta^{15}N$, total organic carbon (TOC), C/N ratio, facies analysis and pollen data, synchronized chronologically with fifteen radiocarbon dated (^{14}C) samples. For this purpose, material extracted from five cores, with depth between 150 and 256 cm, was collected from the eastern coast of Marajó Island.
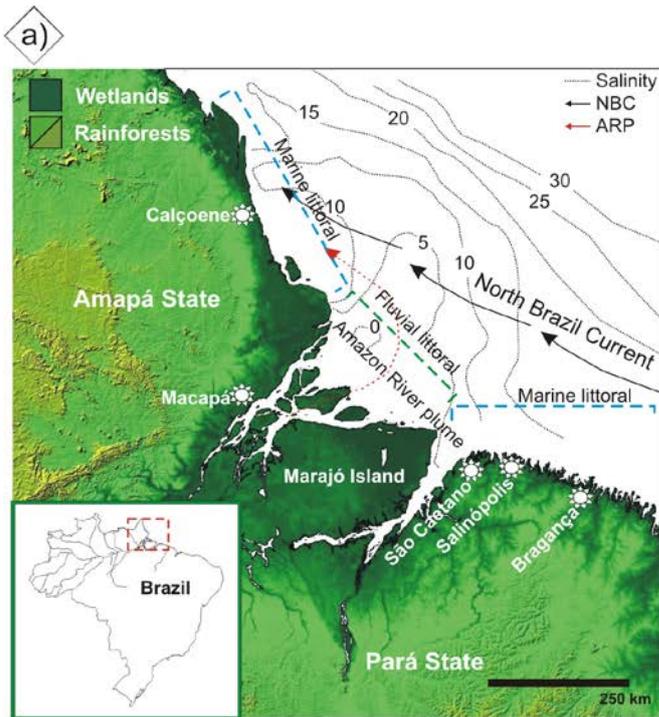
Figure 1 – Location of the study area: a) Sea water salinity, Amazon River plume and North Brazil Current (Santos et al., 2008); b) Marajó Island, which covers approximately 40,000 km², c) Sampling in the mangrove; d) Sampling in the Lake São Luis; e) Mangrove and sand plain; f) Mangrove.

Study site

Geological and geomorphological setting

The Marajó Island has an area of about 40,000 km^2. The study sites are located in the central eastern region of this island (0°39'16.96"S/48°40'13.79"W to 0°55'51.35"S/48°28'16.96"W), northern Brazil, on the coastal plain situated at the mouth of the Amazon River (Cohen et al., 2008; Smith et al., 2011, 2012). Geologically, the island is located in the Pará Platform. The eastern margin presents a topographical range of less than 5 m and extends inland to the maximum extent of the tidal influence zone, which limits the coastal plateau (França and Sousa-Filho, 2006). This region has a low relief, averaging only 4-6 m above modern sea-level (Rossetti et al., 2007, 2008, 2012), and is dominated by Holocene sedimentation, which is slightly depressed relative to the western side (Behling et al., 2004; Rossetti et al., 2007; Lara and Cohen, 2009). Along the eastern portion, the Barreiras Formation is represented by sandstones and mudstones followed by post-Barreiras deposits, that thicken toward the west in the sub-surface (Rossetti et al., 2008).

Regional climate and oceanographic characteristics

The climate is warm and humid tropical with an annual precipitation averaging 2300 mm (Lima et al., 2005). The seasonality of regional precipitation is influenced by several factors, including the migration of the Inter Tropical Convergence Zone (ITCZ), due to changing Atlantic sea surface temperatures (SST), moist trade winds from the tropical Atlantic, evapotranspiration from the forest itself, and the coupled onset and intensity of Amazon convection (Marengo et al., 1993, 2001; Nobre and Shukla, 1996; Fu et al., 2001; Liebmann and Marengo, 2001). The rainy season occurs between the months of December and May and a drier period between June and November. Average temperatures range between 25° and 29° C. The region is dominated by a regime of semidiurnal meso- and macrotides (tidal range of 2 to 4 m and 4 to 6 m, respectively) with variations during the spring tide, between 3.6 and 4.7 m (DHN, 2003). The mean Amazon River discharge is about 170,000 m^3 s^{-1} (at Óbidos city), with maximum and minimum outflow of 270,000 and 60,000 m^3 s^{-1} (ANA, 2003). Consequently, the river discharge and hydrodynamic conditions allow a strong reduction of water salinity along the Amazon River and its adjacent coast (Figure 1a) (Vinzon et al., 2008; Rosario et al., 2009). Furthermore the structure of the Amazon River plume is controlled by the North Brazilian Current, which induces a northwestern flow with speeds of 40–80 cm/s over the continental shelf (Lentz, 1995).

Modern vegetation

The modern vegetation consists of natural open areas dominated by Cyperaceae and Poaceae (herbaceous flats), which occur mainly in the eastern side of Marajó Island. The *várzea* vegetation (swamp seasonally and permanently inundated by freshwater) is composed by wetlands trees such as *Euterpe oleraceae* and *Hevea guianensis,* while the "terra firme" vegetation, represented by the Amazon Coastal Forest (ACF) unit, is characterized by *Cedrela odorata*, *Hymenaea courbaril* and *Manilkara huberi* (Behling et at., 2004; Cohen et al., 2008; Smith et al., 2011, 2012). The *várzea* and ACF dominate the western side of Marajó Island (Figure 1a). Narrow and elongated belts of dense ombrophilous forest are also present along riverbanks (Rossetti et al., 2008). The restinga (shrub and herb vegetation that occurs on sand plains and on dunes close to the shore line) is dominated by Anacardiaceae and Malpighiaceae. The mangroves are colonized by *Rhizophora*, *Avicennia* and *Laguncularia* (Cohen et al., 2008).

The mangrove on the studied island, occurs within specific topographic zones (see Cohen and Lara, 2003; Cohen et al., 2005a, 2005b, 2008, 2009) depending on physical (sediment type, e.g., Duke et al., 1997) and chemical (Hutching and Saenger, 1987; Wolanski et al., 1990) characteristics, and are currently present in small areas in the northeastern coast with 100-700 m width. The mangrove of our study area are classified as *Rhizophora*-dominated "fringe forests" reaching 20 m in height, with a presence of *Avicennia* at highest elevations above mean spring tide level, inundation frequency.

Materials and methods

Analysis of sedimentary facies, pollen, $\delta^{13}C$, $\delta^{15}N$, TOC and C/N ratio were conducted following the results of radiocarbon dating (^{14}C), to assess the development of the Amazonian mangrove and organic matter source. The sediment cores (R-1; R-2 and R-3) were collected during the summer season (November 2008), using Russian sampling equipment (Cohen, 2003) and two others (R-4 and R-5) with a vibracorer (Martin et al., 1995) using an aluminum tube.

Sampling

Five specific sites were selected for shallow coring that represent different morphological aspects and vegetations at Marajó Island (Figure 1b). The sediment cores were sampled from an area colonized by mangroves mainly characterized by *Rhizophora mangle* (R-4, S0º39'37"/W48º29'3" and R-2, S0º40'23"/W48º29'38") and mixture *várzea/*mangrove

(R-1, S0º40'26"/W48º29'37") characterized by *Rhizophora mangle* and others taxa such as Arecaceae (*Euterpe oleracea*; *Mauritia flexuosa*); Araceae (*Montrichardia arborescens*); Aizoaceae (*Sesuvium*); Acanthaceae (*Avicennia germinans*); Cyperaceae; Heliconiaceae; Musaceae; Myrtaceae (*Psidium guajava*); Poaceae (Olyra); Pteridaceae (*Acrostichum auereum*).

The core R-3 (S0º40'25"/W48º29'35") was taken from an area occupied by herbaceous and restinga vegetation characterized by Arecaceae (*Euterpe oleracea*; *Mauritia flexuosa*); Birzonimia; Cyperaceae; Poaceae (*Olyra*); Malpiguiaceae, while the R-5 (S0º55'41"/W48º39'47", 15 km from shoreline) was sampled from an area colonized only by herbaceous vegetation mainly represented by Convovulaceae; Rubiaceae; Cyperaceae and Poaceae.

Facies analysis

For analysis of sedimentary facies, the cores were submitted to X-ray to identify sedimentary structures. The sediment grain size was obtained by laser diffraction using a Laser Particle Size SHIMADZU SALD 2101 in the Laboratory of Chemical Oceanography/UFPA. Approximately 0.5 g of each sample was submitted to H_2O_2 to remove the organic matter, and residual sediments were disaggregated by ultrasound before the determination of grain size (França, 2010). The sediment grain size distribution followed the methods of Wentworth (1922), with sand (2-0.0625 mm), silt (62.5-3.9 µm) and clay fraction (3.9-0.12 µm). The graphics were elaborated using the Sysgran Program (Camargo, 1999). Following the methods of Harper (1984) and Walker (1992). Facies analysis included description of color (Munsell Color, 2009), lithology, texture and structure. The sedimentary facies were codified following Miall (1978).

Pollen analysis

For pollen analysis, 1 cm^3 samples were taken at 2.5 cm intervals along sediment cores R-1, R-2 and R-3 (183 samples), in order to observe a high resolution to vegetation changes. From sediment cores R-4 and R-5, 24 and 36 samples were collected, respectively. Prior to processing, one tablet of exotic *Lycopodium* spores (Stockmarr, 1971) was added to each sediment sample to allow the calculation of pollen concentration (grains cm^{-3}) and pollen influx rates (grains cm^{-2} yr^{-1}). All samples were prepared using standard analytical techniques for pollen including acetolysis (Faegri and Iversen, 1989). Sample residues were placed in Eppendorf microtubes and kept in a glycerol gelatin medium. Reference morphological

descriptions (Roubik and Moreno, 1991; Behling, 1993; Herrera and Urrego, 1996; Colinvaux et al., 1999) and pollen collection of the Laboratory of Coastal Dynamics/Federal University of Pará were consulted for identification of pollen grains and spores. A minimum of 300 pollen grains were counted in each sample. The pollen sum excludes fern spores, algae and micro-foraminifers. Pollen and spore data are presented in diagrams as percentages of the pollen sum (França et al., 2012). Taxa were grouped into mangrove, herbaceous plain elements, *Restinga* (coastal forest vegetation), palms, and Amazon coastal forest (ACF). Software packages TILIA and TILIAGRAPH were used to calculate and plot pollen diagrams (Grimm, 1987).

Organic geochemistry

A total of 236 samples (6-50 mg) were collected at 5 cm intervals from the sediment cores in order to associate to vegetation changes and understand also the organic matter source change. Samples of leaves, roots, etc., were separated and treated with 4% HCl to eliminate carbonates, washed with distilled water until the pH reached 6, dried at $50^{\circ}C$ and homogenized. These samples were used for total organic carbon and nitrogen analyses, carried out at the Stable Isotope Laboratory of the Center for Nuclear Energy in Agriculture (CENA/USP). The results are expressed as a percentage of dry weight, with analytical precision of 0.09 and 0.07%, respectively. The ^{13}C and ^{15}N results are expressed as $\delta^{13}C$ and $\delta^{15}N$ with respect to the VPDB standard and atmospheric air, respectively, using the following conventional notations:

$$\delta^{13}C\ (‰)=[(R_{1sample}/R_{2standard})-1] \cdot 1000$$

$$\delta^{15}N\ (‰)=[(R_{3sample}/R_{4standard})-1] \cdot 1000$$

where $R_{1sample}$ and $R_{2standard}$ are the $^{13}C/^{12}C$ ratio of the sample and standard, as well as $R_{3sample}$ and $R_{4standard}$ are the $^{15}N/^{14}N$, respectively. Analytical precision is $\pm0.2‰$ (Pessenda et al., 2004).

Surface sample sediment cores were collected to verify the isotopic composition of modern organic matter to compare different isotopic signature between them. Leaves of the most representative trees of the study area were also sampled for isotopic $\delta^{13}C$ determination to define photosynthetic characteristics of regional vegetation (Table 1). The application of carbon isotopes is based on the ^{13}C composition of C_3 (trees) and C_4 (grasses) plants and its preservation in SOM (sedimentary organic matter). Especially in the Amazon ecosystem with predominance of C_3 plants values, the isotope values tend to increase towards the deeper

layers, around 3 to 4‰, caused by the fractionation during decomposition of organic matter. However, if the ^{13}C enrichment with depth is large, it is a stronger indication that the signal is due to the previous existence of ^{13}C-enriched vegetation, probably C$_4$ grasses. (Martinelli et al., 1996 and 2003).

Table 1 – List of the current vegetation and their δ^{13}C value.

Division or Family	Species	δ^{13}C ‰ (VPDB)	Biological form	Vegetation units
Acanthaceae	*Avicennia germinans*	-30.88	Tree	Mangrove
Aizoaceae	*Sesuvium*	-13.94	Herb	Herbaceous flat
Araceae	*Montrichardia arborescens*	-27.49	Herb	*Várzea*
Convolvulaceae	*Ipomea asarifolia*	-28.90	Herb	Restinga
Cyperaceae I	unidentified	-29.80	Herb	Herbaceous flat
Cyperaceae II	unidentified	-27.44	Herb	Herbaceous flat
Heliconiaceae	unidentified	-29.27	Herb	Herbaceous flat
Melastomataceae I	unidentified	29.45	Herb	Restinga
Melastomataceae II	unidentified	-27.23	Herb	Restinga
Musaceae	unidentified	-34.32	Tree	Amazon coastal forest
Myrtaceae	*Psidium guajava*	-32.72	Tree	Amazon coastal forest
Myrtaceae	unidentified	-31.64	Tree	Amazon coastal forest
Palmaceae	*Astrocaryum aculeatum*	-34.23	Tree	Amazon coastal forest
Poaceae	*Olyra latifolia*	-32.04	Herb	Herbaceous flat
Poaceae I	unidentified	-11.96	Herb	Herbaceous flat
Poaceae II	unidentified	-12.52	Herb	Herbaceous flat
Pteridaceae	*Acrostichum aureum*	-29.30	Fern	*Várzea*
Pteridaceae	*Acrostichum aureum*	-31.86	Fern	*Várzea*
Rhizophoraceae	*Rhizophora mangle*	-33.63	Tree	Mangrove
Rhizophoraceae	*Rhizophora mangle*	-33.54	Tree	Mangrove
Rubiaceae	Borreria sp.	-30.17	Herb	*Várzea*
Rubiaceae	unidentified	-32.53	Herb	*Várzea*

The δ^{13}C values of C$_3$ plants range from approximately −32‰ to −20‰ VPDB, with a mean of −27‰. In contrast, δ^{13}C values of C$_4$ species range from −17‰ to −9‰, with a mean of −13‰.

The organic matter source is environment-dependent with different δ^{13}C, δ^{15}N and C/N compositions (e.g. Lamb et al., 2006) as follows: The C$_3$ terrestrial plants shows δ^{13}C

values between −32‰ and −20‰ and C/N ratio > 20, while C_4 plants have $\delta^{13}C$ values ranging from −17‰ to −9‰ and C/N > 35 (Deines, 1980; Meyers, 1994; Tyson, 1995; Lamb et al., 2006). In C_3-dominated environments, freshwater algae have $\delta^{13}C$ values between −25‰ and −30‰ (Meyers, 1994; Schidlowski et al., 1983) and marine algae between −24‰ to −16‰ (Haines, 1976; Meyers, 1994). In C_4-dominated environments, algae can have $\delta^{13}C$ values ≤16‰ (Chivas et al., 2001). Bacteria have $\delta^{13}C$ values ranging from −12‰ to −27‰ (Coffin et al., 1989). In general, bacteria and algae have C/N values of 4–6 and <10, respectively (Meyers, 1994; Tyson, 1995).

Fluvial $\delta^{13}C_{POC}$ values (POC-particulate organic carbon) result from freshwater phytoplankton and estuarine dissolved organic carbon-DOC (−25‰ to −30‰) and particulate terrestrial organic matter (−25‰ to −33‰). However, marine $\delta^{13}C_{POC}$ ranges from −23‰ to −18‰ (e.g. Barth et al., 1998; Middelburg and Nieuwenhuize, 1998). Peterson et al. (1994) found values from marine $\delta^{13}C_{DOC}$ between −22‰ and −25‰, and freshwater between −26‰ and −32‰. Thornton and McManus (1994) and Meyers (1997) used $\delta^{15}N$ values to differentiate organic matter from aquatic (>10.0‰) and terrestrial plants (~0‰).

The plants of aquatic environments normally use dissolved inorganic nitrogen, which is isotopically enriched in ^{15}N by 7‰ to 10‰ relative to atmospheric N (0‰), thus terrestrial plants that use N_2 derived from the atmosphere have $\delta^{15}N$ values ranging from 0‰ to 2‰ (Thornton and McManus, 1994; Meyers, 2003).

The geochemistry analyses also included a binary diagram between $\delta^{13}C$ and C/N for each sedimentary core in the study area in order to observe information such as the origin of organic matter preserved in this region (Haines, 1976; Deines, 1980; Schidlowski et al., 1983; Meyers, 1994; Peterson et al., 1994; Tyson, 1995; Middelburg and Nieuwenhuize, 1998; Raymond and Bauer, 2001; Lamb et al., 2006).

Radiocarbon dating

Based on stratigraphic discontinuities that suggest changes in the tidal inundation regime, fifteen bulk samples (10 g each) were selected. In order to avoid natural contamination (e.g. Goh, 2006), sedimentary samples were checked and physically cleaned under the stereomicroscope. The organic matter was chemically treated to remove the eventual presence of a younger organic fraction (fulvic and/or humic acids) and carbonates. This process consisted of extracting residual material with 2% HCl at 60 °C for 4 hours, washing with distilled water to neutralize the pH, and drying at 50 ºC. A detailed description of the chemical treatment for sediment samples can be found in Pessenda and Carmargo

(1991) and Pessenda et al. (1996). A chronologic framework for the sedimentary sequence was provided by conventional and accelerator mass spectrometer (AMS) radiocarbon dating. Samples were analyzed at the C-14 Laboratory of CENA/USP and at UGAMS (University of Georgia – Center for Applied Isotope Studies). Radiocarbon ages were normalized to a $\delta^{13}C$ of -25‰ VPDB and reported in stratigraphical profiles as calibrated years (cal yr BP) (2σ) using CALIB 6.0 (Stuvier et al., 1998; Reimer et al., 2004; Reimer et al., 2009). The dates are reported in the text as the median of the range of calibrated ages by us and other authors' data (Table 2), with some estimated by linear extrapolation based on sedimentation rate. The sedimentation rates were based on the ratio between the depth intervals (mm) and the time range.

Table 2 – Material, Depth, $\delta^{13}C$, ^{14}C conventional and calibrated ages (using Calib 6.0; Reimer et al., 2009).

Cody site and laboratory number	Material	Depth (cm)	Radiocarbon ages (yr B.P.)	CALIB age - 2σ (cal yr B.P.)	Median of age range (cal yr B.P.)	$\delta^{13}C$ (‰)
R-1						
UGAMS4924	Bulk sed.	150-147	540 ± 25	560-520	540	-27,8
R-2						
UGAMS4925	Bulk sed.	150-147	1260 ± 30	1160-1120	1150	-28,2
R-3						
UGAMS4927	Bulk sed.	110-107	40 ± 25	70-30	50	-28,5
UGAMS4926	Bulk sed.	150-147	690 ± 25	680-640	660	-28,8
R-4						
UGAMS4931	Bulk sed.	4-2	Modern	-	-	-29,3
UGAMS5316	Bulk sed.	46-44	Modern	-	-	-27,7
UGAMS5317	Bulk sed.	69-65	620 ± 25	620-560	590	-27,5
UGAMS4932	Bulk sed.	192-190	1530 ± 30	1520-1460	1490	-26,1
UGAMS5318	Bulk sed.	211-209	1510 ± 25	1420-1340	1380	-26,4
UGAMS4933	Bulk sed.	220-218	1760 ± 30	1740-1570	1650	-26,6
R-5						
UGAMS4928	Bulk sed.	24-22	1920 ± 30	1950-1820	1880	-25,3
UGAMS8209	Wood	83-78	5730 ± 30	6640-6580	6610	-30,2
UGAMS4929	Bulk sed.	146-142	5840 ± 30	6740-6600	6670	-27,0
UGAMS8208	Bulk sed.	240-234	5860 ± 30	6780-6770	6770	-29,3
UGAMS4930	Bulk sed.	251-248	6600 ± 30	7530-7440	7500	-27,1

Results

Radiocarbon dates and sedimentation rates

Radiocarbon dates for cores R-1 to R-5 are shown in Table 2 (range since ~7500 cal yr BP). Sedimentation rates are between 0.1 and 10 mm yr^{-1}. Although the rates are nonlinear between the dated points, they are within the vertical accretion range of 0.1 to 10 mm yr^{-1} of mangrove forests as reported by other authors (e.g. Bird, 1980; Spenceley, 1982 and Cahoon and Lynch, 1997; Behling et al., 2004; Cohen et al., 2005a, 2008, 2009; Vedel et al., 2006; Guimarães et al., 2010).

δ^{13}C values of modern vegetation

Twenty-two species of the most representative vegetation were collected at the study site. The δ^{13}C values range between -34.23‰ and -27.23‰, and indicate a predominance of C_3 plants (Table 1). The contribution of C_4 to the δ^{13}C signal in the sediment is restricted to the Poaceae (unidentified) with a mean value of -12.24‰, and Aizoaceae (*Sesuvium*) with a value of -13.94‰.

Facies, pollen description and isotope values of the sediment cores

The cores present dark gray and light brown muddy and sandy silt sediments with an upward increase in grain size. These deposits are massive, parallel laminated or heterolithic. The texture analysis and description of sedimentary structures of the materials collected in the tidal flat, together with pollen records, isotopic (δ^{13}C and δ^{15}N), TOC and C/N values, allowed five facies associations to be defined (Table 3).

Table 3 – Summary of facies association, pollen, isotopes and C/N values, with the proposed interpretation of the depositional environments.

Facies association	Facies description	Pollen, isotopic and C/N values	Interpretation
A	Plastic, massive mud with many roots and root marks (facies Mm), with dwelling structures (facies Mb). Fine grained sand (facies Mms) to very fine grained sand (facies Mp), pale olive silty sand with light gray mottles, many roots and roots traces in growth position and dwelling structures (facies Sb), lenticular heterolithic (facies Hl) and fine to medium-grained cross-stratified sand (facies Sc), with continuous streaks of gray to olive.	Pollen= mangrove vegetation $\delta^{13}C$= -29.3 to -26.9‰ $\delta^{15}N$= -0.6 to 5.0‰ C/N= 11.9 to 45.6	Mangrove tidal flat
B	Plastic, massive mud, gray to dark gray and green, with many roots and root marks (facies Mm), with traces in growth position and dwelling structures (facies Sb). These deposits also have sandy-silt sediments.	Pollen= mangrove and herbs vegetation $\delta^{13}C$= -27.8 to -26.4‰ $\delta^{15}N$= 0.0 to 3.9‰ C/N= 11.1 to 36.3	Mangrove/herb. flat
C	Ligth yellow, moderately sorted, fine-grained massive sand. Mud intraclasts are either disperse or locally form conglomeratic lags (facies Sm) and massive mud with many roots and root marks (facies Mm), preceding the facies association C.	Pollen= mangrove vegetation, ACF and herbs vegetation $\delta^{13}C$= -25.8 to -27.6‰ $\delta^{15}N$= 2.2 to 2.4‰ C/N= 23.8 to 24.2	Lagoon
D	Fine-to-medium grained sand with parallel lamination or stratification (facies Sp). Local association with mud drape and mud intraclasts are either disperse or locally form conglomeratic lags (facies Sm). Gray mud layers interbedded with fine-to-medium-grained sand forming *flaser* structures (facies Hf) and *wavy* structures (facies Hw)	Pollen= no pollen $\delta^{13}C$= -27.6 to -25.0‰ $\delta^{15}N$= 2.2 to 2.6‰ C/N= 22.2 to 24.2	Foreshore
E	Massive mud with many roots and root marks (facies Mm) and dwelling structures and diffuse fine sand following the root traces and benthic tubes (facies Mb).	Pollen= ACF, herbs and aquatic vegetation $\delta^{13}C$= -22.7 to -25.5‰ $\delta^{15}N$= 1.7 to 6.0‰ C/N= 18.7 to 24.2	Lake

R-1 core (mangrove/várzea, 150 cm)

This core is marked by facies associations B and A (Table 3). These deposits consist mainly of massive mud with many roots and root marks with dwelling structures (facies Mm and Mb). It contains clay, silt and fine sand with flat lenses of rippled sand (facies Hl). The top layer displays fine to medium-grained sand (facies Sb). The R-1 core presents mud with

convolute lamination (Figure 2, 90-80 cm), produced by localized differential forces acting on a hydroplastic sediment layer, commonly found on mud flats (Collinson et al., 2006).
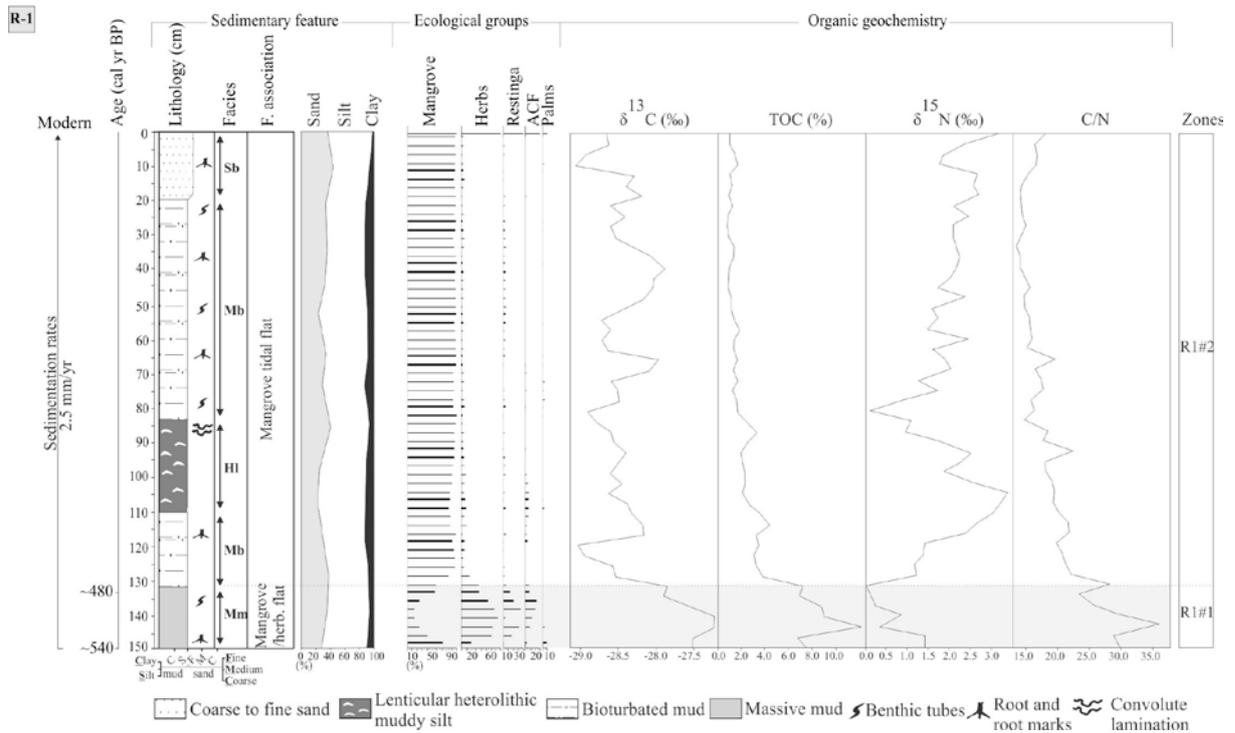
Figure 2 – Summary results for R-1 core: variation as a function of core depth from chronological, lithological profile, pollen analysis and geochemical variables.

The pollen and spore analysis displayed five ecological groups (Figure 2), typically presented on the other profiles. The zone R1#1 (150-135 cm) is characterized by predominance of herbaceous pollen and also by restinga, ACF and the palms group. The mangrove declines slightly. The zone R1#2 (135-0 cm) is marked by a significant increase of mangrove pollen, followed by a decrease of herbaceous pollen, ACF, Restinga and the palms group.

The organic geochemistry results are presented in Figure 2, which indicates that δ^{13}C values are more enriched in the bottom layer (mean $-27‰$) than in the surface layer (around $-29‰$). The δ^{15}N values range from 0.0‰ to +3.3‰ toward the surface, and C/N values are between 36 and 13, displaying high values on the bottom and low values toward the surface. The TOC results show a decreasing trend from bottom to surface, with values between 14% and 1%, respectively.

R-2 core (mangrove, 150 cm)

These deposits consist typically of massive mud (facies Mm), bioturbated mud (facies Mb) and coarse to fine-grained sand (facies Sb), with an increase in sandy sediments at

the surface layers. It also presents many roots and root marks with dwelling structures (Figure 3). The core typically shows two facies associations B and A, with mangrove/herbaceous flat and mangrove tidal flat, respectively (Table 3).
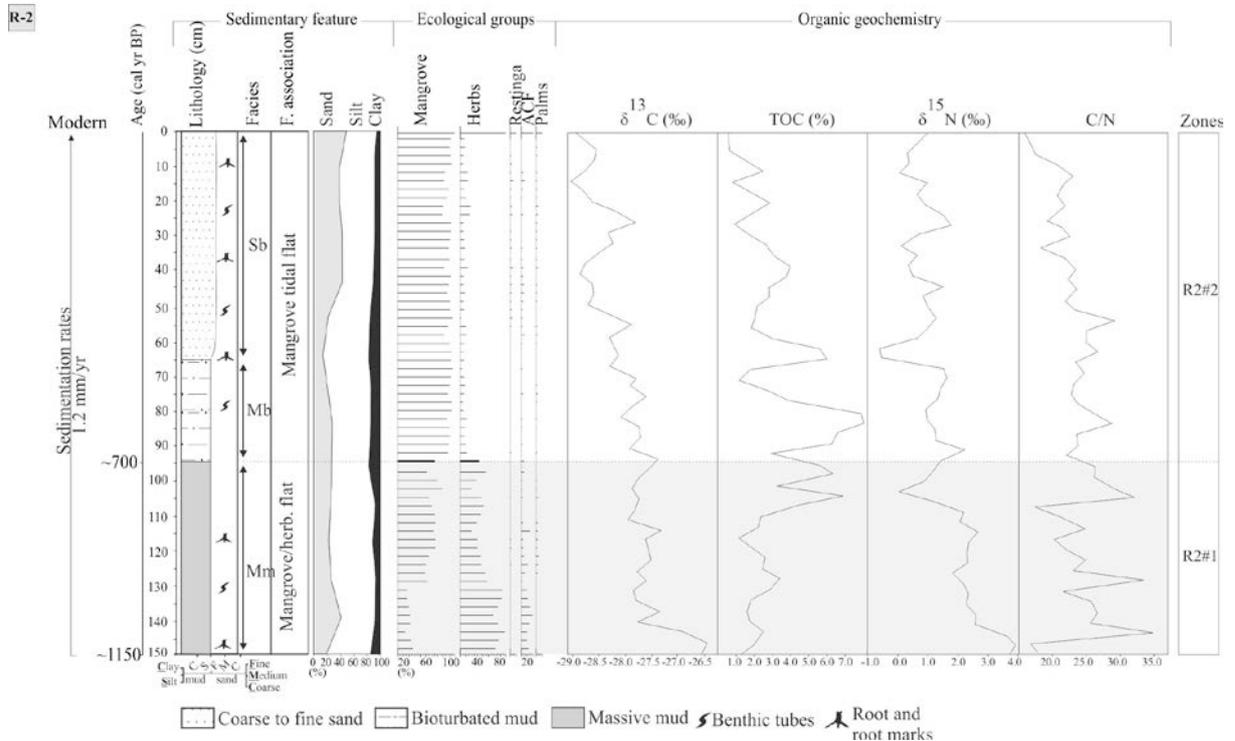
Figure 3 – Summary results for R-2 core: variation as a function of core depth from chronological, lithological profile, pollen analysis and geochemical variables.

The pollen and spore analyses present five ecological groups (Figure 3). The interval between 150 and 95 cm is characterized by herbaceous and mangrove pollen, while the top sequence is dominated by mangrove pollen.

The organic geochemistry results show isotope and elemental data that indicates an upward depleting trend of $\delta^{13}C$ values from −26 to −29‰, while the $\delta^{15}N$ values oscillate between −0.6‰ and +3.9‰. The C/N presents an upward decreasing trend from 35 to 16. The TOC values range between 0.5% and 7.9%. (Figure 3).

R-3 core (herbaceous plain/mangrove, 150 cm)

The core consists of bioturbated mud (facies Mb), which are interbedded with lenticular muddy silt (facies Hl) and sand cross-lamination (facies Sc). Near the top it is possible to record fine to medium-grained sand (facies Sb) with an upward increase in grain size. This core presents facies associations A and B (Table 3), with mangrove tidal flat and mangrove/herbaceous flat (Figure 4).
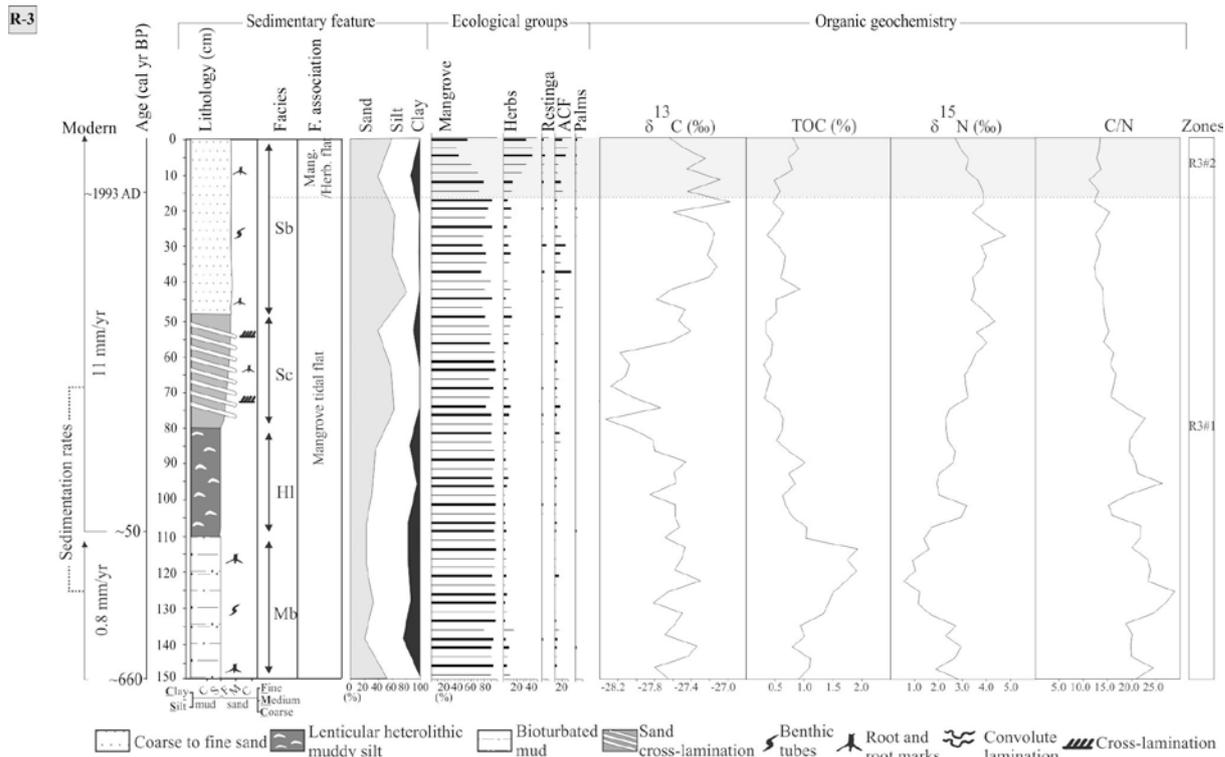
Figure 4 – Summary results for R-3 core: variation as a function of core depth from chronological, lithological profile, pollen analysis and geochemical variables.

The interval between 150 and 15 cm is marked by a dominance of mangrove pollen, while the top is marked by a decrease in mangrove, and an increase in herbaceous pollen, and trees and shrubs from ACF.

The isotope data and elemental analysis results are presented in Figure 4. The $\delta^{13}C$ values oscillate between $-28.3‰$ and $-27‰$. The $\delta^{15}N$ values present an upward increase from $+0.6‰$ to $+4.8‰$. The C/N shows a decreasing trend from 26.2 to 11.1 in surface. The TOC results exhibit values between 0.3% and 2% with higher values at 120 cm.

R-4 core (mangrove, 225 cm)

The deposits are dominantly sandy sediments at the bottom, with mud present at shallow depth. This core grades downward into heterolitic deposits (facies Hf and Hw), consisting of massive sand (facies Sm) or, less commonly, parallel laminated, fine to very fine-grained sand (facies Sp). Plant debris and overload structures are locally present. These deposits show association D, C and A (Table 3), thus a phase of foreshore, with tidal channel (facies Hf and Hw), lagoon with mangrove and mangrove tidal flat, respectively (Figure 5).
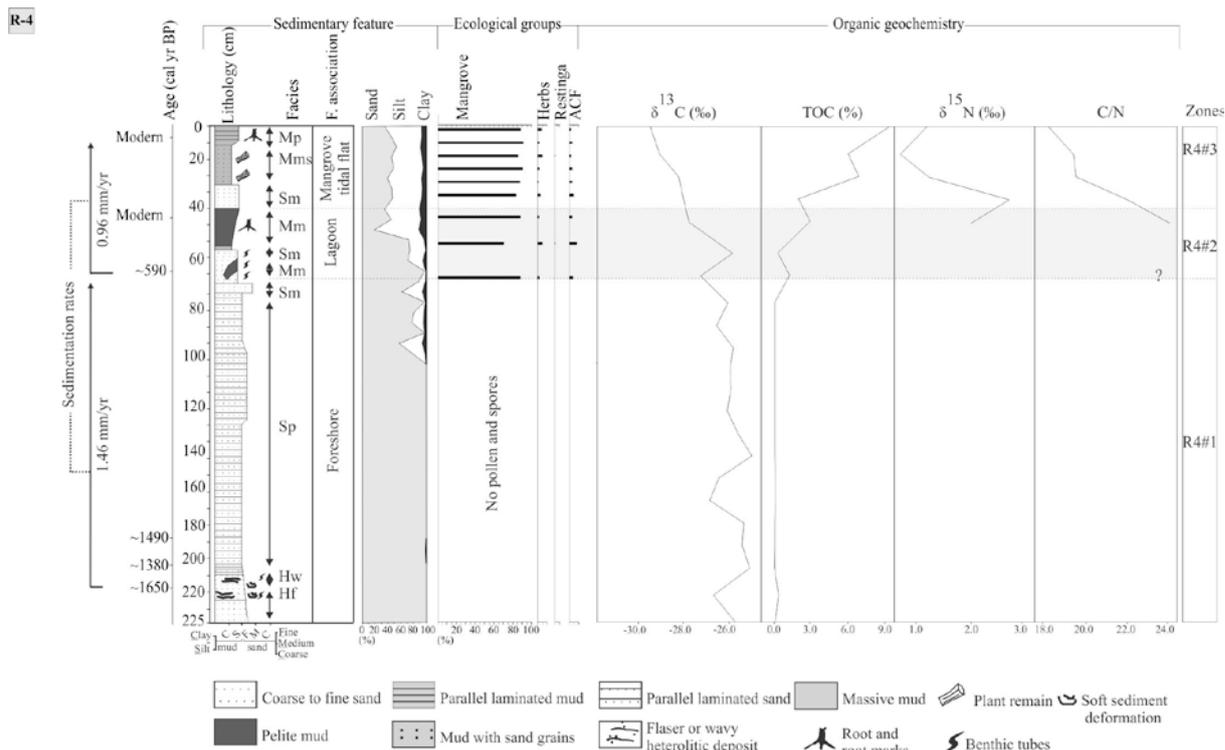
Figure 5 – Summary results for R-4 core: variation as a function of core depth from chronological, lithological profile, pollen analysis and geochemical variables.

The interval between 225 and 70 cm is characterized by the absence of pollen, probably due to the presence of sandy sediments, coinciding with foreshore facies association, while the section between 70 and 40 cm is marked by the onset of mangrove development. The top (40-0 cm) is marked by an increase of mangrove pollen, characterizing the mangrove tidal flat facies association.

The organic geochemical results obtained in the bottom zone were only $\delta^{13}C$ (between −27‰ and −25‰) and TOC values (around 0-1%). At the shallow depth, where the mangrove occurs, the $\delta^{13}C$ values are more depleted (between −26‰ to −29‰). The modern sediments show $\delta^{15}N$ results between +0.5‰ and +2.5‰ and C/N with a decreasing trend to approximately 18 at the surface. The TOC values are 0% between 225 and 80 cm, with an upward increase to 9% to the top (Figure 5).

R-5 core (lake/herbaceous plain, 256 cm)

The sediment consists typically of massive mud (facies Mm) and parallel laminated mud (facies Mp), with plant fragments, leaves and benthic structures. Near the surface bioturbated mud (facies Mb) are observed. These deposits have characteristics related to the associations A and E (Figure 6 and Table 3), indicating a phase of a mangrove tidal flat and lake stage, respectively.
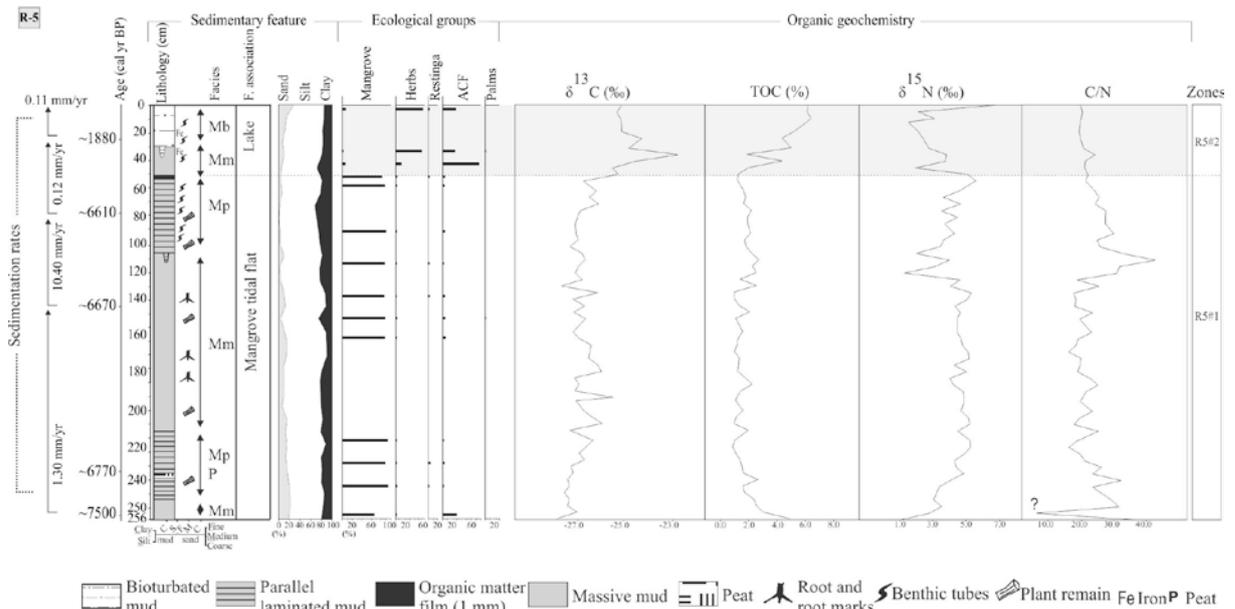
Figure 6 – Summary results for R-5 core: variation as a function of core depth from chronological, lithological profile, pollen analysis and geochemical variables.

The base (255-55 cm) of this core is marked mainly by mangrove pollen, while the top (55-0 cm) presents a decrease of mangrove pollen, replaced by herbaceous and ACF pollen.

The organic geochemical results show a contrast between the two depositional periods (Figure 6). During the time interval ~7500 BP and ~3200 cal yr BP (estimated age), the mangrove tidal flat was characterized by $\delta^{13}C$ values between −28‰ and −25‰. The $\delta^{15}N$ results during the mangrove phase were +1‰ to +5‰ and C/N values between 9 and 45. The TOC results in the bottom of the core are relatively higher (2.6-4.9%) than the middle (0.9-2.7%), and at the top around 6%. The upper facies, deposited by the lake since ~3200 cal yr BP, shows $\delta^{13}C$ values with an enrichment trend from −26.5‰ to −22‰. The $\delta^{15}N$ values occur between 1‰ and 6‰, C/N values around 17 and 20 and an increase in the TOC concentration to 6%.

Interpretation and discussion

Generally, sediment cores sampled from lakes include pollen and organic matter sourced from the lake and its surroundings (e.g. Davis, 2000; Xu et al., 2012), while cores sampled from tidal flats accumulate pollen and organic matter originating relatively near to the sampling site (Behling et al., 2001). For this reason, core R-5 (sampled from a lake in the central region of the island) between depths of 0 and 55 cm, is likely more representative of

vegetation and organic matter of eastern Marajó Island than the records from cores R-1, R-2, R-3 and R-4, collected from tidal flats with a smaller spatial representativeness of vegetation and organic matter (Cohen et al., 2008; Smith et al., 2011; 2012).

Thus, the results obtained from sedimentary features, pollen and geochemical analyses from Marajó Island suggest significant changes in vegetation and organic matter source during at least the last seven thousand years. The data suggest the delimitation of three phases, with a tidal flat colonized by mangrove in the central region of the island between ~7500 and ~3200 cal yr BP (estimated age), and with relatively higher contributions of estuarine organic matter between ~7500 and ~6500 cal yr BP, as recorded in core R-5 (Figures 6, 7 and 8). During ~3200 and ~1150 cal yr BP in the hinterland of Marajó Island, mangroves were largely replaced by herbaceous vegetation, characterizing the second phase. The third phase is marked by migration and isolation of mangrove to the east coast of the island since ~1150 cal yr BP at the earliest (i.e, core R-2), and is recorded in cores R-1, R-4 and R-3 at ~540, ~580 and ~660 cal yr BP, respectively (Figure 8).
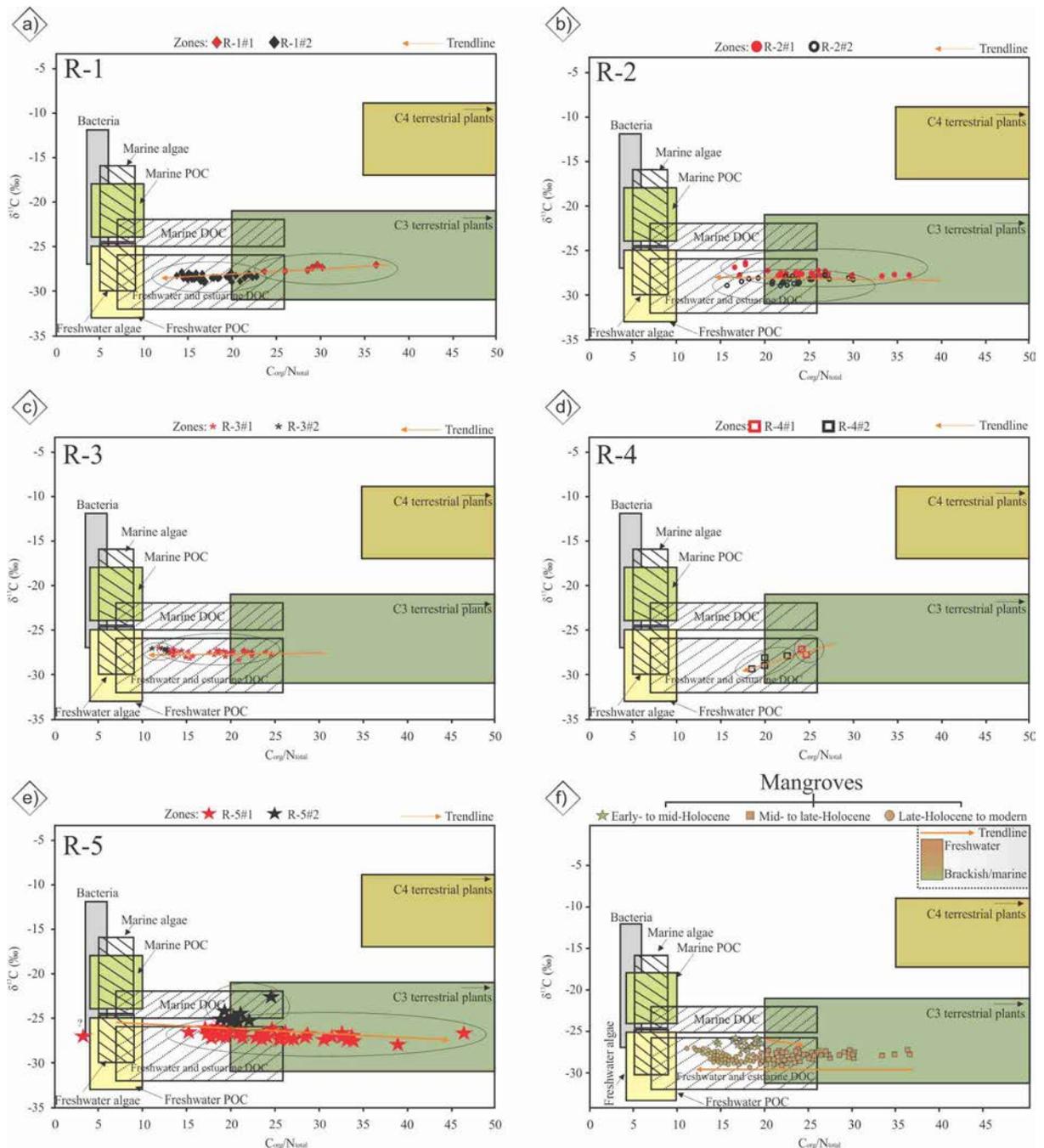
Figure 7 – Binary diagram between $\delta^{13}C$ x C/N for the different studies cores and different zones: a) R-1; b) R-2; c) R-3; d) R-4 and e) R-5 core. 7f) It represents the integration of $\delta^{13}C$ and C/N data of organic matter preserved along the facies association Mangrove tidal flat. The different fields in the $\delta^{13}C$ x C/N plots correspond to the member sources for organic matter preserved in sediments and trendline, on red line (modified from Meyers, 1997 and Lamb et al., 2006).
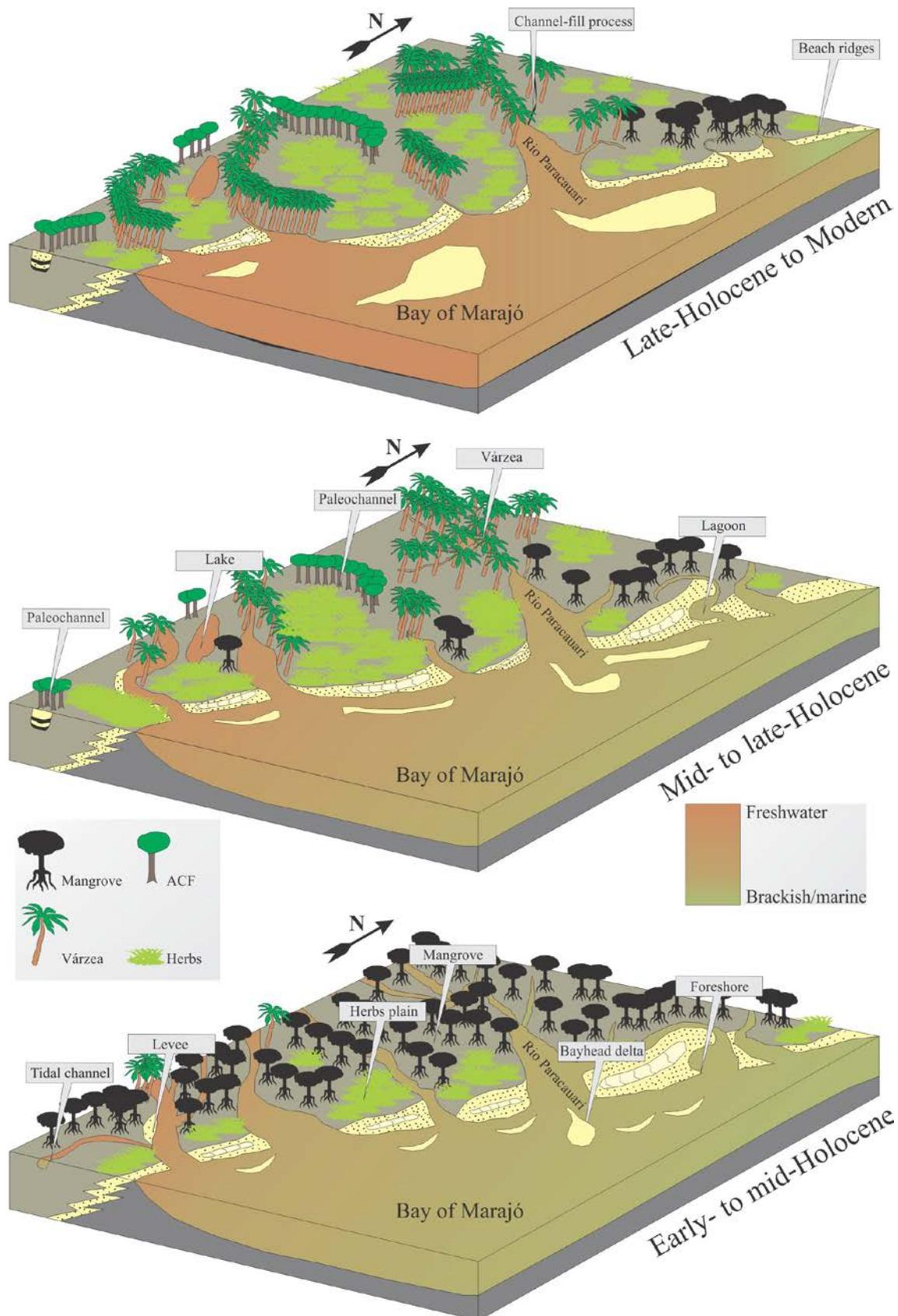
Figure 8 – Schematic representation of successive phases of sediment accumulation and vegetation change in the study area according to marine-freshwater influence gradient.

First phase (Early- to mid-Holocene – mangrove): ~7500 to ~3200 cal yr BP

The tidal mud flats were occupied by mangroves since at least ~7500 cal yr BP, and remained in the area of R-5 until ~3200 cal yr BP (Figure 8). The relationship between $\delta^{13}C$ and C/N values indicates an influence of estuarine organic matter, with dominance of C_3 plants ($\delta^{13}C= -32‰$ to $-21‰$, Deines, 1980) and a mixture of freshwater algae ($\delta^{13}C= -26‰$ to $-30‰$, Schidlowski et al., 1983; Meyers, 1994) with brackish water algae ($\delta^{13}C= -22‰$ to $-25‰$, Peterson et al., 1994). The $\delta^{13}C$ values (around $-27‰$) of organic matter recorded during this phase are 3‰ enriched in relation to $\delta^{13}C$ values range of mangrove vegetation (-33 to -30‰, table 1), with pollen percentage between 60 to 95% and mixture with some herbs also C_3. These isotope values difference may be attributed to the natural trend of $\delta^{13}C$ to increase towards the deeper layers, around 3 to 4‰, caused by the fractionation during decomposition of organic matter. The $\delta^{15}N$ values (1.3 to 5.0‰) suggest a mixture of terrestrial plants and aquatic organic matter (~5.0‰, Sukigara and Saino, 2005). The C/N values (15-42) also indicate a mixture of organic matter from vascular plants and algae (< 10 algae dominance and > 12 vascular plants, Meyers, 1994; Tyson, 1995).

Second phase (Mid- to late-Holocene. – lake): ~3200 to ~1880 cal yr BP

This phase is marked by massive mud sedimentation, with organic matter film (1mm), and some benthic tubes, root and root marks (R-5, 42 cm) that indicate stagnant conditions with vegetation development (herbaceous plain and ACF influence). The relationship between $\delta^{13}C$ ($-25.5‰$ to $-22.7‰$) and C/N values (< 20) indicate a mixture of continental organic matter, dominance of C_3 plants with a slight C_4 plant (herbaceous) influence and aquatic contribution (Figures 6, 7 and 8), allowing the inference of a lacustrine environment since ~3200 cal yr BP at the earliest. During this stage a reduction of mangrove occurs (<8%) that is replaced by herbaceous vegetation (20 to 55%), ACF (30 to 75%) and some aquatics elements with freshwater influence. The interruption of mangrove development during this period indicates unfavorable conditions to mangrove development, which may be due to a decrease in porewater salinity. During this interval, the ACF and herbaceous plain, which had adapted to freshwater flooding, expanded in this area. The mangroves were isolated in the most northeastern areas of Marajó Island (about 40 km away from R-5 core), where the tidal water salinity remained relatively higher.

Third phase (Late Holocene to modern – mangrove): ~1700 cal yr BP to modern

The foreshore facies association (R-4, Figure 5) was recorded between ~1700 and ~600 cal yr BP. This period is marked by low TOC and absence of pollen. It may be caused by various external factors (sediment grain size, microbial attack, oxidation and mechanical forces), as well as factors inherent to the pollen grains themselves (sporopollenine content, chemical and physical composition of the pollen wall) (Havinga, 1967). In this case the sediment grain size and energy flow can be considered the main cause of the pollen absence, since the sandy sediments are not favorable to pollen preservation.

During the foreshore facies association, it was not possible to measure the C/N and $\delta^{15}N$ values due to low concentration of nitrogen in sedimentary organic matter. Thus, it is not possible to identify the origin of organic matter (terrestrial or marine) preserved in these sediments. The $\delta^{13}C$ values (around -26‰) may indicate continental C_3 plants (-32‰ to -21‰, Deines, 1980) and/or freshwater algae (-26‰ to -30‰, Schidlowski et al., 1983; Meyers, 1994).

This phase is marked by mangrove presence since ~1150 cal yr BP (R-2) at the earliest, and is recorded in cores R-1, R-4 and R-3 at ~540, ~580 and ~660 cal yr BP, respectively. Data presented by Behling et al. (2004) shows that mangrove vegetation became established at about ~2800 cal yr BP along the northeastern Marajó Island. The vegetation development in this region was marked by four ecological groups (herbs, Restinga, ACF and palms).

During the last thousand years the relationship between $\delta^{13}C$ and C/N shows a trend from continental organic matter to organic matter originating from estuarine algae during mangrove establishment (Figure 7). This indicates an increase in tidal influence on the R-1, R-2, R-3 and R-4 areas, mainly during the last century.

Amazon River and Relative Sea Level (RSL) controlling mangrove dynamics

The Amazon climate change within the Holocene is often offered as a causal mechanism underlying the modern biodiversity and biogeography of Amazonia (e.g. Bush, 1994; Colinvaux, 1998, Bush et al., 2004; Weng et al., 2004; Hermanowski et al., 2012). Main climatic factors may have driven changes in vegetation as temperature, precipitation, seasonality and CO_2 concentration (Bush et al., 2004). However, the development of mangroves is regulated by continent-ocean interactions and their expansion is determined by the topography relative to sea-level (Gornitz 1991; Cohen and Lara, 2003), and flow energy (Woodroffe, 1989; Chapman 1976), where mangroves preferentially occupy mud surfaces. On the mud tidal flats, this ecosystem is controlled by tidal inundation frequency, nutrient

availability, and porewater salinity (Hutchings and Saenger, 1987, Lara and Cohen, 2006). Mangroves are tolerant to soil salinity and sediment salinity is mostly controlled by flooding frequency (Cohen and Lara, 2003) and estuarine salinity gradients (Lara and Cohen, 2006).

Therefore, despite that mangroves are influenced by coastal variables (Blasco et al. 1996), climatic changes recorded in Amazon basin during the Holocene (Absy et al., 1991; Desjardins et al., 1996; Gouveia et al., 1997; Pessenda et al., 1998a) must be affecting the Amazon River discharge, and consequently, its estuarine salinity gradients and the area flooded by estuarine waters at the mouth of the Amazon River (Smith et al., 2011; 2012; Guimarães et al., 2012).

The data indicate a tidal mud flat colonized by mangroves with influence of estuarine organic matter between at least ~7500 and ~3200 cal yr BP (Figures 7f and 8). Probably it is due to the relatively higher marine influence favored by reduced Amazon River discharge caused by a dry period during the early and middle Holocene (Pessenda et al., 2001; Behling and Hooghiemstra, 2000; Freitas et al., 2001; Sifeddine et al. 2001; Weng et al., 2002; Bush et al., 2007). Mangrove expansion during the early Holocene was likely caused by the post-glacial sea-level rise which, combined with tectonic subsidence (Rossetti et al., 2008; Rossetti, et al., 2012), led to a marine transgression. This event caused a marine incursion along the littoral of northern Brazil, where the RSL stabilized at its current level between 7000 and 5000 yr BP (e.g. Cohen et al., 2005a; Vedel et al., 2006). A transgressive phase occurred on Marajó Island in the early to middle Holocene. Subsequently, there was a return to more continental conditions that prevail currently in the study area (Rossetti et al., 2008).

During the late Holocene, there was a decrease of mangrove vegetation in the area of R-5 and the contribution of freshwater organic matter is higher than early and middle Holocene (Figure 7f), suggesting a decrease in marine influence as recorded by Smith et al. (2012). This led to the isolation of mangroves in the eastern Marajó Island since at least ~1150 cal yr BP (Figure 3), indicating a gradual migration of mangroves from the central region to the current coastline (Figure 8). An increment in Amazon River discharge during the more humid late Holocene in the Northern and Northeastern regions of Brazil (Pessenda et al.,1998a, 2001, 2004, 2010) constitutes a hypothesis for this isolation (Guimarães et al., 2012; Smith et al., 2011; 2012). This process could be responsible for the modern decrease in tidal water salinity along the littoral (0–6 ‰, Santos et al., 2008). It is clearly observed in the relationship between C/N and $\delta^{13}C$ (Figure 7), which shows a trend of increasing aquatic organic matter (R-1, R-2, R-3 and R-4).

Conclusions

The sediment deposits from Marajó Island offer a valuable opportunity to investigate past climate and RSL, and its effects on vegetation and sedimentary organic matter. Changes in vegetation, sediment deposition and organic matter input should be related to the interaction between Amazon climate and the RSL. The data indicate a tidal mud flat colonized by mangroves with estuarine organic matter in the interior of Marajó Island between ~7500 and ~3200 cal yr BP. It was caused by the post-glacial sea-level rise, which combined with tectonic subsidence, produced a marine transgression. Likely, the relatively higher marine influence along the studied area was favored by reduced Amazon River discharge caused by a dry period during the early and middle Holocene.

During the late Holocene, there was a reduction of mangrove vegetation in the interior of Marajó Island and the contribution of freshwater organic matter was higher than during the early and middle Holocene. It suggests a decrease in marine influence that led to a gradual migration of mangroves from the central region to the northeastern littoral, and consequently, its isolation since at least ~1150 cal yr BP. These likely results from lower tidal water salinity caused by a wet period that resulted in greater river discharge during the late Holocene.

As reported by this work, using a combination of proxies is efficient for establish a relationship between changes in estuarine salinity gradient and depositional environment/vegetation.

CHAPTER IV:

LANDSCAPE EVOLUTION DURING THE LATE QUATERNARY AT THE DOCE RIVER MOUTH, STATE OF ESPÍRITO SANTO, SOUTHEASTERN BRAZIL

Abstract

The sedimentary deposits of delta plain of the Doce and Barra Seca Rivers, Southeastern Brazil, were studied by facies analysis, pollen records, δ^{13}C, C/N analysis and ^{14}C- dating by AMS. Today, this deltaic plain is dominated by beach ridges and sandy terraces occupied by arboreal and herbaceous vegetation. Between at least ~47,500 and ~29,400 cal yr B.P., a deltaic system was developed in response mainly to eustatic sea-level fall. Despite of the stratigraphic sequence studied presents compatibility with the trend of global sea-level fall, the position of old sea-level, suggested by the deltaic system, is above the expected for the MIS3 stage. Probably, a tectonic uplift occurred during the late Quaternary and raised this sedimentary sequence. The post-glacial sea-level rise caused a marine incursion with invasion of embayed coast and broad valleys, and it favored the evolution of an estuary with wide tidal mud flats occupied by mangroves between at least ~7400 and ~5100 cal yr B.P. Probably, the high river sand supply and/or the relative sea-level fall in the late Holocene lead to seaward and downward translation of the shoreline during normal/forced regression, producing progradational deposits with mangrove shrink and expansion of marsh colonized by herbaceous vegetation. Therefore, stratigraphic architecture and evolution of the Doce River delta plain suggest that fluvial sediment supply and relative sea-level fluctuations related to Quaternary global climatic changes and tectonism exerted a major control on sedimentation through the variation of accommodation space and base-level changes.

Keywords: climate change; isotopes; palynology; sea-level changes; sedimentary facies

Introduction

Systematic studies of the Holocene sea-level in the eastern Brazilian coastline show a post-glacial sea-level rise, and that a middle Holocene sea-level highstand occurred along the whole coast, with a subsequent fall to the present time (e.g., Angulo et al., 2006). The sea-level change and the local balance of the coastal sediments are the main factors that control the evolution of the sedimentary plains in the Brazilian coast. Associated to these plains, several ecosystems and coastal systems, such as mangroves, beaches, lagoons, and deltas undergo the influence of those factors and interact among themselves composing an integrated system that cannot be analyzed in isolation (e.g., Woodroffe, 2002).

Considering a sandy coastal zone with an equilibrium profile determined by the local hydrodynamics and the grain size of the sediments, the profile is constantly being destroyed by hydrodynamic changes due to tides, waves and litoraneous currents. However, over a sufficiently long period of time, a standard equilibrium profile will be established. This equilibrium may be disturbed by the relative sea-level rise (SLR), but it would be re-established by a landward displacement of the beach profile. This results in an accelerated erosion of the beach prism and transfer of eroded sands toward the inner shelf, with the rise of the inner shelf bottom by a height equal to that of SLR (Bruun, 1962; Schwartz, 1965; 1968; Woodroffe, 2002).

Under conditions of rising sea-level on a gently sloping sandy coast, a barrier island with lagoons and/or estuaries are the dominant depositional systems (Swift, 1975), and beach-ridge plains are virtually absent. Regarding estuaries, its response to sea-level changes is affected by tidal range, nearshore wave climate, river inflow, and the nature and supply of sediments. All estuaries assumed their present form during the rise of sea-level that followed the Last Glacial Maximum (LGM), about 20 thousand years ago (Chappell and Woodroffe, 1994). In contrast, a sea-level fall creates highly unfavorable conditions for the genesis and maintenance of estuaries, lagoons and bays, especially in wave dominated coasts. The continued river sediment supply results in shoreline progradation, and it may generate a delta (Suter, 1994). Lagoons and bays become emergent and beach ridge plains rapidly prograde, resulting in regressive sand sheets (Martin and Suguio, 1992).

If the littoral is colonized by mangroves, they can be used as indicators of coastal dynamics, since their position within the intertidal zone are strongly influenced by SLR (Woodroffe et al., 1989; Woodroffe, 1995). Over a range of SLR scenarios, coastal wetlands adjust towards an equilibrium with sea-level (e.g., D'Alpaos et al., 2007; Kirwan and Murray, 2007). Equilibrium models predict that coastal wetlands have a number of feedbacks that

allow wetlands to maintain their position relative to the position of mean tide (Cohen et al., 2005a,b). For example, surface accretion, often through sediment inputs, increases with the depth of tidal inundation (e.g., French and Stoddart, 1992; Furukawa and Wolanski, 1996), leading to increments in surface elevation that allow the wetland to keep pace with sea-level rise (Cahoon et al., 2006). Fringe mangroves have kept up and could accommodate eustatic SLR rates of 4 mm year^{-1}. If eustatic rates exceed 5 mm year^{-1}, then the mangroves would not be likely to persist (Mckee et al., 2007).

The northern littoral of the Espírito Santo presents a deltaic plain associated to the Doce River. According to Martin and Suguio (1992), during the middle Holocene, almost all sediments supplied by the Doce River were retained within large lagoons located behind a barrier island. This system of deposition was formed during the Holocene relative sea-level highstand, about 5.5 ky B.P. About 2.5 ky B.P., the coastal lagoons became completely filled.

Today, this area is characterized by vast strandline sandy progradation, and mangroves are restricted to lagoon margins. The aim of this study is to improve the reconstruction of landscape evolution in the Doce River delta plain according to the interaction among sedimentary processes, vegetation dynamics and sea-level fluctuations during the late Pleistocene and Holocene based on facies analysis, pollen records, δ^{13}C, C/N analysis and AMS dating.

Study area

Location

The study site comprises the deltaic plain of the Doce River near the Barra Seca River. Six sediment cores were sampled following a landward transect and named of Li, in reference to the Linhares city, 30 km southwest from the study area: Li 31 (S 19° 11' 16"/W 39° 49' 33"); Li 01 (S 19° 10' 53"/W 39° 51' 55"); Li 33 (S 19° 10' 19.16"/W 39° 53' 10"); Li 26 (S 19° 07' 4"/W 39° 52' 57"); Li 23 (S 19° 08' 58"/W 39° 53' 29"), and Li 24 (S 19° 09' 8"/W 39° 55' 47"). The core Li 24 was sampled from the margin of a paleochannel in the most proximal sector of the studied coastal plain (Figure 1c), while the Li 31 was taken from a lake confined between beach ridges. The Li 23, 26 and 33 were sampled from the coastal plain dominated by beach ridges, and the Li 01 (positioned 10 km from the Li24) was collected from the margin of the Bonita Lake, which is a freshwater lake inserted in the lower course of Barra Seca River (Figure 1c) inside the Sooretama Federal Biological Reserve. The lake is 30 km far from the Doce River and 15 km far from the sea at the southeastern wave-dominated coast of Brazil (Dominguez, 2009).
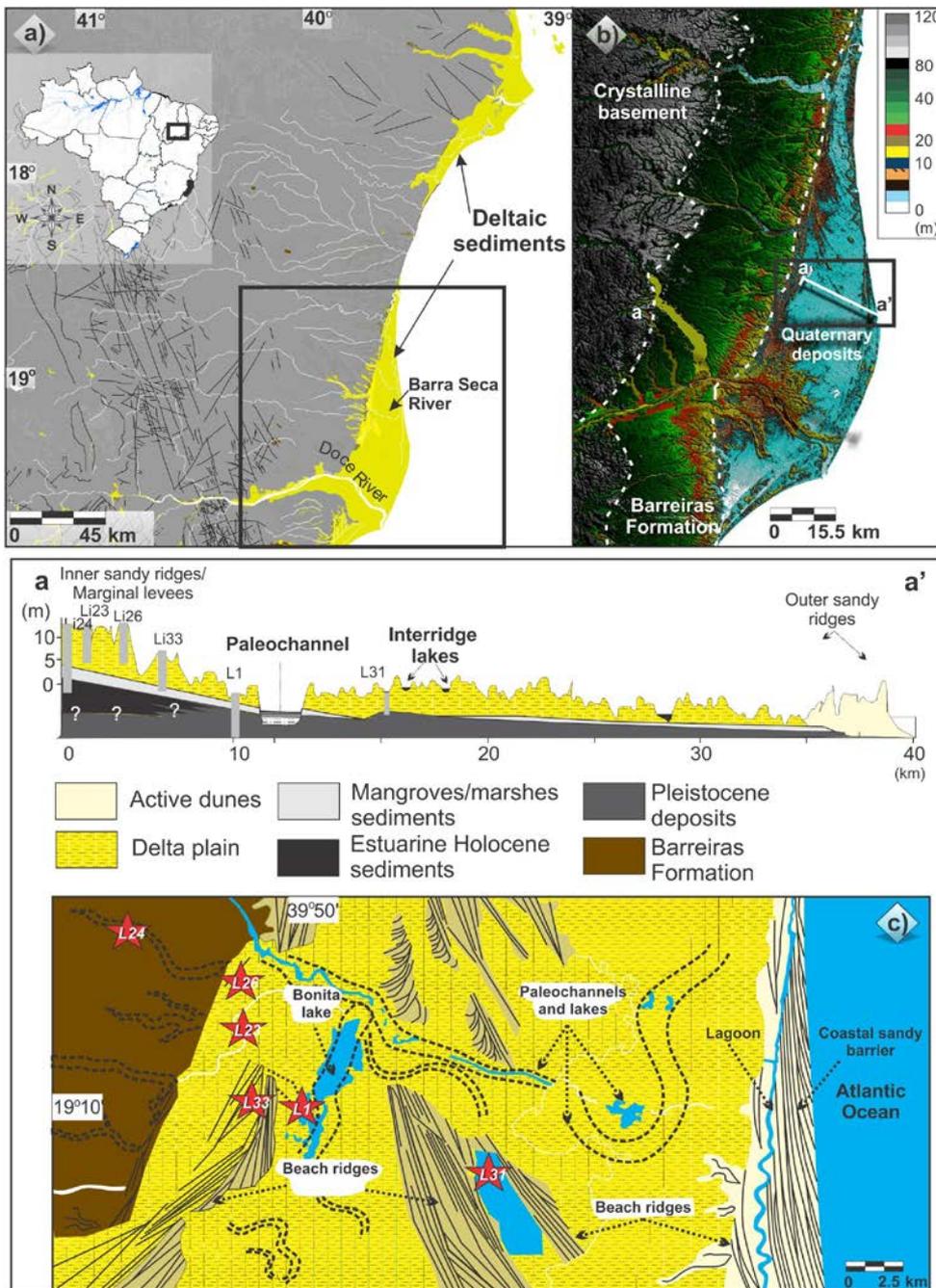
Figure 1 – a) Location of the study area, and its geological context. b) SRTM-DEM topography of the study site and lithostratigraphic profiles. C) Location of studied sediment cores and the spatial distribution of main geomorphological features.

Geology and geomorphology

Four geomorphological units are recognized in the area: (1) the mountainous area, represented by Precambrian crystalline rocks, with a multidirectional rectangular dendritic drainage net; (2) a tableland area composed of the Barreiras Formation, which is constituted by sandstones, conglomerates, and mudstones attributed mainly to Neogene fluvial and alluvial fan deposits, but possibly including marine deposits originated from a coastal onlap associated to Neogene transgressions (Arai, 2006; Dominguez, 2009); (3) a coastal plain area, with fluvial, transitional and shallow marine sediments, which were deposited during changes in sea-level in the Quaternary (Martin and Suguio, 1992); and (4) an inner continental shelf area (Asmus et al., 1971). Several W-E, NW–SE and NE–SW tectonic lineaments revel the importance of regional tectonic in the development of many modern drainage systems (Fig. 1a).

Currently, the Doce River shows a mostly W-E trending "straight" pattern, flowing on basement crystalline rocks and into the littoral plain through a low valley with Holocene terraces (Figure 1). The terraces, with a 0.45% longitudinal gradient, consist of a mixture of sediments from the Barreiras Formation, and are transported by rivers that originate in mountainous areas and Neogene tablelands. They are composed mainly of moderately sorted, coarse- to very-coarse grained sands that are distributed along the coastline forming beach ridges. Downstream, sandy silt sediments of the Doce River spread over its floodplain (Figure 1). Residual and very poorly preserved mangrove vegetation close to marine influence occurs in the margin of the barrier and coastal lagoon system. An elongated coastal sand barrier occurs parallel to the shore and are separated from the mainland by a lagoon. It displays 37 and 3.6 km in length and width, respectively, and present multiple beach ridges, that likely represent successive shoreline positions formed during coastline progradation associated to sea-level fall (Otvos, 2000).

The studied delta plain covers an area of ~2700 km^2 and displays fluvial channels and an extensive paleochannel network. The abandoned channels present straight to meandering patterns, and they maintain the shape and typical concavity of the original channel, resulting in the formation of lakes and lake belts (Figure 1). Avulsion may have been responsible for the partial or complete abandonment of several channels due to the rapid sand sedimentation.

Considering the sandy ridges, they present extensive, straight to slightly curved sand bodies colonized by herbaceous vegetation, and exhibit N-S and NW-SE orientations, elevation between 4 and 11 m, 2 to 20 km in length with interridge spacing between 30 and 200 m (Figure 1). Additionally, the studied delta plain presents three topographic groups of

sandy ridges, named inner (~9 m), intermediated (~5 m) and outer sandy ridge (~10 m) with maximal width of about 3.5; 75 and 3.6 km, respectively. The inner and intermediate sandy ridges are interpreted as beach ridges, while the outer sandy ridges occur as dune ridges. Some interridge depressions present standing water. These shallow interridge lakes are subjected to overbank crevassing, resulting in a sediment influx into the lake. They show ~2 m depth, water salinity of ~0‰, and ephemeral behavior due to the seasonality of climate and hydrology. The deposits consist of thick peat layers, laminated, mud and bioturbated mud, which are colonized by freshwater marshes.

Climate

The region is characterized by a warm and humid tropical climate with annual precipitation averaging 1400 mm (Peixoto and Gentry, 1990), and concentrated in the summer, between November and January. The dry fall-winter season occurs between May and September. It is regulated by the position of the Inter Tropical Convergence Zone (ITCZ) and South Atlantic Convergence Zone (SACZ) (Carvalho et al., 2004). The study area is entirely located within the South Atlantic trade winds belt (NE-E-SE) that is related to a local high-pressure cell and the periodic advance of the Atlantic Polar Front during the autumn and winter, generating SSE winds (Dominguez et al., 1992, Martin et al., 1998). The average temperature ranges between 20º and 26º C.

Vegetation

The modern vegetation is composed mainly by tropical rainforest. The most representative plant families are Fabaceae, Myrtaceae, Sapotaceae, Bignoniaceae, Lauraceae, Hippocrateaceae, Euphorbiaceae, Annonaceae and Apocynaceae (Peixoto and Gentry, 1990). In the proximal portion of the delta plain occurs a herbaceous plain mainly represented by Cyperaceae and Poaceae with some trees and shrubs on edge of the plain. A gradual transition occurs to the distal portion of the delta plain where dominates the *restinga* vegetation, which occurs on sand plains and dunes close to the shoreline. It is represented by shrub and herbs. Palm trees as well as orchids and bromeliads that grow on the trunks and branches of larger trees occurs also along the shoreline. *Ipomoea pes-caprae* (Convolvulaceae), *Hancornia speciosa* (Apocynaceae), *Chrysobalanus icaco* (Chrysobalanaceae), *Hirtella Americana* (Chrysobalanaceae)*, Cereus fernambucensis* (Cactaceae), *Anacardium occidentale*

(Anacardiaceae) and *Byrsonima crassifolia* (Malpighiaceae) are also found. Mangroves represented by *Rhizophora* and *Avicennia* are restricted to the margin of the barrier and coastal lagoon systems. The vegetation inside the lake and at its margins comprises land plants such as *Tabebuia cassinoides*, *Alchornea triplinervia* and *Cecropia sp*., and emergent, submerged, floating-leaved and floating plants like *Typha sp*., Cyperaceae, Poaceae, *Salvinia sp*., *Cabomba sp*., *Utricularia sp*. and *Tonina sp*. A freshwater marsh composed by herbaceous vegetation colonizes the Barra Seca Valley.

Methods

Remote Sensing

The morphological aspects of the study area were characterized based on the analysis of Landsat images 5-TM, obtained in August 2008 by INPE-Brazilian National Institute for Space Research, as well as topographic data acquired during the Shuttle Radar Topographic Mission (SRTM-90 m) distributed by the National Aeronautics and Space Administration (NASA). The SRTM data were processed using customized shading schemes and palettes to highlight topographic and morphological features. We interpreted elevation data using the software Global Mapper (Global Mapper Software LLC, Olathe, KS, USA).

Sampling processing and facies description

Fieldwork was undertaken in November 2009, during the dry season. Using a Percussion Drilling (Hammer Cobra TT), the sediment cores were taken up to a depth of 12m.

Following the proposal of Harper (1984) and Walker (1992), facies analysis included descriptions of lithology, texture and structures. The sedimentary facies were codified following Miall (1978). The sediment grain size distribution, following Wentworth (1922), was analyzed by laser diffraction in a Laser Particle Size SHIMADZU SALD 3101.

Pollen and spore analysis

For pollen analyses, 1 cm^3 samples were taken at 10 cm intervals along the cores Li 01 and Li24. Preparation followed standard pollen analytical techniques including acetolysis (Faegri and Iversen, 1989). Pollen and spores were identified by comparison with reference collections of about 4,000 Brazilian forest taxa and various pollen keys (Salgado-Laboriau, 1973; Absy, 1975; Markgraf and D'Antoni, 1978; Roubik and Moreno, 1991; Colinvaux, et al., 1999) jointly with the reference collection of the Laboratory of Coastal Dynamics – Federal University of Pará and [14]C Laboratory of the Center for Nuclear Energy in

Agriculture (CENA/USP) to identify pollen grains and spores. A minimum of 300 pollen grains were counted for each sample. In specific depths 100-200 grains were counted due to low pollen concentration. Microfossils consisting of spores, algae and some fungal were also counted, but not included in the sum. Pollen data are presented in pollen diagrams as percentages of the total pollen sum. Taxa were grouped into broad ecological categories including mangrove, trees and shrubs, herbs, palms, fern spores, and micro-foraminifer. The software TILIA was used for calculations, and CONISS and TILIAGRAPH for the cluster analysis of pollen taxa and to plot the pollen diagrams (Grimm, 1987).

Isotopic and chemical analysis

Ninety-four samples (1 cm^3) were collected along the cores Li01 and Li24. Samples were separated and treated with 4% HCl to eliminate carbonates, washed with distilled water until pH ~ 6, dried at 50ºC, and homogenized. These samples were used for total organic carbon (TOC) and total nitrogen (TN) analyses, carried out at the Stable Isotope Laboratory of the Center for Nuclear Energy in Agriculture (CENA/USP). The results are expressed in percent of dry weight, with an analytical precision of 0.09 and 0.07%, respectively. The ^{13}C results are expressed as δ^{13}C with respect to the VPDB standard using the following conventional notations:

$$\delta^{13}C \; (‰)=[(R_{1sample}/R_{2standard})-1] \; . \; 1000$$

where RS$_1$ and RS$_2$ are, respectively, the ^{13}C/^{12}C ratios in the sample, RPDB the ^{13}C/^{12}C ratio for the international standard (VPDB). The results are expressed in delta per mil (δ ‰) notation, with analytical precision better than 0.2 ‰ (Pessenda et al., 2004).

Radiocarbon dating

Thirteen samples of ~ 2g each of sedimentary organic matter and one shell were used for radiocarbon dating (Table 1). The sediment samples were physically treated by removing roots and vegetal fragments under the microscope. The residual material was then chemically treated with 2 % HCl at 60°C during 4 hours, washed with distilled water until neutral pH and dried (50 ºC), in order to remove eventual younger organic fractions (fulvic/humic acids) and carbonates. A chronologic framework for the sedimentary sequence was provided by conventional and accelerator mass spectrometer (AMS) radiocarbon dating. Samples were analyzed at the ^{14}C Laboratory of Fluminense Federal University (LACUFF) and at the

University of Georgia – Center for Applied Isotope Studies (UGAMS). Radiocarbon ages were normalized to a $\delta^{13}C$ of -25‰ VPDB and reported as calibrated years (cal yr B.P.) (2σ) using CALIB 6.0 (Reimer et al., 2009). The dates are reported in the text as the median of the range of calibrated ages.

Table 1 – Radiocarbon dates of studied sediment cores.

Lab. Number	Sample	Depth (m)	Dated material	Ages (14C yr BP, 1σ)	Ages (cal yr BP, 2σ)	Mean (cal yr BP, 2σ)
UGAMS 10565	LI-1	1.65-1.75	sed. org. matter	6710±30	7556-7622	~7600
UGAMS 10566	LI-1	3.7-3.75	sed. org. matter	24,610±70	29,226-29,678	~29,500
LACUFF13018	LI-1	6,20 - 6,30	shell	33,358±948	36,105-40,014	~38,000
UGAMS11693	LI-1	8.80-8.86	sed. org. matter	31,220 ± 100	35,162-36,321	~35,700
LACUFF00038	LI-1	11.52-11.7	sed. org. matter	44,232±812	45,775-49,391	~45,500
UGAMS 10567	LI-24	1	sed. org. matter	Modern	Modern	Modern
UGAMS 10568	LI-24	3	sed. org. matter	1480±25	1313 - 1405	~1350
UGAMS 10569	LI-24	5	sed. org. matter	4500±25	5047 - 5201	~5100
UGAMS 10570	LI-24	9	sed. org. matter	6330±30	7171 - 7317	~7200
UGAMS 10571	LI-24	14	sed. org. matter	6560±30	7425 - 7509	~7500
UGAMS 10572	LI-31	1.05-1.1	sed. org. matter	4320±25	4840 - 4893	~4860
UGAMS 10573	LI-31	4.95-5.0	sed. org. matter	3600±20	3845 - 3933	~3890
UGAMS 10574	LI-31	6.55-6.65	sed. org. matter	25,970±80	30,465-31,022	~30,700

Results

Radiocarbon dates and sedimentation rates

Thirteen sedimentary organic matter and one shell were dated, and range from 49,391 - 45,775 cal yr B.P. to modern age. The sedimentation rates were based on the ratio between the mean of depth intervals (mm) and the mean time range. The filling of the estuary, represented by core Li24, is recorded by an upward decrease of sedimentation rates, with 22.4 mm/yr (14-9 m), 1.9 mm/yr (9-5 m), 0.5 mm/yr (5-3 m) and ~1.4 mm/yr (3-1 m). A partial overlapping of ages were identified in the Li01, between 6.2 and 8.8 m, and a age inversion in the Li31, between 1.10 and 5m (Figures 2 and 3). In the case of Li01, this may be attributed to the content of dated material, because a shell and sedimentary organic matter were dated in

6.20–6.30 and 8.8-8.86 m depth, respectively (Figure 3). Generally, organic matter, found in marine sediments, are suited for radiocarbon dating, since it is assumed the temporal relation between the material dated and the timing of sedimentation. However, is possible overgrowth of calcite in mollusks, and some gastropods incorporate old carbon from limestone or calcareous sediments into their shells and, therefore, yield radiocarbon ages that are ~3000 ^{14}C years too old (Rubin et al., 1963; Evin et al., 1980; Goodfriend, 1987; Goodfriend and Stipp, 1983; Pigati et al., 2013). Regarding the Li31, the age inversion was recorded in the base and top of the facies association fluvial channel. This may reflect a rapid filling of the channel and/or rework of sedimentary organic matter along its pathway (Figure 2).
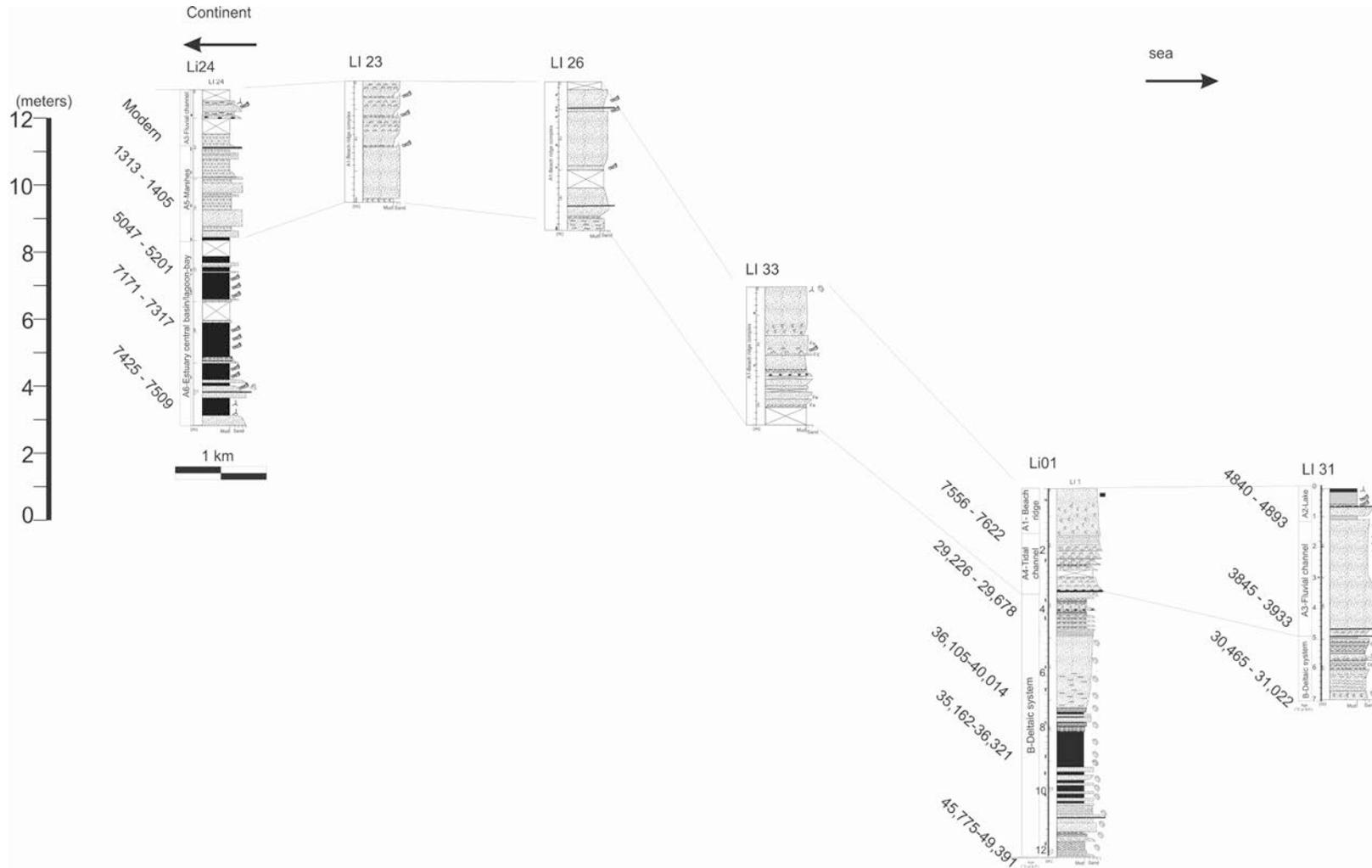
Figure 2 – Topographic correlation among the facies associations identified in the studied cores.
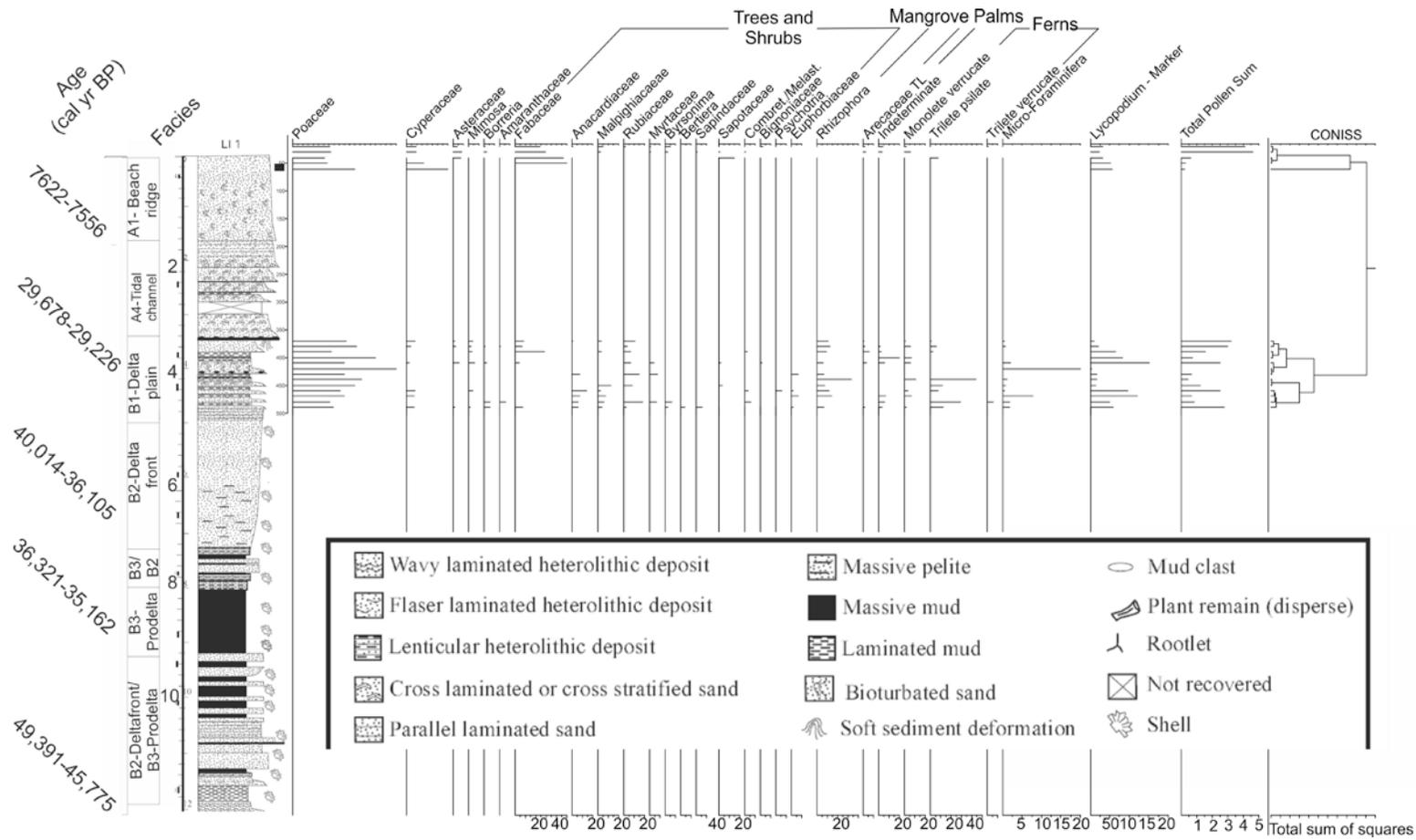
Figure 3 – Stratigraphic description for Li01 with lithological profile, pollen analysis and geochemical variables.

Facies description

      The studied cores record sedimentary successions encompassing massive sand and mud, parallel laminated/cross stratified sand and wave laminated/heterolithic lenticular deposits (Figure 2). Pollen, spore, shell records and δ^{13}C values were added to facies characteristics in order to define nine facies associations.

Delta plain and Estuary central basin/lagoon-bay (A)

      The delta plain deposits occur along the studied cores. They are represented by five facies associations related to high and low energy proximal environments of the deltaic system. The sedimentary deposits of the estuary central basin/lagoon-bay occur only in the base of the Li24.

Facies Association A1- Beach ridge complex

      This facies association occurs in the Li01, between 0 and 1.8 m depth; Li23, between 0 and 2.2 m; Li26, between 0 and 5 m, and along the Li33. It is characterized by deposits of silty to fine-grained sands, with laminated mud and plant remains that grade upward into sandy deposits with cross-laminated or cross-stratified sand, characterizing coarsening upward successions, and forming several coarsening upward cycles. In Li33, it consists of cross-laminated and cross-stratified sands. Association A1 ranges in thickness from a few cm up to 2 m thick (Figure 2).

      Considering the Li01, a pollen assemblage was identified mainly in the finer-grained layers, and it is predominantly characterized by herbs (30-100%) represented by Poaceae (30-60%), Cyperaceae (9-40%) and Asteraceae (0-7%); and trees and shrubs, evidenced mainly by Fabaceae (0-50%) and Sapotaceae (0-17%) pollen.

Facies Association A2- Lake

      This facies association occurs only in the Li31 between 0 and 1.2 m in the upper part of the Facies Association Fluvial Channel. It is characterized by massive mud with plant remain, being interbedded with a sand level in its basis.

Facies Association A3-Fluvial channel

This association occurs in Li24 (0-1.8 m) and Li31 (1.2-4.6 m). It consists of several thin fining upward successions of massive, cross-stratified or cross-laminated, fine- to coarse-grained sands in the Li24 and massive medium to coarse-grained sands in the Li31. These deposits are typically bounded at the base by sharp and erosional surfaces, which might be mantled by a lag of quartz granules or mud clasts. The pollen assemblage in the finer-grained layers in the Li24 presents arboreal (70-86%) pollen as the most representative, followed by herbaceous (10-15%) pollen (Figure 4). The δ^{13}C values range between -28‰ and -26‰. The C/N values are between 6 and 12 (Figures 4 and 5).
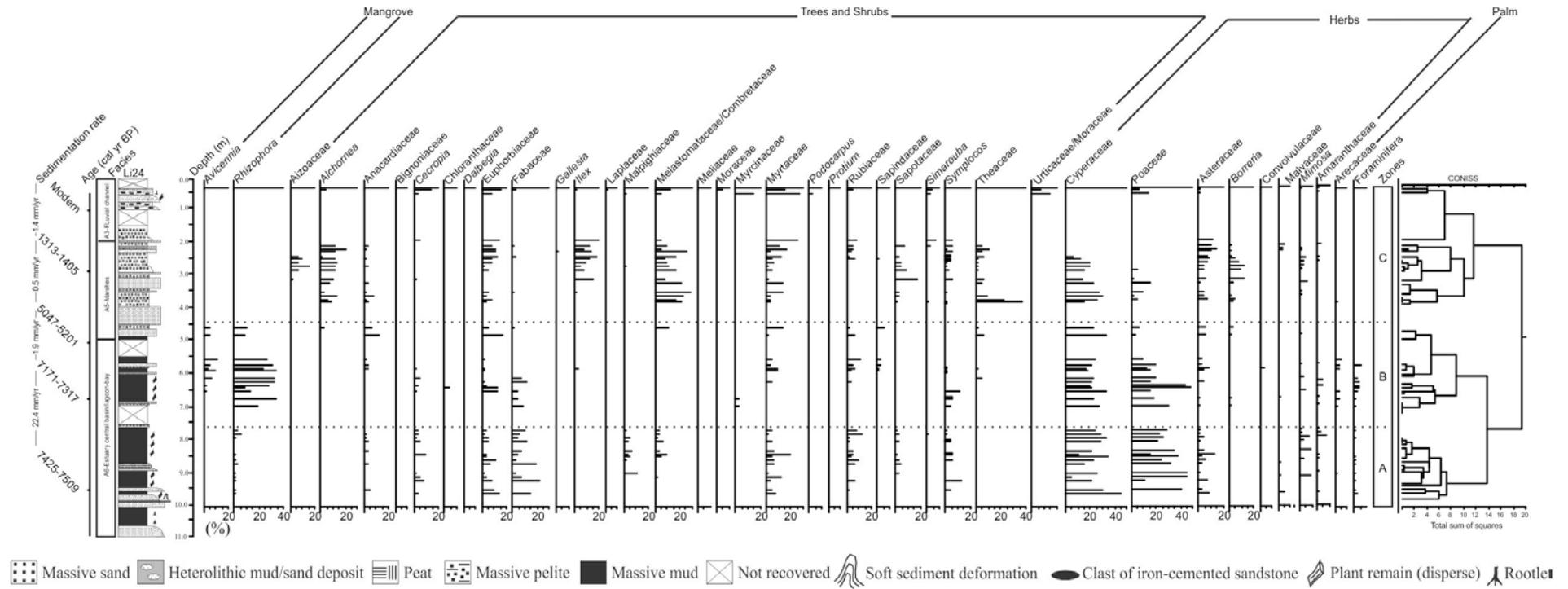
Figure 4 – Stratigraphic description for Li24 with lithological profile, pollen analysis and geochemical variables.
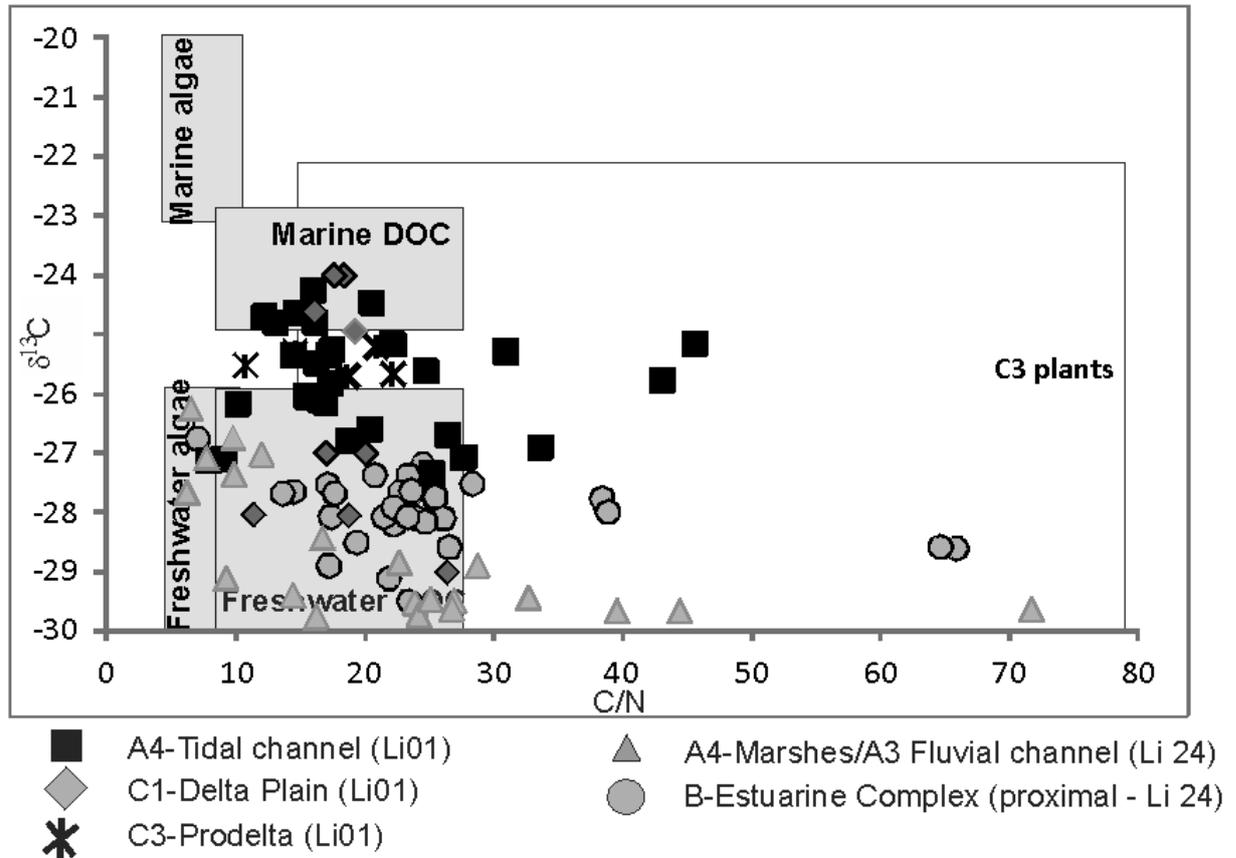
Figure 5 – Diagram illustrating the relationship between $\delta^{13}C$ and C/N for the different sedimentary facies, with interpretation according to data presented by Lamb et al. (2006) and Meyers (2003).

Facies Association A4-Tidal channel

This association is represented by the Li01 (1.6-2.6 m). It consists of several thin fining upward successions of massive, cross-stratified or cross-laminated, fine- to coarse-grained sands (Figure 3). This facies association is characterized by $\delta^{13}C$ values between -28‰ and -24‰, and C/N values between 7 and 46 (Figure 5).

Facies Association A5- Marshes

This association occurs in Li24, between 1.8 and 5 m depth, and presents organic mud (peat layer) interbedded with sand layers. This interval is characterized by arboreal pollen (60-85%), mainly represented by Melastomataceae/Combretaceae (0-30%), *Alchornea* (0-20%), Myrtaceae (0-25%), Euphorbiaceae (0-15%), *Ilex* (0-20%) and Sapotaceae (0-20%),

followed by herbs pollen (20-60%) mainly composed by Cyperaceae (1-30%), Poaceae (0-15%), *Borreria* (0-15%), Aizoaceae (0-20%), Asteraceae (0-15%) and *Mimosa* (0-5%) (Figure 4). The δ^{13}C values range between -26‰ and -30‰, and the C/N values occur between 9 and 71 (Figure 5).

Facies Association A6- Estuary central basin/lagoon-bay

This facies association was recorded in core Li24 between 4.5 and 11 m, represented by massive mud with plant remain, being interbedded with sand levels deposited during the early Holocene. This phase is characterized by arboreal and herbaceous pollen (Figure 4). In contrast to the facies associations from coastal plain, these deposits are dominantly muddy. It grades upward into tidal flat colonized by mangroves with thickening and coarsening upward successions. Trees and shrubs (20-45%) and herbs (35-73%) pollen, followed by mangrove (15-43%) pollen represented by *Rhizophora* (10-30%) and *Avicennia* (5-10%), are preserved, occurring between 4.5 and 7 m in a massive mud with sand. Between 7 and 11 m occurs trees and shrubs (20-60%) and herbaceous (40-75) pollen (Figure 4). This facies association is characterized by δ^{13}C values between -29 and -27‰. The C/N values display a range of variation between 8 and 66 (Figure 5).

Deltaic system (B)

This depositional system is recorded between 5 and 7 m in the Li31 (Figure 2) and 3.4 and 12 m depth in the Li01 (Figure 3). It is represented by three facies associations: B1-Delta Plain, B2-Deltafront and B3-Prodelta.

Facies Association B1-Delta Plain

It is mainly characterized by gray massive and laminated mud with massive sandy levels between 7 and 5 m in the Li31 (Figure 2), and between 3.6 and 5.0 m in Li01 (Figure 3). The pollen assemblages in this interval in the Li01 is characterized by the predominance of herbs pollen (35-96%) represented by Poaceae (36-96%), Cyperaceae (0-8%), Asteraceae (0-5%), *Mimosa* (0-5%), *Borreria* (0-5%) and Amaranthaceae (0-5%). The trees and shrubs are represented mainly by Fabaceae (0-28%), Anacardiaceae (0-14%), Malpighiaceae (0-12%), *Byrsonima* (0-5%), Rubiaceae (0-18%) and Myrtaceae (0-5%). The mangrove is characterized by *Rhizophora* (5-32%). Arecaceae and ferns occurred also during this phase (Figure 3). This

facies association is characterized by $\delta^{13}C$ values between -26 and -25‰. The C/N values display a range of variation between 11 and 23 (Figure 5).

Facies Association B2-Delta Front

This facies association was record along the 5-8 m and 9.2-12 m intervals in the Li01 (Figure 3). Between 5-7.5 m, it presents a dark silt to medium-grained quartz sand, and contains shells (*Olivella mutica, Glycymeris sp., Halistylus columna, Corbula cymellain, Mulinia cleryana, Tivela sp., Strigilla mirabilis and Miltha childrenae*) that may be scattered within the sediment or concentrated in layers. These species are found in sandy-muddy sediments from coastal areas near the mouths of rivers or oceanic islands (Da Costa, 1778; Say, 1822; Dall, 1881; Dall, 1890). The *Mulinia cleryana* may be found in coastal regions, between 0 to 30 m (Orbigny, 1846). The *Tivela sp.* occurs between 0 and 20 m (Link, 1807). *Olivella mutica* is found up to 113 m (Say, 1822). The *Halistylus columna* occurs between 18 and 108 m (Dall, 1890), while the *Strigilla mirabilis* and *Miltha childrenae* may be found between 10 and 65 m depth (Gray, 1825; Orbigny, 1841; Philippi, 1841).

The 7.5-8 m and 9.2-12 m intervals present characteristics of deltafront and prodelta with massive sand and dark clay level. These intervals contain shells (*Anachis isabellei, Natica sp., Olivella floralia, Anadara ovalis*) scattered in the sediment. These species are found in sandy-muddy sediments from coastal areas near the mouths of rivers or oceanic islands (Bruguière, 1789; Orbigny, 1841; Duclos, 1840), while the *Anadara ovalis* may be found in coastal waters associated with carbonate and coral reefs (Bruguière, 1789).

Facies Association B3-Prodelta

It occurs between 8 and 9.2 m, and is represented by massive dark clay. Shells are present along this interval, however, due to its poor preservation, we could not identify them. This facies association is characterized by $\delta^{13}C$ values between -25 and -23‰. The C/N values display a range of variation between 13 and 19 (Figure 5).

Palaeoenvironmental Interpretation

Likely, the base of the Li01 (12-9.2m) characterizes a transition zone between delta front and prodelta accumulated between ~47,500 and ~35,000 cal yr B.P., while the upward succession deposited in 9.2-8 and 8-7.5 m intervals were accumulated in a prodelta and prodelta/delta front environment, respectively (Figure 6). The prodelta is entirely subaqueous and presents the finest-grained portion of a delta. Sediments here are deposited mostly from

suspension, or from dilute turbidity currents flows. The finest sediments are found at the greatest depths, and usually a coarsening-upward signature is present. Relatively slow or intermittent deposition can permit marine organisms to colonize the sediments of the prodelta (Suter, 1994).
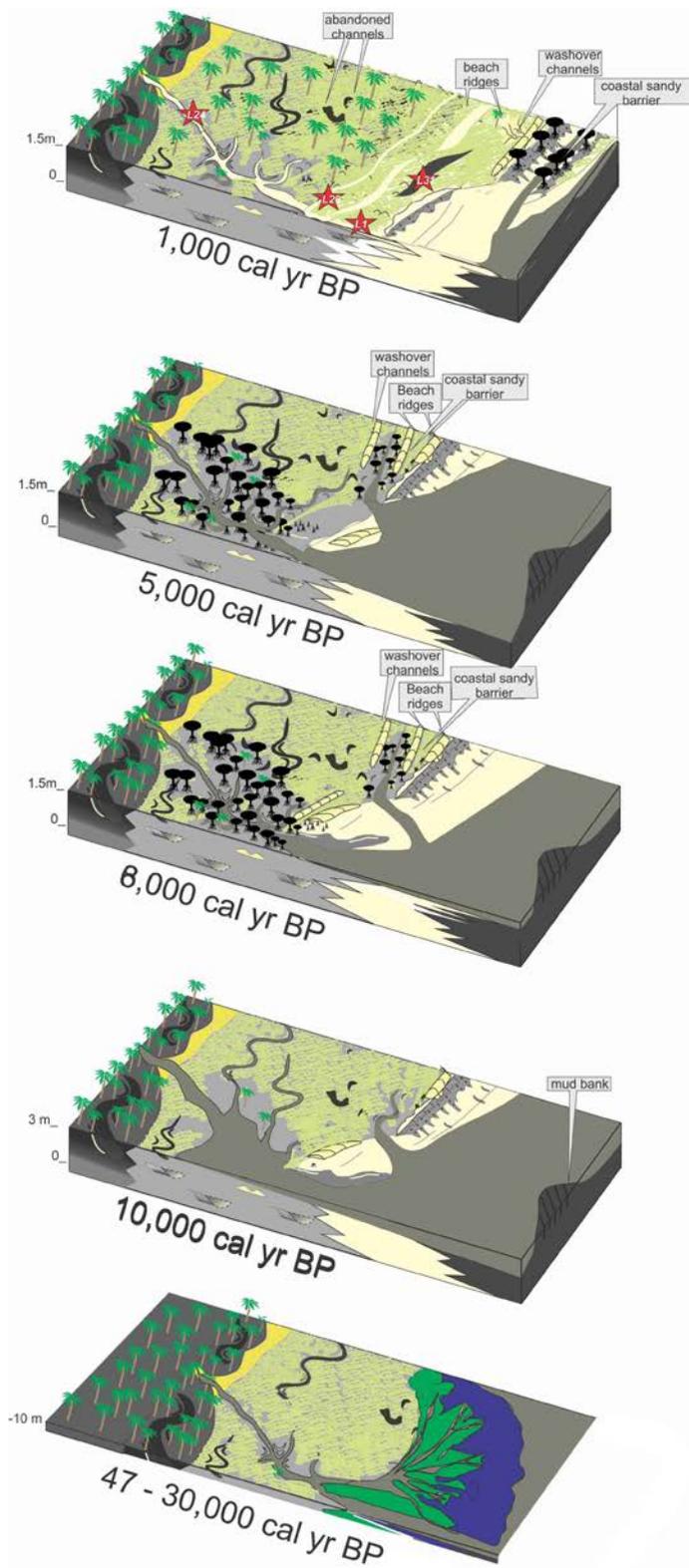
Figure 6 – Schematic representation of successive phases of sediment accumulation and vegetation change in the study area according to relative sea-level changes and sediment supply. (★ cores location).

Probably, the sediments accumulated between 7.5 and 5 m record a delta front that is the transition zone from the fluvial to the marine environment. The delta front includes distal bar silts, distributary mouth bar sands, and redistributed marine deposits such as tidal ridges and shoreface deposits. The process of river mouth sedimentation and seaward fining of sediments results in the deposition of the coarsest material in a short distance from the river mouth, on the upper parts of the delta front (Suter, 1994). The sedimentary deposits between 5 and 3.6 m should represent a delta plain with its tidal flats, lagoons, mangroves and creeks (Suter, 1994; Figures 3 and 6). The deltaic sediments, accumulated between ~47,500 and ~29,000, presents $\delta^{13}C$ values, ranging between -26‰ and -23‰, and C/N values between 11 and 23 (Fig. 5), indicating continental organic matter (C3 plants) and freshwater/marine algae influence (-30‰ to -26‰ and -23‰ to -16‰, respectively, Schidlowski et al., 1983; Meyers, 1994).

Regarding the facies association A6 (Estuary central basin/lagoon-bay) accumulated during the early and middle Holocene (Figure 4), it presents low flow energy, likely in a depositional environment characterized by shallower water protected from direct wave action. However, it is subjected to some currents, as indicated by the presence of lenticular heterolithic mud deposits with sand levels and locally cross laminated sand. The C/N between 8 and 66, and $\delta^{13}C$ values, ranging between -29‰ and -27‰ (Figure 5) indicate continental organic matter (C3 plants) and freshwater algae influence (Figure 5) (Schidlowski et al., 1983; Meyers, 1994), reveling a proximal portion developed in an estuary, and in particular in the central portion of the estuary where the low-energy part occurs (Figure 6). Within an estuary, sediment is coarsest within the marine- and river-dominated zones, and finest in the central zone (Dalrymple et al., 1992). However, the formation of barrier islands during the early Holocene may have contributed to the deposition of this sedimentary deposit, as described by Martin et al. (2003) and França et al. (2013). Then, the facies association A6 may have been deposited in an estuary central basin or in a lagoon-bay influenced by river with its edge colonized by mangroves and herbaceous vegetation passing upward into marshes of the association A4 (Figures 3 and 6).

Today some mangroves occur immediately behind the coastal sandy barriers, which it favor the lagoons development. Its tidal inlets undergo a longshore migration, and the inlet channel is often obliterated as the sands from the adjacent barriers migrate.

The facies associations A1, A2, A3, A4 and A5 are compatible with a delta plain setting, since the studied area today presents several sandy ridges sequence and displays fluvial channels, lake belts and an extensive paleochannel network (Figure 1).

The association A4 in the Li01 (Figure 3) may correspond to a tidal channel established during the early Holocene, and represent the distal portion of the delta plain, relatively more influenced by marine organic matter, as evidenced by the relationship $\delta^{13}C$ and C/N values (Figures 5 and 6). The sandy deposits occur in the tidal channels that run along the length of the estuary (Woodroffe et al., 1989; Dalrymple et al., 1990). Nevertheless, the energy minimum is the site of the finest channel sands. Muddy sediments accumulate primarily in tidal flats and marshes along the sides of the estuary. Then, the facies association A4 is related to marshes (A5) and estuary central basin/lagoon-bay (A6).

The succession A4-A2 in the Li31 likely evidence abandonment phases of a channel by avulsion during the middle Holocene. The concavity of the some abandoned channel, product of avulsion process, may result in formation of lakes (Figures 1 and 2).

The facies association A1 is related to beach ridge complex based on the sandy nature and coarsening upward nature and on the relationship with the other coastal associations. The wave-deposited deposits run parallel to a shoreline, and, generally, inasmuch the relative sea-level fall, the interridges depressions form shallow lakes subjected to overbank crevassing, resulting in an influx of sediment into the lake ending with its siltation as identified in facies association A1 (Figure 2, Li23).

Regarding the pollen, isotopic and C/N data, the sequence of facies association A presents $\delta^{13}C$ values predominantly around -28‰ (Li24, Figure 5) and -26‰ (Li01, Figure 5). The C/N values oscillate between 6 and 72 in the Li24, while in the Li01 presents values between 10 and 45. These values indicate contribution of C_3 plants along the facies association A3 and A4, as evidenced by the pollen analysis (Figure 5).

Climate and sea-level changes during the late Quaternary

Globally, the climates during the Marine Isotope Stage 3 (MIS3, Figure 7), the phase that precedes the LGM, are 2°C warmer than LGM (van Meerbeeck et al., 2008), and in the South America, paleoecology studies indicate that the climate was colder (4 - 5°C lower compared to modern) during the MIS3 (e.g. Colinvaux et al., 2000; Urrego et al., 2005; Whitney et al., 2011).
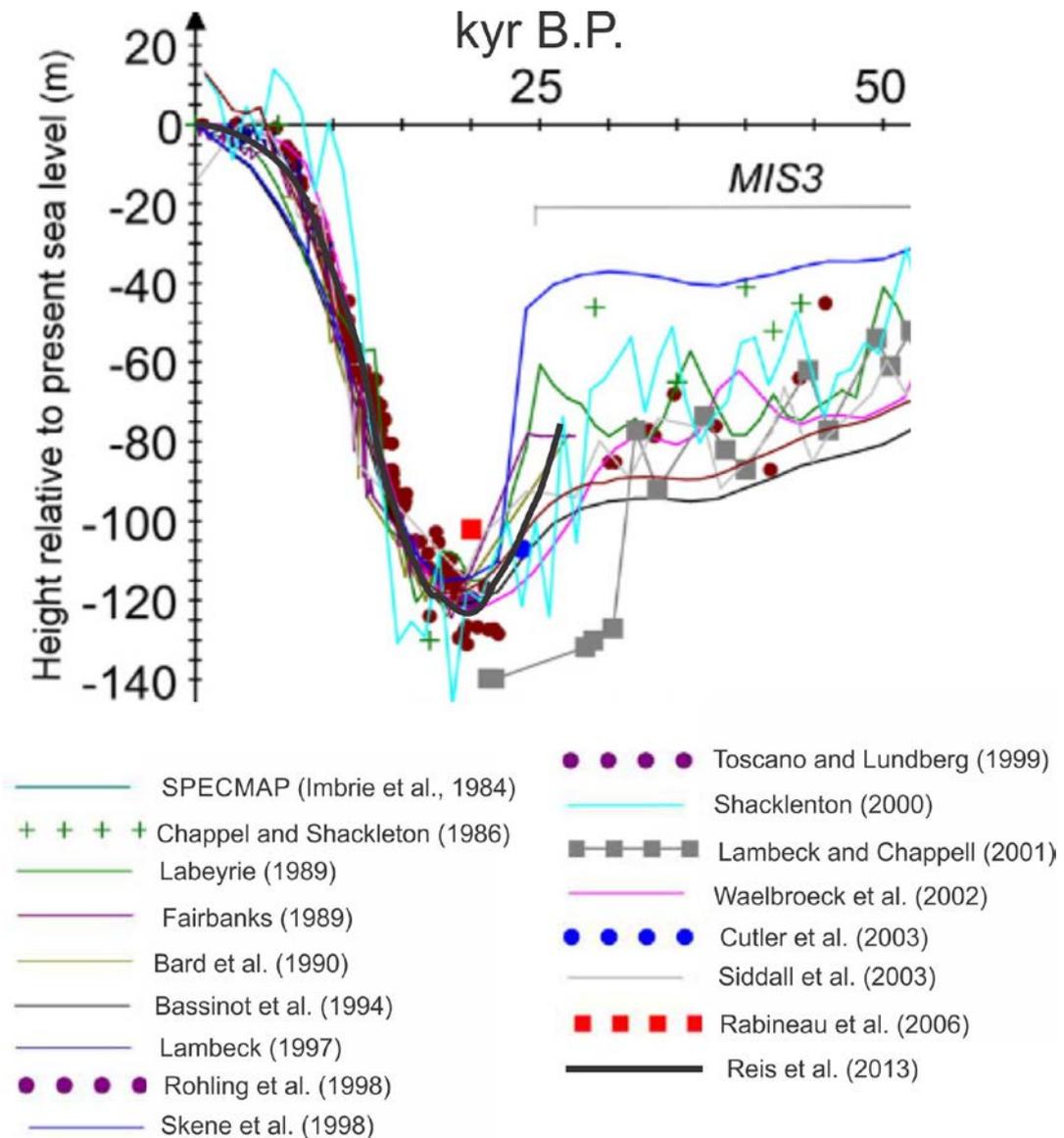
Figure 7 – Global sea-level curves to the late Quaternary.

Regarding the LGM in the South America, the temperatures were between 5 and 9°C colder than present (Wright et al., 1989; Stute et al., 1995; Colinvaux et al., 1996; Klein et al., 1998; Porter, 2001; Ledru and Mourguiart, 2001; Mourguiart and Ledru, 2003a;b; Paduano et al., 2003; Bush et al., 2004). The onset of the LGM is defined as the time sea-levels first approached their minimum levels at about 30 ky cal B.P. (Lambeck et al., 2002). Based on this definition they suggest a duration of 10,000 yrs for the LGM (between 30 and 19 ky cal B.P.). However, Peltier and Fairbanks (2006) suggest that LGM must have started 26 ky cal B.P. having duration of about 5000-7000 years (between 26 and 19 ky cal B.P.).

During that time, the North Atlantic temperature was cooled by 8°C or more and sea ice was more extensive than it is today (e.g. Ruddiman, 2008). Changes in sea-level are

directly related to changes in global ice volume, where with each 1-m rise of sea-level equivalent to 0.4 million km^3 of ice (Ruddiman, 2008). According to global sea-level data based on independent proxies and modelled reconstruction (Figure 7), the global sea-level in 50 ky cal B.P. was between 40 and 80 m below the present, and the sea-level fell gradually until 30 – 25 ky cal B.P., when the it dropped abruptly (100 – 140 m below the modern sea-level) until ~20 ky cal B.P. After the end of the LGM the global sea-level rose dramatically fast (e.g. Fairbanks, 1989; Bard et al., 1990, 1996; Lambeck and Bard, 2000; Lambeck et al., 2002, 2004; Berné et al., 2007; Clark, 2009; Bard et al., 2010; Bard, 2012). Based on geomorphic indicators, similar trend was recorded along the continental shelf of Rio de Janeiro State (Reis et al., 2013).

Considering the present work, the observed succession of facies association B and A might be a product of driving forces regulated by cyclic mechanism leading to a delta, estuary and following to a delta plain environment. Probably, the changes in this depositional environment were driven by the equilibrium between the relative sea-level changes and fluvial sediment supply during the late Pleistocene and Holocene. Probably, this depositional architecture of the late Pleistocene coastal system evolving from a prodelta to a delta front, followed by the delta plain in response to relative sea-level fall between ~47,500 and ~29,400 cal yr B.P. (Figures 6 and 7).

The sediments accumulated during the LGM and the late Pleistocene/Holocene transition were not characterized. Probably, from ~ 29,400 cal yr B.P. to ~7500 cal yr B.P in Li01, and ~30,000 cal yr B.P. to ~3900 cal yr B.P. in Li31, a sedimentary hiatus occurred, related to an erosive event associated to the rapid post glacial sea-level rise. Similar erosive event between ~ 19,000 cal yr B.P. and ~2200 cal yr B.P. has been recorded at the Cardoso Island, southern coastal region of São Paulo State, southeastern Brazil (Pessenda at al., 2012).

Although the stratigraphic sequence studied present compatibility with the trends of global sea-level changes, the position of the old sea-level, suggested by sedimentary deposits interpreted as a deltaic system, is at least 20 meters above the sea-level of the MIS3 stage. A tectonic uplift in the study area during the late Quaternary may justify this difference in the paleo sea-levels, since the late Pleistocene marine terrace deposits in northeastern Brazil suggests that the littoral zone may have been uplifted by at least 10 – 12 m since 120 ky B.P. (Barreto et al., 2002). In addition, regressive–transgressive events recorded along the Brazilian coast likely responded to a combination of eustatic sea-level fluctuations and local factors such as tectonic activity (Rossetti et al., 2013). It may contribute to accumulation of old marine deposits close to the modern coastline (Rossetti et al., 2011), as recorded in the

Li01 with marine/brackish organic matter, marine shells and mangrove pollen along the deltaic system (Figure 3).

Regarding the estuary with mangroves recorded in the Li24, it was formed during the high relative sea-level of the Holocene. Likely, these environments were formed during the early and middle Holocene as a response of an eustatic sea-level rise that resulted in significant changes in the coastal geomorphology (Figure 6). During the early Holocene, the arboreal and herbaceous vegetation dominated the coastal plain, and the equilibrium between the relative sea-level and fluvial sediment supply created conditions to the development of an estuarine system with fluvial and tidal channels, and tidal flats colonized by mangroves (Figure 6).

The upward succession composed by the transition estuarine complex with mangrove into the coastal plain colonized by marshes in the Li24 suggests a decrease of marine influence and form the regressive part of the cycle after the post glacial sea-level rise. Thus, the upper sequence of the Li24 (A5 and A3) should have been accumulated following a relative sea-level fall or a high fluvial sediment supply during the middle and late Holocene. Considering the increase in the sand input by fluvial channels, the fluvial sediment was reworked by wave and caused the sandy ridges with replacement of mangroves by the groups of trees/shrubs and herbaceous vegetation according to a marine regression.

Sea-level changes and fluvial sediment supply

According to Posamentier et al. (1992), the term "regression" describes a retreat of the sea and a concomitant seaward expansion of the land. Regression can occur in two specific ways: (1) if sediment flux delivered to the shoreline exceeds the amount of space added for sediment to fill; and (2) if there is a relative sea-level fall. In either case, the shoreline migrates seaward. In the situation 1, sufficient sediment is entering into the coastal system so as to overwhelm the amount of space available. This can occur during stillstands or rises of relative sea-level (which is a function of sea surface movement, i.e., eustasy and sea floor movement, the latter due to tectonics, thermal cooling, loading by sediments or by water, and sediment compaction) and is referred to as a "normal" regression. However, in certain cases, regression may not occur despite high volumes of sediment flux, if the dispersive energy of the littoral environmental (i.e., waves or tidal currents) is high. Under these circumstances, supplied sediment is distributed over a widespread area commonly beyond the immediate area, thus preventing progradation of the shoreline.

When no sediment is delivered to the shoreline during a relative sea-level fall, the regression is said to be forced because a seaward shift of the shoreline must occur, even if the volume of sediment supplied is zero. This is in marked contrast to "normal" regression, which occur in response to the balance between variations of sediment flux and new space added (Posamentier et al., 1992).

In the first situation, regression can occur under conditions of eustatic sea-level rise, since the rate of sediment flux is greater than the rate of increase of accommodation. Consequently, in areas of relatively high sediment flux, such as deltas, regression will continue longer following a sea-level rise, than in areas of relatively low sediment flux. Thus, despite of the eustatic sea-level rise recorded to the southeastern Brazilian littoral during the early and middle Holocene, followed by a relative sea-level fall (e.g., Suguio et al., 1985; Angulo et al., 2006), the high sediment flux of the Doce and Barra Seca River may have contributed to the regressive sequence since the middle Holocene.

Conclusion

Between at least ~47,500 and ~29,400 cal yr B.P., a deltaic system was developed in response mainly to eustatic sea-level fall of the MIS3 stage. Even though the stratigraphic sequence studied presents compatibility with the trend of global sea-level fall, the position of old sea-level, suggested by the deltaic system, is above the sea-level for the MIS3 stage. Probably, a tectonic uplift occurred during the late Quaternary and raised this sedimentary succession. The rapid post glacial sea-level rise caused the erosion of the sedimentary sequences accumulated during the LGM and the late Pleistocene/Holocene transition in the studied area. This eustatic sea-level rise produced a marine incursion with invasion of embayed coast and broad valleys, and favored the evolution of an estuary with wide tidal mud flats occupied by mangroves between at least ~7400 and ~5100 cal yr B.P. During the late Holocene, the high river sand supply and/or the relative sea-level fall lead to seaward and downward translation of the shoreline during normal/forced regression, producing progradational deposits with mangrove shrink and expansion of marsh colonized by herbaceous vegetation.

Therefore, the case study of the delta plain of Doce River illustrates a stratigraphic sequence with development of deltaic systems and estuary produced by the interplay of eustatic sea-level fluctuations and local factors such as sediment supply and tectonic activity.

CHAPTER V:

MANGROVE VEGETATION CHANGES ON HOLOCENE TERRACES OF THE DOCE RIVER, SOUTHEASTERN BRAZIL

Abstract

High-resolution sedimentological, geochemical and pollen analysis on sediment core from the coastal plain of the Doce River, southeastern Brazil, revealed changes in the depositional system and vegetation caused by combined action of oscillations in relative sea-level (RSL) and sedimentary supply during the Holocene. Two main phases were discerned using sedimentary features, $\delta^{13}C$, $\delta^{15}N$, total organic carbon (TOC), total nitrogen (N), C/N and cluster analysis of pollen data, temporally synchronized with radiocarbon age dating. The data indicates the presence of a lagoon system surrounded by a tidal plain colonized by mangroves and its sedimentary organic matter sourced from C_4 plants between ~8050 and ~7115 cal yr BP. However, during the mid and late-Holocene the mangroves shrank and freshwater vegetation expanded (C_3 plants), probably, due to a marine regression. During this phase, the development of a lacustrine environment was followed by the colonization of herbs, trees and shrubs. The continuous sediment infilling into the lake allowed the expansion of a herbaceous plain as seen today. This geomorphologic and vegetation evolution is in agreement with the mid-Holocene RSL maximum above present RSL and subsequent fall to the present time.

Introduction

Several studies have presented coastal environmental shifts in response to Holocene sea-level changes (Woodroffe, 1981; Parkinson et al., 1994; Blasco et al., 1996; Fujimoto et al., 1996; Behling et al., 2001, 2004; Yulianto et al., 2004, 2005; Cohen et al., 2005a,b; Ellison, 2005; Horton et al., 2005; Engelhart et al., 2007; Monacci et al., 2009, 2011; Guimarães et al., 2012; 2013; Smith et al., 2012; Cohen et al., 2012). The effect of relative sea-level (RSL) changes is apparent in coastal environments, where significant geomorphological changes (Giannini et al., 2007) extend to the mangrove dynamics (Behling et al., 2001, 2004; Lara et al., 2002; Cohen and Lara, 2003; Cohen et al., 2004; 2005a,b; Vedel et al., 2006; França et al., 2012; Guimarães et al., 2012; Smith et al., 2012). The expansion or contraction of mangrove areas is dependent on temperature, soil type, salinity, inundation frequency, sediment accretion, tidal and wave energy (Lugo and Snedaker, 1974). Specifically the mangrove has special physiological and morphological adaptations that allow it to grow in intertidal environments (Blasco et al., 1996; Cahoon and Lynch, 1997; Alongi, 2008; Sanders et al., 2012). Thus this ecosystem may be used as indicator of coastal change and RSL fluctuations (Blasco et al., 1996).

Along the Brazilian coast, mangroves are found from the extreme northern Brazilian coast in the Oiapoque River (04°20′N) to Laguna (28°30′S) in the southern coast (Schaeffer-Novelli et al., 2000). In northern Brazil the mangroves are extremely irregular and jagged, occurring throughout bays and estuaries (Souza-Filho et al., 2006), with meso- and macrotidal ranges (tidal range of 2 to 4 m and 4 to 6 m, respectively). On the southeastern and southern coast, mangroves are restricted to microtidal (tidal range below 2 m) bays, lagoons or estuarine inlets (Schaeffer-Novelli, 1990), which are strongly controlled by climate and oceanographic characteristics (Soares et al., 2012).

Some studies have shown post-glacial sea-level rise at the Brazilian littoral (Bittencourt et al., 1979; Suguio et al., 1985; Angulo and Suguio, 1995; Martin et al., 1996; Angulo and Lessa, 1997; Angulo et al., 1999; Bezerra et al., 2003; Martin et al., 2003; Angulo et al., 2006), which inundated inland valleys (Martin et al., 1996; Scheel-Ybert, 2000; Cohen et al., 2005a,b; Souza-Filho et al., 2006), causing changes in depositional systems and also in mangrove area (Scheel-Ybert, 2000; Cohen et al., 2005a,b; Amaral et al., 2006, 2012; Smith et al., 2012; Guimarães et al., 2012).

Investigations in northern Brazil utilizing sedimentological, palynological and geochemical data revealed displacement of the mangrove ecosystem during the Holocene. This shift is attributed to climate, river discharge and RSL changes (Behling et al., 2004;

Cohen et al., 2005a, 2008, 2009; Lara and Cohen, 2009; Smith et al., 2011, 2012; Guimarães at al., 2012; França et al., 2012). However, in southeastern Brazil, the mangrove dynamics are mainly related to RSL changes (Buso Junior, 2010; Buso Junior et al., 2013 – *in press*) and sediment transport (Amaral et al., 2006).

For the southeastern Brazilian coast environmental reconstructions based on inter-proxy analysis are still scarce, and the response of mangrove ecosystems to Holocene sea-level changes remains poorly understood. In this work we present a study about mangrove development on the coastal plain of the Doce river, State of Espírito Santo, southeastern Brazil, during the Holocene, recorded by multiple proxies such as sedimentary features, δ^{13}C and δ^{15}N, C/N , pollen data and radiocarbon dating.

Modern settings

Study area and geological setting

The study site is located in the coastal plain between two large rivers (Figure 1), Doce and São Mateus, northern Espírito Santo – Brazil, running along a nearly N-S section between Conceição da Barra and Barra do Riacho (Suguio et al., 1982; Bittencourt et al., 2007). The Holocene sedimentary history in this sector is strongly controlled by RSL changes, fluvial supply and longshore transport. The formation of a barrier island/lagoonal system began about 7000 yr BP (Suguio et al., 1982; Martin et al., 1996; Martin et al., 2003).

The study area is composed of a Miocene age plateau of Barreiras Formation continental deposits, whose surface is slightly sloping to the ocean. The site is characterized by the presence of many wide valleys with flat bottoms, resulting from Quaternary deposition of silty sediments (Martin et al., 1996). The study area is part of a larger area of tectonically stable Precambrian crystalline rocks. Four geomorphological units are recognized in the area: (1) a mountainous province, made up of Precambrian rocks, with a multidirectional rectangular dendritic drainage net; (2) a tableland area composed of Barreiras Formation constituted by sandstones, conglomerates and mudstones attributed mainly to Neogene fluvial and alluvial fan deposits, but possibly including deposits originating from a coastal overlap associated with Neogene marine transgressions (Arai, 2006; Dominguez et al., 2009). The drainage catchment slopes gently down towards the sea; and (3) a coastal plain area, with fluvial, transitional and shallow marine sediments, which were deposited during RSL changes (Martin and Suguio 1992) and (4) an inner continental shelf area (Asmus et al., 1971).
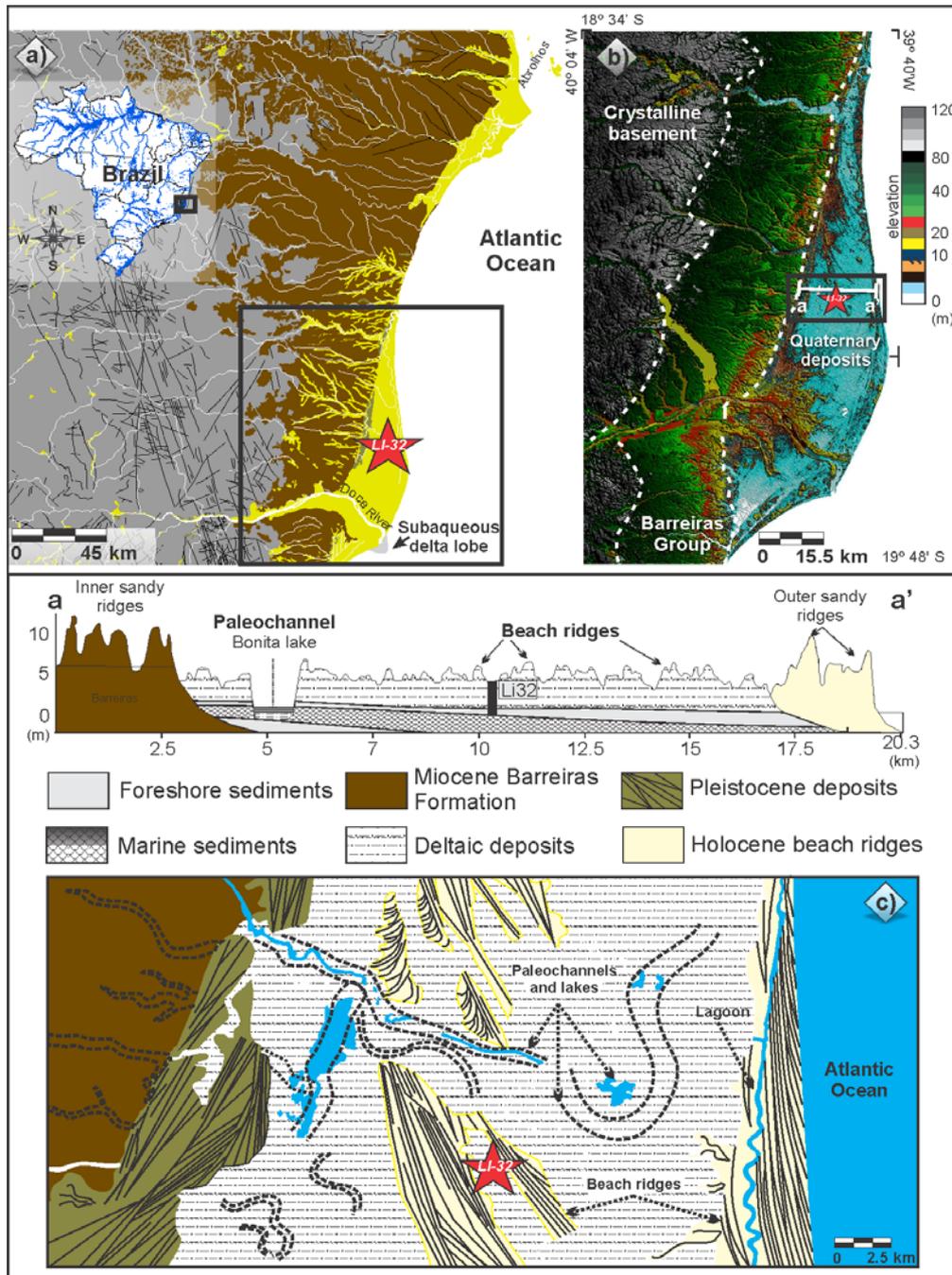
Figure 1 – Location of the study area: a) Miocene Barreiras Formation and coastal plain of the Doce River; b) RGB Landsat composition – SRTM, with a topographical profile obtained from SRTM digital elevation data illustrating a large area slightly more depressed on coastal plain of the Doce River. Note a morphometric profile along the main geological features and morphological units (a-a'); c) palaeodrainage networks preserved, with lagoons and lake system originated at the Holocene. Note the presence of Pleistocene deposits. Observe also, the beach ridges which are related to coastal progradation.

Climate

The region is characterized by a warm and humid tropical climate with annual precipitation averaging 1400 mm (Peixoto and Gentry, 1990). Precipitation generally occurs

in the summer with a dry fall-winter season, controlled by the position of the Inter Tropical Convergence Zone (ITCZ) and the position of the South Atlantic Convergence Zone (SACZ) (Carvalho et al., 2004). The area is entirely located within the South Atlantic trade winds belt (NE-E-SE) that is related to a local high-pressure cell and the periodic advance of the Atlantic Polar Front during the autumn and winter, generating SSE winds (Dominguez et al., 1992, Martin et al., 1998). The rainy season occurs between the months of November and January with a drier period between May and September. The average temperature ranges between 20º and 26º C.

Vegetation

The region is composed mainly of tropical rainforest, where the most representative plant families are Annonaceae, Fabaceae, Myrtaceae, Sapotaceae, Bignoniaceae, Lauraceae, Hippocrateaceae, Euphorbiaceae, and Apocynaceae (Peixoto and Gentry, 1990). In the sandy coastal plain, vegetation is characterized by palm trees as well as orchids and bromeliads that grow on the trunks and branches of larger trees. *Ipomoea pes-caprae*, *Hancornia speciosa*, *Chrysobalanus icaco*, *Hirtella Americana* and *Cereus fernambucensis* are also found. The coastal plain of the Doce River is characterized by forest pioneering freshwater species such as *Hypolytrum* sp., *Panicum* sp and also brackish/marine water species such as *Polygala cyparissias*, *Remiria maritima*, *Typha* sp., *Cyperus* sp., *Montrichardia* sp., *Tapirira guianensis* and *Symphonia globulifera*. A mangrove dominated ecosystem is also present, characterized by *Rhizophora mangle*, *Laguncularia racemosa* and *Avicennia germinans*, which are currently restricted to the northern littoral part of the coastal plain (Bernini et al., 2006). Herbaceous vegetation dominates the sampling site, represented by Araceae, Cyperaceae and Poaceae with some trees and shrubs on edge of the plain (Figure 2).
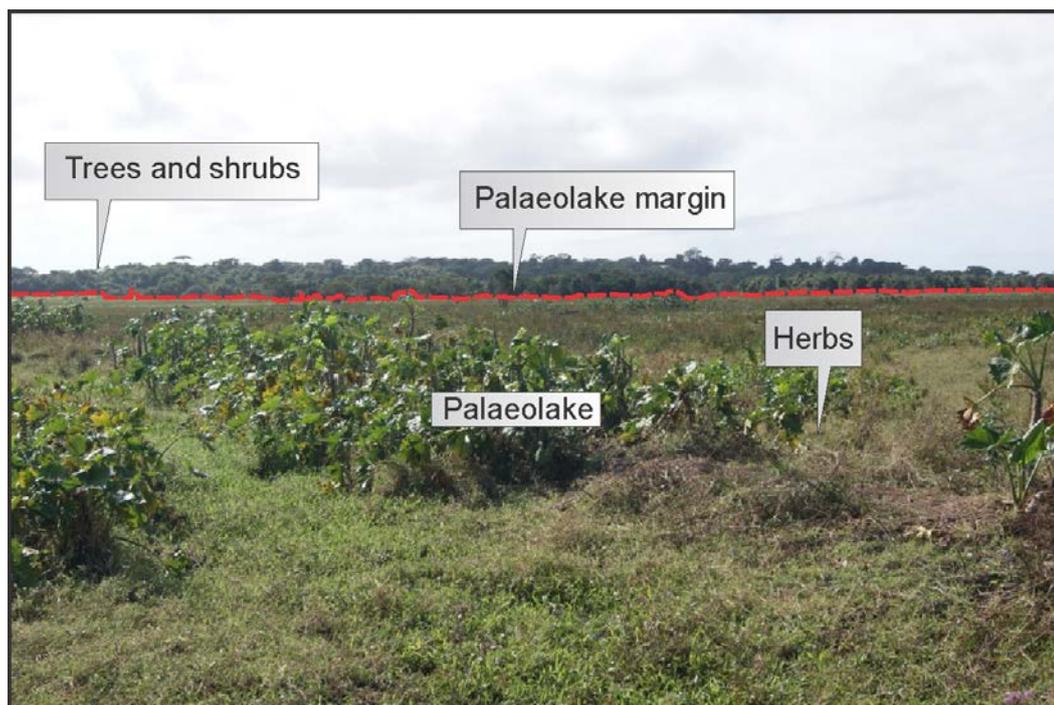
Figure 2 – The sharp contact between arboreal vegetation and herbaceous vegetation indicates the transition zone between palaeolake and the edge at the coastal plain of the Doce River. The herbs are the current vegetation which has been developed during the past 3,043 cal yr BP on the palaeolake.

Materials and methods

Field work and sampling processing

A LANDSAT image acquired on July 2011 was obtained from INPE (National Institute of Space Research, Brazil). A three-colour band composition (RGB 543) image was created and processed using the SPRING 3.6.03 image processing system to discriminate geological features. Topographic data were derived from SRTM-90 data, downloaded from USGS Seamless Data Distribution System (http://srtm.usgs.gov/data/obtainingdata.html). Imagem interpretation of elevation data was carried out using software Global Mapper 12.

The fieldwork was carried out in July 2011. The sediment core LI-32 (5.75 m) (S 19° 11' 56.1"/ W 39° 48' 1.8") was taken between Holocene sandy ridges (Figure 1) from a herbaceous plain using a Russian Sampler (Cohen, 2003). It is located approximately 30 km from Doce River and 10 km from the current southeastern wave-dominated coast (Dominguez et al., 2009). The geographical position of the core was determined by GPS (Reference Datum: SAD69).

Facies description

The core was X-rayed in order to identify internal sedimentary structures. As recorded in the figure 3, without the radiography of the core, would not be possible to evidence such structures. Grain size was determined by laser diffraction using a Laser Particle Size SHIMADZU SALD 2101 in the Laboratory of Chemical Oceanography/UFPA. Prior to identify the grain size, approximately 0.5 g of each sample was immersed in H_2O_2 to remove organic matter and residual sediments were disaggregated by ultrasound (França, 2010). The grain-size scale of Wentworth (1922) was used in this work with sand (2-0.0625 mm), silt (62.5-3.9 µm) and clay fraction (3.9-0.12 µm). Although the equipment presents reading range between 1000 and 0.03 µm, in the studied core was not recorded sediment fraction higher than 1 mm or lower than 0.12 µm. Following the methods of Harper (1984) and Walker (1992), facies analysis included description of color (Munsell Color, 2009), lithology, texture and structure. The sedimentary facies were codified following Miall (1978).
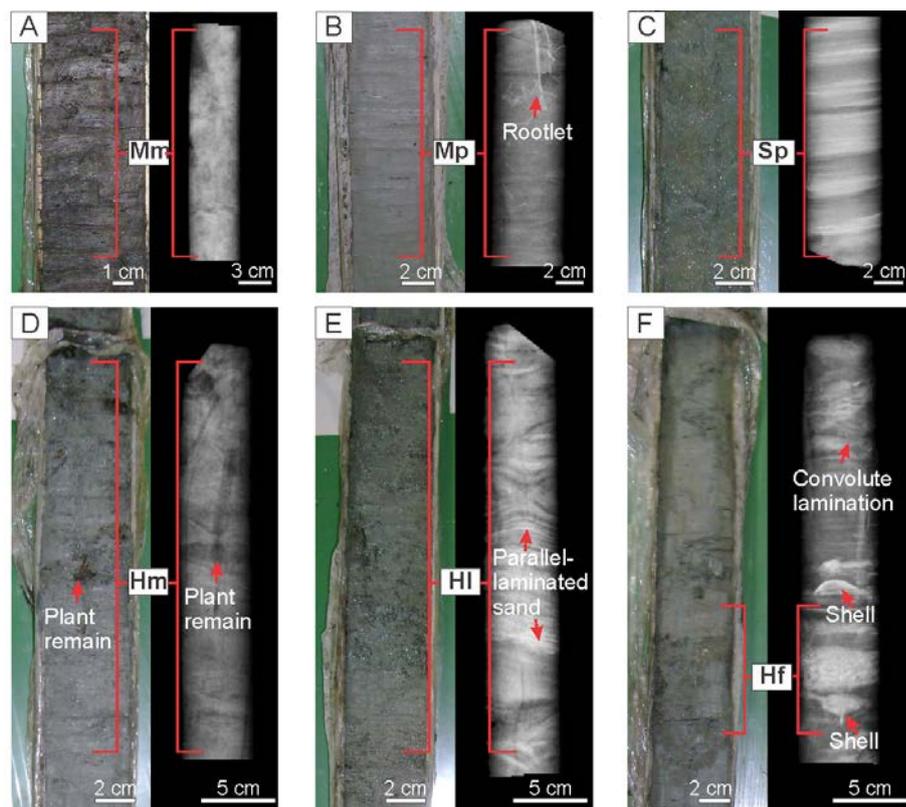
Mm - Massive mud **Mp** - Parallel laminated mud **Hm** - Heterolithic mud/sand deposit
Sp - Parallel-laminated sand **Hl** - Lenticular heterolithic muddy silt **Hf** - Flaser or wavy heterolithic deposit

Figure 3 – The X-ray of the core with examples of sedimentary facies of the tidal plain deposits, illustrating: a) massive mud (facies Mm); b) parallel laminated mud (facies Mp), with rootlets and root marks; c) parallel-laminated sand (facies Sp); d) heterolithic mud/sand deposit with plain remain (facies Hm); e) lenticular heterolithic muddy silt with cross lamination (facies Hl); f) sandy layer, heterolithic mud/sand deposit with convolute lamination and shells (facies Hf).

Palynological analysis

Considering the interpretative significance of pollen data, there often exists two pollen components in sediment—pollen from ''local'' vegetation (the crown of the hat), and background pollen from ''regional'' vegetation (the brim of the hat) (Andersen 1967; Janssen 1966, 1973; Sugita, 1994). The terms are useful, even though the distinction cannot be drawn sharply: the transition between the crown and brim is gradual, and the sizes of the crown and brim will differ for each pollen taxon (Davis, 2000).

The pollen records of sediment cores in lakes assume that pollen accumulating in a lake represents the vegetation on all sides of the lake, on the assumption that breezes blow from various directions and the drainage basin area of the lake receive the pollen production. Thus, the strength of the pollen signal from each vegetation is distance-weighted (e.g. Davis, 2000). According to Cohen et al. (2008), pollen profiles from tidal plains present a smaller spatial representativeness of the vegetation than pollen records from lakes. Considering the palaeo-lagoon described in this work as a shallow body of water separated from the ocean by a barrier islands, the pollen signal in its bottom sediment should reflect the regional palaeovegetation, while the pollen preserved in foreshore sediment may represent the pollen transported by rivers and tidal channels to the littoral.

For pollen analysis 1.0 cm^3 samples were taken at 5.0 cm intervals downcore, for a total of 116 samples. All samples were prepared using standard pollen analytical techniques including acetolysis (Faegri and Iversen, 1989). Sample residues were mounted on slides in a glycerin gelatin medium. Pollen and spores were identified by comparison with reference collections of about 4,000 Brazilian forest taxa and various pollen keys (Salgado-Laboriau, 1973; Absy, 1975; Markgraf and D'Antoni, 1978; Roubik and Moreno, 1991; Colinvaux et al., 1999) jointly with the reference collection of the Laboratory of Coastal Dynamics – Federal University of Pará and ^{14}C Laboratory of the Center for Nuclear Energy in Agriculture (CENA/USP) to identify pollen grains and spores. A minimum of 300 pollen grains were counted for each sample. The total pollen sum excludes fern spores, algae, and foraminiferal tests. Pollen and spore data are presented in pollen diagrams as percentages of the total pollen sum. The *taxa* were grouped according to source: mangroves, trees and shrubs, palms, herbs and aquatics pollen. The software TILIA and TILIAGRAF were used for calculation and to plot the pollen diagram (Grimm, 1990). CONISS was used for cluster analysis of pollen *taxa*, permitting the zonation of the pollen diagram (Grimm, 1987).

Isotopic and chemical analysis

A total of 232 samples (6-50 mg) were collected at 5 cm intervals from the sediment core. Sediments were treated with 4% HCl to eliminate carbonate, washed with distilled water until the pH reached 6, dried at 50°C, and finally homogenized. These samples were analyzed for total organic carbon and nitrogen, carried out at the Stable Isotope Laboratory of the Center for Nuclear Energy in Agriculture (CENA/USP). The results are expressed as a percentage of dry weight, with analytical precision of 0.09% (TOC) and 0.07% (TN), respectively. The ^{13}C and ^{15}N results are expressed as δ^{13}C and δ^{15}N with respect to VPDB standard and atmospheric air, using the following notation:

$$\delta^{13}C\ (‰) = [(R_{1sample}/R_{2standard}) - 1] \cdot 1000$$

$$\delta^{15}N\ (‰) = [(R_{3sample}/R_{4standard}) - 1] \cdot 1000$$

where $R_{1sample}$ and $R_{2standard}$ are the ^{13}C/^{12}C ratio of the sample and standard, and $R_{3sample}$ and $R_{4standard}$ are the ^{15}N/^{14}N, respectively. Analytical precision is ±0.2‰ (Pessenda et al., 2004).

Radiocarbon dating

Based on stratigraphic discontinuities that suggest changes in the tidal inundation regime, four bulk samples (10 g each) were selected for radiocarbon analysis. In order to avoid natural contamination by shell fragments, roots, seeds, etc., (e.g. Goh, 2006), the sediment samples were checked and physically cleaned under the stereomicroscope. The organic matter was chemically treated to remove the presence of a younger organic fraction (fulvic and/or humic acids) and to eliminate adsorbed carbonates by placing the samples in 2% HCl at 60 °C for 4 hours, followed by a rinse with distilled water to neutralize the pH. The samples were dried at 50 ºC. A detailed description of the chemical treatment for sediment samples can be found in Pessenda et al. (2010 and 2012).

A chronologic framework for the sedimentary sequence was provided by conventional and accelerator mass spectrometer (AMS) radiocarbon dating. Samples were analyzed at the ^{14}C Laboratory of CENA/USP, LACUFF (Fluminense Federal University) and at UGAMS (University of Georgia – Center for Applied Isotope Studies). Radiocarbon ages were normalized to a δ^{13}C of -25‰ VPDB and reported as calibrated years (cal yr BP) (2σ) using CALIB 6.0 (Reimer et al., 2009). The dates are reported in the text as the median of the range of calibrated ages (Table 1).

Table 1 – Sediment samples selected for Radiocarbon dating and results from LI-32 core (coastal plain of the Doce River) with material, depth, δ^{13}C, ^{14}C conventional and calibrated ages (using Calib 6.0; Reimer et al., 2009).

Cody site and laboratory number	Depth (m)	Material	Ages (^{14}C yr BP, 1σ)	Ages (cal yr BP, 2σ deviation)	Median of age range (cal yr BP)	Sedimentation rates
LACUFF13019	0.67-0.72	Bulk sed.	2877 ± 79	3246-2840	3043	0.2 mm/yr
LACUFF12039	1.40-1.45	Bulk sed.	6237 ± 66	7278-6955	7116	0.2 mm/yr
UGAMS11695	3.40-3.45	Bulk sed.	6330 ± 30	7318-7172	7245	15.0 mm/yr
UGAMS11694	4.30-4.35	Bulk sed.	6380 ± 30	7339-7259	7300	16.0 mm/yr
LACUFF12040	5.45-5.50	Bulk sed.	7186 ± 54	8161-7933	8047	1.50 mm/yr

Results

Radiocarbon date and sedimentation rates

The radiocarbon dates are shown in Table 1 (range since ~ 8050 cal yr BP) and no age inversions were observed. The sedimentation rates were based on the ratio between the depth intervals (mm) and the time range. The calculated sedimentation rates are 1.5 mm/yr (5.50-4.35 m), 16 mm/yr (4.35-3.45 m), 15 mm/yr (3.45 - 1.45 m), 0.2 mm/yr (1.45- 0.72 m) and 0.2 mm/yr (0.72-0 m). Although the rates are non linear between the dated points, they are same magnitude order with the vertical accretion range of 0.1 to 10 mm yr^{-1} of mangrove forests reported by other authors (e.g. Cahoon and Lynch, 1997; Bird, 1980; Spenceley, 1982; Behling et al., 2004; Cohen et al., 2005a; 2008; 2009; Guimarães et al., 2010; Vedel et al., 2006).

Facies, pollen description and isotopes values from sediment core

The sediment is composed mostly of greenish gray or dark brown sandy silt with grain size fining upward. The sediment facies are characterized by massive mud, parallel laminated mud, cross stratified sand, parallel-laminated sand, lenticular and heterolithic mud/sand, with peat present near the surface (Figures 3 and 4). The texture, grain size, sedimentary structures and pollen content, complemented with isotopic and geochemical data (δ^{13}C, δ^{15}N, TOC, N and C/N), define four facies associations representative of foreshore, lagoon, lake, and herbaceous plain environments (Table 2).
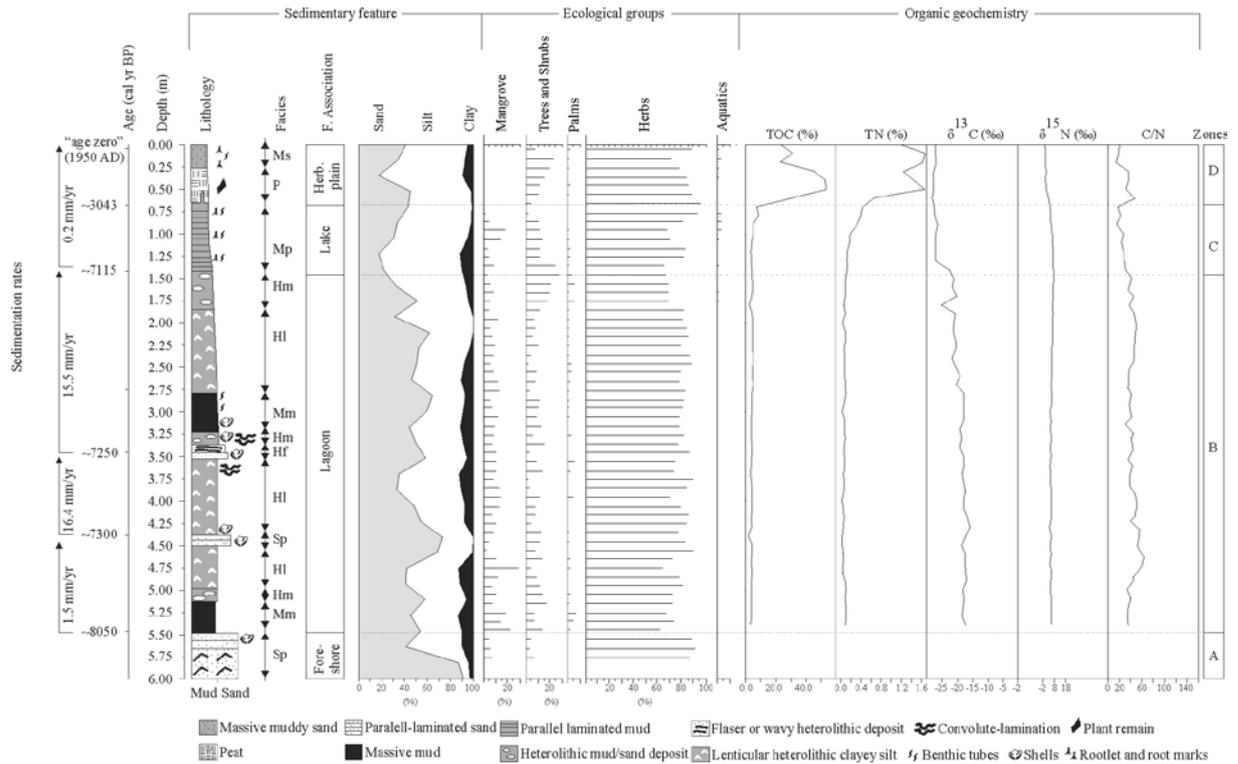
Figure 4 – Summary results for sediment core (LI-32): variation as a function of core depth showing chronological and lithological profile with sedimentary features and facies, pollen analysis with ecological groups, organic geochemical variables and characteristics of organic matter influence. Pollen data are presented in pollen diagrams as percentages of the total pollen sum.

Table 2 – Summary of facies association with sedimentary characteristics, pollen groups and geochemical data.

Facies association	Facies description	Pollen predominance	Geochemical data	Interpretation
A	Fine to medium-grained, parallel-laminated sand (facies Sp) and cross-stratified (facies Sc). Greenish gray sand with shells and poorly sorted.	Herbs, mangrove, trees and shrubs		Foreshore
B	Massive mud (facies Mm) greenish gray, with many roots and root marks. Lenticular to streaky (facies Hl), heterolithic mud with sand deposit (facies Hm). Silty sand and sandy silt, fine to medium-grained poorly sorted and locally flaser (facies Hf) with parallel-laminated sand (facies Sp) and with also massive sand, shells and convolute lamination.	Herbs, mangrove, trees and shrubs	$\delta^{13}C$= -27 to -15‰ $\delta^{15}N$= +3.6 to +7‰ TOC= 1.7 to 5.2% C/N= 30 to 60	Lagoon
C	Parellel-laminated mud (facies Mp), yellowish brown, with many roots and root marks and dwelling structures and sandy silt.	Herbs, trees, shrubs and mangrove	$\delta^{13}C$= -28 to -23‰ $\delta^{15}N$= +4.5 to +7‰ TOC= 3.4 to 8.7% C/N= 15 to 32	Lake
D	Plastic, massive mud and some sandy silt, gray to dark gray and green, with many roots and root marks (facies Ms) and peat deposit (P).	Herbs, trees and shrubs	$\delta^{13}C$= -28 to -26‰ $\delta^{15}N$= -0.14 to +7‰ TOC= 7.4 to 53% C/N= 16 to 47	Herbaceous plain

Facies association A (foreshore)

Facies association A occurs in the base of the sediment core until ~8050 cal yr BP (Figure 4). It consists mainly of fine to medium-grained sands which are poorly selected, sand cross-stratified (facies Sc) and parallel-laminated sand (facies Sp), with locally rippled sand and cross-lamination. Shell fragments are present.

The pollen and spore analysis revealed three ecological groups; herbs, mangroves, and trees and shrubs (Figure 4). The first pollen zone (A) is characterized mainly by a herbaceous pollen represented by Poaceae (~80%), Asteraceae (~18%) and Amaranthaceae (~2%). The mangrove pollen presents a small fraction represented by *Rhizophora* (~8%). Trees and shrubs are generally represented by Euphorbiaceae (~6%) and Rubiaceae (~3%) (Figure 5).

Facies association B (lagoon)

This facies association corresponds to the depth interval from 5.5 m (~8050 cal yr BP) to 1.5 m (~7115 cal yr BP). These deposits consist of massive mud (facies Mm), which are interbedded with heterolithic mud and sand deposits (facies Hm), lenticular heterolithic muddy silt (facies Hl), parallel-laminated sand (facies Sp) and flaser or wavy heterolithic deposit (facies Hf). Cross lamination is present at 2.1 m and convoluted laminations are present between ~3.5 and 3.75 m. Shell fragments and dwelling structures produced by the benthic fauna are also visible (Figure 4).

The pollen assembly is characterized by five ecological groups (Figures 4 and 5), defined by the presence of herbs such as Poaceae (30–80%), Cyperaceae (3–30%), Asteraceae (2–5%), *Borreria* (1–5%), Malvaceae (1–4%), *Smilax* (1–3%), Amaranthaceae (1–3%) and *Polygonum* (~1%). Within this facies association mangrove pollen represented by *Rhizophora* (4–30%) and *Avicennia* (1–3%) is also observed. Tree and shrub species are present as Euphorbiaceae (2–8%), Fabaceae (2–7%), *Mimosa* (1–6%), Rubiaceae (1–5%) and Myrtaceae, Malpighiaceae, Sapindaceae, Meliaceae, *Podocarpus* with less than 4%, respectively. The Arecaceae occurs between 1–5%, while aquatic species are represented by *Typha* (~2%).

The $\delta^{13}C$ values exhibit a depleted trend from −15 to −27‰ (mean= −20 ‰) between 5.5 and 1.35 m. The $\delta^{15}N$ record shows stable values between 3.6 and 7.0‰ (mean= 5.3‰). The TOC and N results were also relatively stable between 1.77 to 5.20% (mean= 3.48%) and 0.03 to 0.11% (mean= 0.07%), respectively. The C/N values showed considerable variation between 30 and 60 (mean= 40).

Facies association C (lake)

Facies association C was identified from 1.5 (~7115 cal yr BP) to 0.8 m (~3274 cal yr BP). The grain size of this facies ranges between sandy silt and silty sand, and is poorly sorted, with heterolithic mud/sand (facies Hm) and parallel laminated mud (facies Mp) along with roots, root marks and dwelling structures produced by benthic fauna (Figure 4).

The pollen record is marked by the shrinkage and eventual disappearance of mangroves, which was mainly constituted by *Rhizophora* (3−15%) and *Avicennia* (1−2%). The others four ecological groups were stable, such as herbs represented by Cyperaceae (25−55%), Poaceae (15−40%), Araceae (5−8%), Amaranthaceae (2−7%), Malvaceae (2−6%), *Borreria* (2−5%) and *Smilax* (1−3%). The trees and shrubs section of this facies is represented by *Alchornea* (2−6%), Anacardiaceae (2−5%), Fabaceae (2−4%), Euphorbiaceae (1−4%), *Mimosa* (1−4%), Moraceae (2−3%), Rubiaceae (2−3%), Myrtaceae (~2%), Sapotaceae (~2%), Meliaceae (2%) and Melastomataceae/Combretaceae (1%). The Palms (2−5%) and aquatics pollen groups are represented by *Potamogeton* (1−3%) and *Typha* (~2%) (Figure 5).

The isotope and elemental data showed different results relative to facies association B, where the δ^{13}C values exhibit relatively depleted values between −28 and −23‰ (mean= −26‰). The δ^{15}N values range between 4.5 and 7.2‰ (mean= 5.9‰). The C/N values decrease from 32 to 15 (mean= 23).

Facies association D (herbaceous plain)

The herbaceous plain facies begins at a depth of 0.7 m and continues to the surface. Probably, it was developed during the late-Holocene. These deposits are represented by peat and sandy silt sediments (facies Ms), poorly sorted, with plant debris and evidence of bioturbation (Figure 4).

The pollen assemblages of this association correspond to zone D, which is composed of four ecological groups (Figures 4 and 5), and the mangrove group was not present. This zone is characterized by pollen from herbs, trees and shrubs, palms and some aquatics. The herbaceous pollen is represented by Cyperaceae (10−35%), Poaceae (20−30%), Araceae (15−25%), *Smilax* (2−10%), Malvaceae (3−7%) and *Borreria* (2−4%), followed by Amaranthaceae, *Apium*, Asteraceae, *Begonia*, *Coccocypselum*/*Declieuxia*, Convovulaceae, *Polygonum*, *Sauvagesia* and *Xyris* in percentages below 3%. The trees and shrubs pollen is represented mainly by *Mimosa* (2−6%), Anacardiaceae (2−6%), Rubiaceae (2−5%),

Malpighiaceae (2−4%), *Alchornea* (2−3%) and Fabaceae (1−2%), followed by *Anadenanthera*, Melastomataceae/Combretaceae, Meliaceae and Mytaceae at around 1−2%, respectively. The palm and aquatic pollen were below 2%, colonized by Arecaceae, *Hydrocleis*, *Typha* and *Utricularia*.

The sediment $\delta^{13}C$ values ranged between −28 and −26‰ (mean= −27‰). The range for $\delta^{15}N$ values was between −0.1 and 7‰. The C/N ratio varies between 47 and 16 (mean= 29).
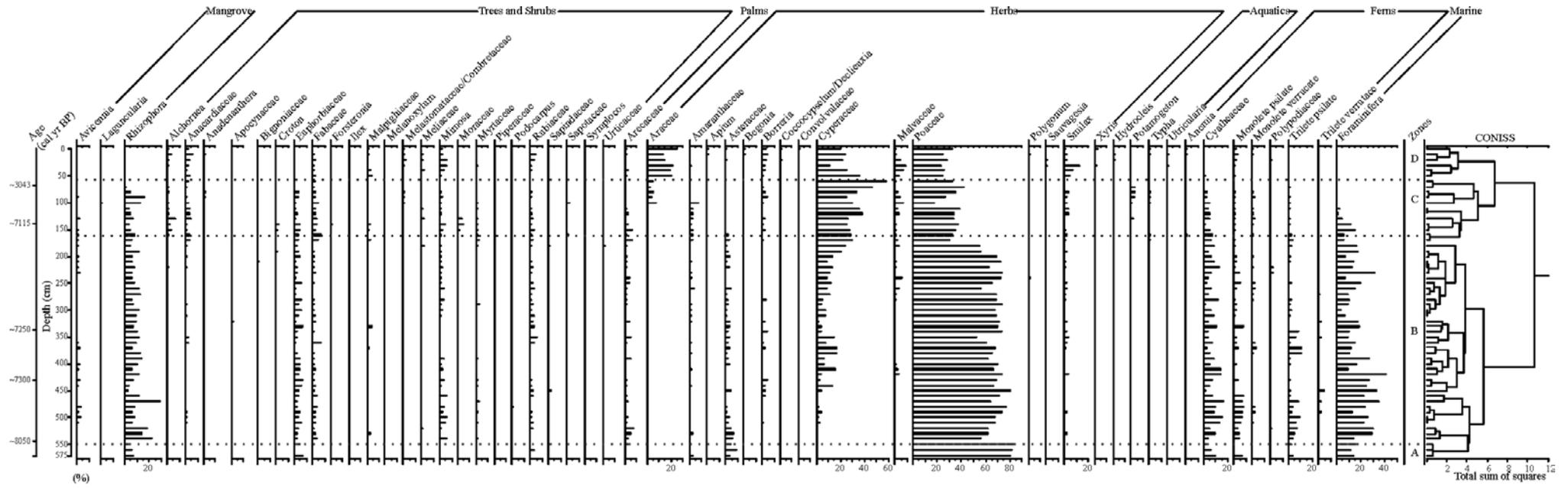
Figure 5 – Pollen diagram record with percentages of the most frequent pollen taxa, samples age, zones and cluster analysis.

Interpretation and discussion

The data suggest two phases of wetland development: (i) tidal flat colonized by mangroves in the margin of the lagoon, where flow energy oscillated. In addition, the geochemical data showed organic matter was influenced by C_4 plants between ~8050 and ~7115 cal yr BP. The phase (ii) was characterized by mangrove extinctions, with an increased influence of C_3 plants and freshwater/estuarine dissolved organic matter, which occurred in the lake and, then the development of a herbaceous plain, probably, during the late-Holocene (Figure 7).

Early Holocene: foreshore to lagoon

The foreshore to lagoon phase was initially marked by a foreshore facies association which exhibits shell fragments in cross-stratified sand and parallel-laminated sand (Figure 4), which record the action of relatively weak currents shaping the bedform. These currents induced the migration of small sand ripples (Reineck and Singh, 1980) between 6 and 5.60 m depth. The ecological record for this region is characterized by mangrove development associated with herbs, trees and shrubs (Figures 5 and 7). The lagoon facies is represented by massive mud, heterolithic mud/sand, lenticular heterolithic muddy silt, parallel-laminated sand, and flaser or wavy heterolithic deposits and cross-laminations. This assemblage of structures may indicate tidal influence. During this period, the tidal flat in the margin of the lagoon was occupied by mangroves, herbs, palms, trees and shrubs (Figure 7). Also during this time, the development of the mangrove was largely represented by *Rhizophora* (4−30‰), which is associated with trees and shrubs (2−25‰), and may have contributed to the upward decrease of $\delta^{13}C$ values from −15‰ to −23‰. It may represent a mixture of C_3, C_4 plants and aquatic organic matter, as indicated by the binary diagram between the $\delta^{13}C$ and C/N rate (Figure 6). The C_4 plants may be sourced from marine herbs, which have lower $\delta^{13}C$ values (between −17‰ and −9‰, Boutton, 1996). The $\delta^{15}N$ values (mean= 5.2‰) suggest a mixture of terrestrial plants and aquatic organic matter (~5.0‰, Sukigara and Saino, 2005).
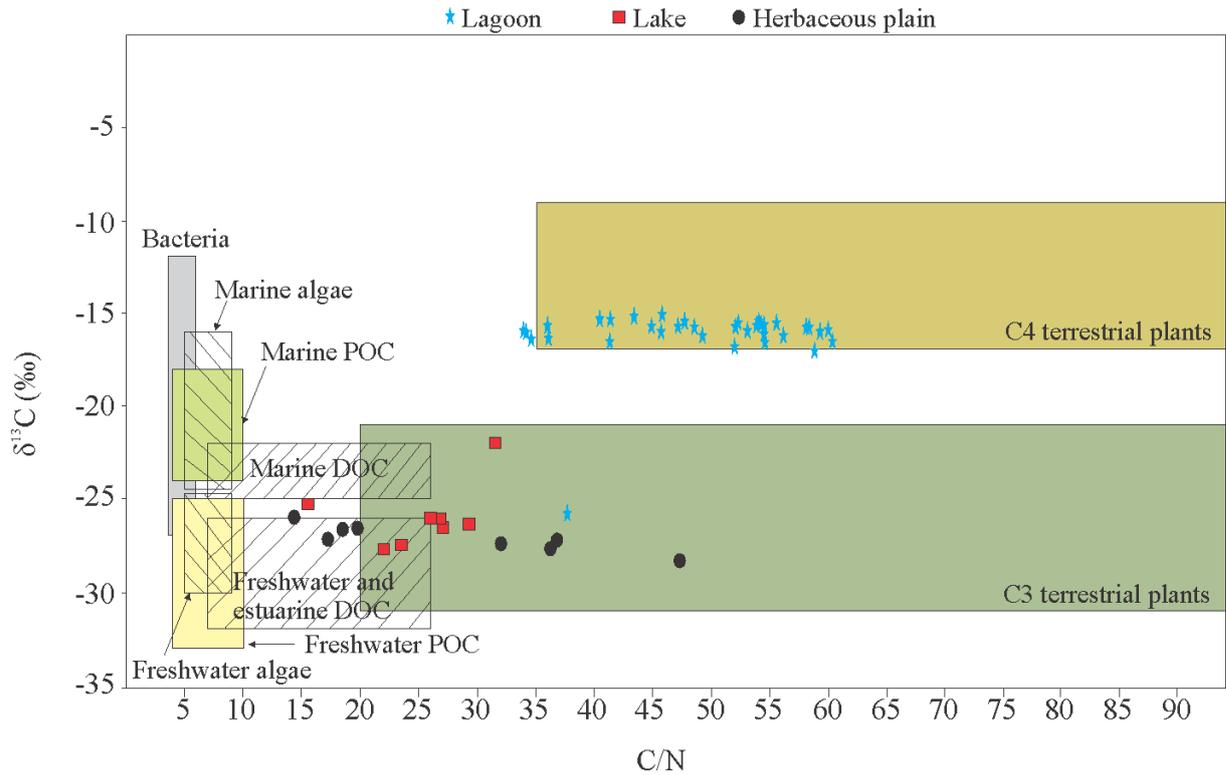
Figure 6 – Diagram illustrating the relationship between $\delta^{13}C$ and C/N ratio for the different sedimentary facies (foreshore, lagoon, lake and herbaceous plain), with interpretation according to data presented by Lamb et al. (2006); Meyers (2003) and Wilson et al. (2005) showing C_4 plants with marine/brackish water influence and C_3 plants with freshwater influence.
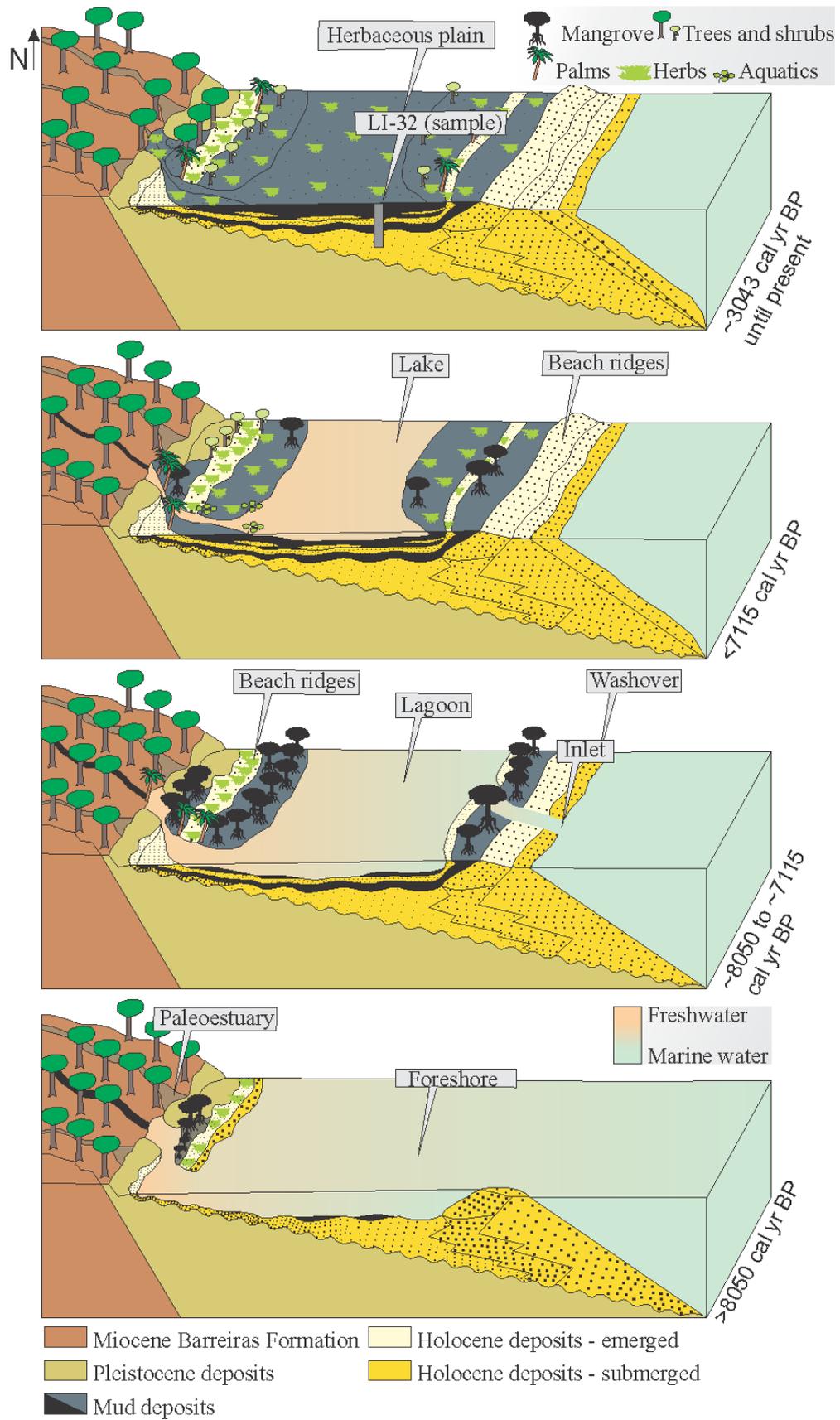
Figure 7 – Model of the geomorphology and vegetation development with successive phases of sediment accumulation according to relative sea-level changes during the Holocene.

Middle-Late Holocene: Lagoon/lake transition to herbaceous flat

The transition from a lagoon system to lake/herbaceous flat occurred after 7115 cal yr BP. This environment is marked by increased influence of C_3 plants. The sediment is composed of sandy silt, parallel-laminated mud and some benthic tubes, roots, and root marks, which indicate stagnant conditions. In this phase the mangrove ecosystem became extinct at the study site. The disruption of the mangrove ecosystem during this period indicates unfavorable conditions for mangrove development, which may have been due to decreased pore water salinity. This salinity decrease would have allowed the colonization of herbs, trees, shrubs, palms, and aquatic vegetation in the study site. The $\delta^{13}C$ values from $-23‰$ to $-28‰$, indicate an increased influence of C_3 plants ($-32‰$ to $-21‰$; Deines, 1980). The relationship between $\delta^{13}C$ and C/N values indicate a mixture of continental and aquatic organic matter, which was dominantly composed of C_3 plants. The presence of aquatic material (Figure 5) indicates a lacustrine environment. The accumulation of mud and organic matter into the lake led to the filling of lake depressions and expansion of a herbaceous plain during the late-Holocene. During this time the vegetation was characterized mainly by herbs, trees, and shrubs with distinctive isotopic signals and C/N values from C_3 plants (Figure 6). The $\delta^{15}N$ values exhibit a decreasing trend from 4.3‰ to $-0.1‰$ in sediments close to the surface ($0.7-0$ m), suggesting a increased amount of terrestrial organic matter ($\delta^{15}N$ ~1‰, Peterson and Howarth, 1987; Fellerhoff et al., 2003). Normally aquatic plants take up dissolved inorganic nitrogen, which is isotopically enriched in ^{15}N by 7‰ to 10‰ relative to atmospheric N (0‰), and thus terrestrial plants that use N_2 derived from the atmosphere have $\delta^{15}N$ values ranging from 0‰ to 2‰ (Meyers, 2003). The C/N ratio (mean= 29) also indicates organic matter from vascular plants (>12 vascular plants, Meyers, 1994; Tyson, 1995). The binary diagram of $\delta^{13}C$ vs. C/N ratio reveals the contribution of C_3 terrestrial plants (Figure 6).

Holocene sea-level changes, climate and vegetation dynamics

The data suggest mangrove vegetation and C_4 plants on a tidal flat surrounding a lagoon between ~8050 and ~7115 cal yr BP. This phase was followed by a decrease in mangrove habitat and an expansion of C_3 terrestrial plants represented by herbs, trees and shrubs. These results suggest a transition from marine to freshwater influence, likely due to the combined action of RSL fall and sedimentary supply during the mid and late-Holocene.

During the lagoon phase (~8050 and ~7115 cal yr BP) the sedimentation rates (16.4 - 15.5 mm/yr) were higher than the lacustrine and herbaceous plain phase (0.2 mm/yr) over the

past ~7115 cal yr BP (Figure 4). It may be related to the post-glacial sea-level rise in the early-Holocene, when more space was created to accommodate new sediments (Figure 8), while during the mid and late-Holocene occurred RSL fall with the decrease in accommodation space.

Changes in the RSL, sedimentary supply and river discharge during the Holocene are important process that influenced not only the relative position of the shoreline, but also the characteristics of coastal stratigraphic systems and vegetation dynamics (Scheel-Ybert, 2000; Cohen et al., 2005a,b; Buso Jr., 2010; Guimarães et al., 2012; Smith et al., 2012; França et al., 2012, Cohen et al., 2012) (Figure 8). Probably, the RSL changes along the Brazilian littoral must be the main driving force controlling the mangrove dynamics, while the sedimentary supply, mainly in the southern Brazil, and tidal water salinity, mainly in the northern Brazil, may be considered as secondary causes (Cohen et al., 2012).
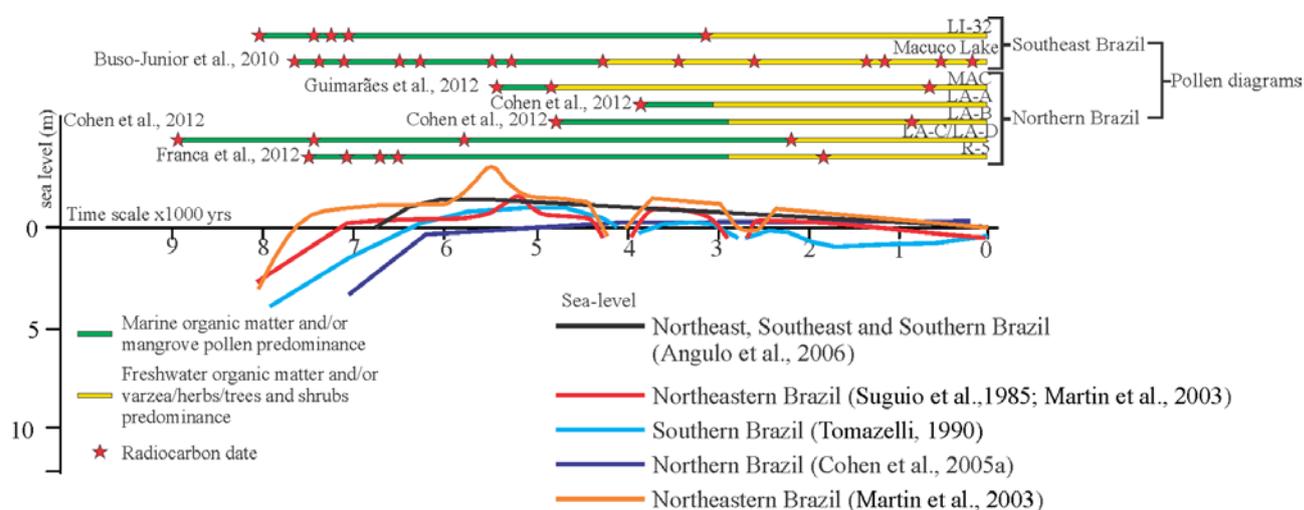
Figure 8 – RSL curves of the eastern Brazilian coast during the Holocene with comparative pollen diagrams from northern and southeast Brazil coastline.

Considering the RSL changes, references to the highstand along eastern coast of Brazil can be found in several publications, including Suguio et al. (1985), Dominguez et al. (1990), Angulo and Suguio (1995), Angulo and Lessa (1997), Angulo et al. (1999), Souza et al. (2001), Bezerra et al. (2003), Martin et al. (2003) and Angulo et al. (2006).

The RSL curve during the mid- to late-Holocene, along northeastern Brazil, was reconstructed by Martin et al. (2003), who showed that RSL exceeded the present level around 7700 cal yr BP and 5600 cal yr BP, followed by fast regression between 5300 and 4200 cal yr BP when the RSL may have been below the current level. (Figure 8). A fast rise occurred again approximately 3700 cal yr BP with a maximum of 3.5 ± 0.5 m above the

present RSL, followed by a steady and slow decrease between 3500 and 2800 cal yr BP. At 2800 cal yr BP, sea level fell quickly, falling below the current level by 2600 cal yr BP. About 2300 cal yr BP, RSL began to rise, reaching 2.3 ± 0.5 m above the present level by 2100 cal yr BP. After 2100 cal yr BP RSL fell steadily to its current position (Figure 8). Others studies performed along the eastern and southeastern Brazilian coast also showed the existence of three paleo-sea-levels higher than the present (Suguio et al., 1982, 1985; Martin et al., 1987, 1996). However, Angulo et al. (2006) proposed a mid-Holocene RSL maximum above present RSL and subsequent fall to the present time, without subsequent oscillation (Figure 8).

Along the coast of southeastern Brazil, higher RSL led to the formation of numerous lagoons (Sallun et al., 2012), and estuaries as observed in a recent study developed in the region (Buso Jr., 2010). This information is relevant to our study because between >8050 and ~7115 cal yr BP the sedimentary features reveal a facies association typically of foreshore and lagoon systems with mangrove, likely a consequence of high RSL during this time (Figure 8). During the mid and late-Holocene there was a retraction of mangrove and expansion of herbaceous vegetation, trees and shrubs followed by an increase in the contribution of freshwater organic matter. During this phase, a lake was developed following a regressive phase. During this period C_3 plants became the dominant vegetation in the study region. The flow of sediments led to siltation and infilling of the lacustrine setting, causing the expansion of the herbaceous plain ecosystem seen today (Figure 7).

Conclusion

This study indicates the presence of a lagoon system surrounded by a tidal plain colonized by mangroves, and its sedimentary organic matter sourced from C_4 plants, between ~8050 and ~7115 cal yr BP. However, during the mid and late-Holocene the mangroves shrank and freshwater vegetation expanded (C_3 plants), probably, due to the combined action of RSL fall and sedimentary supply. During this time, the development of a lacustrine environment was followed by the colonization of herbs, trees and shrubs. The continuous infilling of sediment into the lake allowed the expansion of a herbaceous plain, as seen today. The geomorphologic and vegetation evolution is in agreement with the mid-Holocene RSL maximum above present RSL and subsequent fall to the present time, as proposed by Angulo et al. (2006).

REFERENCES

Absy, M.L., 1975. Polen e esporos do Quaternário de Santos (Brasil). Hoehnea 5, 1-26.

Absy, M.L., Cleef, A., Fournier, M., Martin, L., Servant, M., Sifeddine, A., Ferreira da Silva, M., Soubies, F., Suguio, K., Turcq, B., Van Der Hammen, T.H., 1991. Mise en evidence de quatre phases d'overture de la forêt dense dans le sud-est de l'Amazonie au cours des 60,000 dernieres annees. Premiere comparision avec d'autres regions tropicales. Comptes Rendus de l'Académie des Sciences. Paris t.312, 673–678 (Serie II).

Alongi, D.M., Sasekumar, A., Tirendi, F., Dixon, P., 1998. The influence of stand age on benthic decomposition and recycling of organic matter in managed mangrove forests of Malaysia. Journal of Experimental Marine Biology and Ecology 225. 197–218.

Alongi, D.M., Tirendi, F., Dixon, P., Trott, L.A., Brunskill, G.J., 1999. Mineralization of Organic Matter in Intertidal Sediments of a Tropical Semi-enclosed Delta. Estuarine, Coastal and Shelf Science 48, 451–467.

Alongi, D.M., Tirendi, F., Clough, B.F., 2000. Below-ground decomposition of organic matter in forests of the mangrove Rhizophora stylosa and Avicennia marina along the arid coast of Western Australia. Aquatic Botany 68, 97–122.

Alongi, D.M., 2002. Present state and future of the world's mangrove forests. Environmental Conservation 29, 331-349.

Alongi, D.M., 2008. Mangrove forests: Resilience, protection from tsunamis, and responses to global climate change. Estuarine, Coastal and Shelf Science 76, 1–13.

Altabet, M.A., McCarthy, J.J., 1985. Temporal and spatial variations in the natural abundance of ^{15}N in PON from a warm-core ring. Deep-Sea Res. 32, 755–772.

Amaral, P.G.C., Ledru, M.P., Branco, F.R., Giannini, P.C.F., 2006. Late Holocene development of a mangrove ecosystem in southeastern Brazil (Itanhaém, state of São Paulo). Palaeogeography, Palaeoclimatology, Palaeoecology 241, 608–620.

Amaral, P.G.C., Giannini, P.C.F., Sylvestre, F., Pessenda, L.C.R., 2012. Paleoenviromental reconstruction of a Late Quaternary lagoon system in southern Brazil (Jaguaruna region, Santa Catarina state) based on multi-proxy analysis. Journal of Quaternary Science 27, 181–191.

Amarasekera, K. N., Lee, R.F., Williams, E.R., Eltahir, E.A.B., 1997. ENSO and the natural variability in the flow of tropical rivers. Journal of Hydrology 200, 24–39.

ANA, 2003. *Hydrological information system*. Brazilian National Water Agency. On line dataset, 14.3 MB, http://hidroweb.ana.gov.br/baixar/mapa/Bacia1.zip.

Andersen, S.T., 1967. Tree-pollen rain in a mixed deciduous forest in south Jutland (Denmark). Review Palaeobotany Palynology 3, 267–275.

Andersen, S.T., 1970. The relative pollen productivity and pollen representation of north European trees, and correction factors for tree pollen spectra. Dan. Geol. Surv. Trans. Ser. 2 (96), 1–99.

Angulo, R.J., Suguio, K., 1995. Re-evaluation of the Holocene sea-level maxima for the State of Paraná, Brazil. Palaeogeography, Palaeoclimatology, Palaeoecology 113, 385–393.

Angulo, R.J., Lessa, G.C., 1997. The Brazilian sea-level curves: a critical review with emphasis on the curves from Paranaguá and Cananéia regions. Marine Geology 140, 141–166.

Angulo, R.J., Giannini, P.C.F., Suguio, K., Pessenda, L.C.R., 1999. Relative sea-level changes in the last 5500 years in southern Brazil (Laguna – Imbituba region, Santa Catarina State) based on vermitid ^{14}C ages. Marine Geology 159, 323–339.

Angulo, R.J., Lessa, G.C., Souza, M.C., 2006. A critical review of the mid- to late Holocene sea-level fluctuations on the eastern brazilian coastline. Quaternary Science Reviews 25, 486–506.

Angulo, R.J., de Souza, M.C., Assine, M.L., Pessenda, L.C.R., Disaró, S.T., 2008. Chronostratigraphy and radiocarbon age inversion in the Holocene regressive barrier of Paraná, southern Brazil. Marine Geology 252, 111–119.

Arai, M., 1997. Dinoflagelados (Dinophyceae) miocênicos do Grupo Barreiras no nordeste de Estado do Pará (Brasil). Guarulhos: Revista Universidade Guarulhos, Geociências II (n° especial): 98-106.

Arai, M., 2006. A grande elevação eustática do Mioceno e sua influência na origem do Grupo Barreiras. Geologia USP Série Científica 6, 1–6.

Asmus, H.E., Gomes, J.B., Pereira, A.C.B., 1971. Integração geológica regional da bacia do Espírito Santo – Anais do XXV Congresso Brasileiro de Geologia, v.3: 235–254, São Paulo.

Baltzer, F., 1970. Etude sédimentologique du marais de Mara (Côte ouest de la Nouvelle Calédonie) et de formations quaternaires voisines. Mémoires expédition française sur lês récifs coralliens de la Nouvelle Calédonie. Foundation Singer-Polignac 4, 146–169.

Baltzer, F., 1975. Solution of silica and formation of quartz and smectite in mangrove swamps and adjacent hypersaline marsh environments. Proceedings of the International Symposium on Biology and Management of Mangroves, University of Florida, Orlando, Florida, pp. 482–498.

Bard, E., Hamelin, B., Fairbanks, R.G., 1990. U–Th ages obtained by mass spectrometry in corals from Barbados: sea level during the past 130,000 years. Nature 346, 456–458.

Bard, E., 2012. A review on sea-level changes during deglaciations. Quaternary International 279–280, 9–120.

Barreto, A. M. F., Bezerra, F. H. R., Suguio, K., Tatumi, S. H., Yee, M., R.P. Paiva., C.S. Munita. 2002. Late Pleistocene marine terrace deposits in northeastern Brazil: sea level change and tectonic implications. Palaeogeography, Palaeoclimatology, Palaeoecology 179, 57-69.

Barth, J.A.C., Veizer, J., Mayer, B., 1998. Origin of particulate organic carbon in the upper St. Lawrence: Isotopic constraints. Earth and Planetary Science Letters 162, 111–121.

Bassinot, F., Labeyrie, L., Vincent, E., Quidelleur, X., Lancelot, N.J., Lancelot, Y., 1994. The astronomical theory of climate and the age of the Brunhes–Matuyama magnetic reversal. Earth and Planetary Sciences Letters 126, 91–108.

Behling, H., 1993. Untersuchungen zur Spätpleistozänen und Holozänen Vegetations und Klimageschichte der Tropischen Küstenwälder und der Araukarienwälder in Santa Catarina (Südbrasilien). Dissertationes Botanicae, Berlin, Deutschland.

Behling, H., Hooghiemstra, H., Negret, A.J., 1998. Holocene history of the Choco rain forest from Laguna Piusbi, southern Pacific lowlands of Colombia. Quaternary Research 50 (3), 300–308.

Behling, H., Costa, M.L., 2000. Holocene environmental changes from the Rio Curuá record in the Caxiuanã region, eastern Amazon Basin. Quaternary Research 53, 369–377.

Behling, H., Costa, M.L., 2001. Holocene vegetational and coastal environmental changes from the Lago Crispim record in northeastern Pará State, eastern Amazonia. Review of Paleobotany and Palynology 114, 145–155.

Behling, H., Hooghiemstra, H., 2000. Holocene Amazon rainforest–savanna dynamics and climatic implications: high-resolution pollen record from Laguna Loma Linda in eastern Colombia. Journal of Quaternary Science 15, 687–695.

Behling, H., 2001. Late Quaternary environmental changes in the Lagoa da Curuca region (eastern Amazonia) and evidence of *Podocarpus* in the Amazon lowland. Vegetation History and Archaeobotany, 10, 175–183.

Behling, H., Cohen, M.C.L., Lara, R.J., 2001. Studies on Holocene mangrove ecosystem dynamics of the Bragança Peninsula in north-eastern Pará, Brazil. Palaeogeography, Palaeoclimatology, Palaeoecology 167, 225–242.

Behling, H., Cohen, M.C.L., Lara, R.J., 2004. Late Holocene mangrove dynamics of the Marajó Island in northern Brazil. Vegetation History and Archaeobotany 13, 73–80.

Behling, H., Pillar, V.D., Müller, S.C., Overbeck, G.E., 2007. Late-Holocene fire history in a forest-grassland mosaic in southern Brasil: implications for conservation. Applied Vegetation Science 10, 81–90.

Bemerguy, R.L., 1981. Estudo sedimentológico dos paleocanais da região do Rio Paracauari, Ilha do Marajó – Estado do Pará. 1981. 95p. Dissertação de Mestrado – NCGG-UFPA. Belém (PA).

Berger, U., Rivera-Monroy, V.H., Doyle, T.W., Dahdouh-Guebas, F., Duke, N.C., Fontalvo-Herazo, M.L., Hildenbrandt, H., Koedam, N., Mehlig, U., Piou, C., Twilley, R., 2008. Advances and limitations of individual-based models to analyze and predict dynamics of mangrove forests: A review. Aquatic Botany 89, 260–274.

Bernini, E., Silva, M.A.B., Carmo, T.M.S., Cuzzuol, G.R.F., 2006. Composição química do sedimento e de folhas das espécies do manguezal do estuário do Rio São Mateus, Espírito Santo, Brasil. Revista Brasileira de Botânica 29, 689–699.

Bezerra, F.H.R., Barreto, A.M.F., Suguio, K., 2003. Holocene sea-level history on the Rio Grande do Norte State coast, Brazil. Marine Geology 196, 73–89.

Bird, E.C.F., 1980. Mangroves and coastal morphology. The Victorian Nauralist 97, 48–58.

Bittencourt, A.C.S.P., Martin, L., Vilas-Boas, G.S., Flexor, J.M., 1979. Quaternary marine formations of the coast of the State of Bahia, Brazil. Coastal Evolution in the Quaternary, 232–253.

Bittencourt, A.C.S.P., Dominguez, J.M.L., Martin, L., Silva, I.R., De-Medeiros, K.O.P., 2007. Past and current sediment dispersion pattern estimates through numerical modeling of wave climate: an example of the Holocene delta of the Doce River, Espírito Santo, Brazil. Anais da Academia Brasileira de Ciências 79, 333–341.

Blasco, F., Saenger, P., Janodet, E., 1996. Mangrove as indicators of coastal change. Catena 27, 167–178.

Boutton, T.W., 1996. Stable carbon isotope ratios of soil organic matter and their use as indicators of vegetation and climate change. In: Boutton, T.W., Yamasaki, S.I. (Eds.). Mass spectrometry of soils. Marcel Dekker, New York, NY.

Bruguière, L.G., 1789. Encyclopedie methodique. Histoire naturelle des Vers: Paris and Liege, Panckouche & Plomteux. A. Bul.

Bruun, P., 1962. Sea level rise as a cause of shore erosion. Am. Soc. Civ. Eng. Proc., J. Waterw. Harb. Div. 88, 117–130.

Brush, G.S., Brush, L.M.J., 1972. Transport of pollen in a sediment laden channel: a laboratory study American Journal of Science 272, 359–381.

Bush M.B., Colinvaux P.A., 1988. A 7000-year pollen record from the Amazon lowlands, Ecuador. Vegetatio 76, 141–154.

Bush, M.B., 1994. Amazonian speciation: a necessarily complex model. Journal Biogeography 21, 5–18.

Bush, M.B., Silman, M.R., Urrego, D.H., 2004. 48.000 years of climate and forest change from biodiversity hotspot. Science 303, 827–829.

Bush, M.B., Silman, M.R., Listopad, C.M.C.S., 2007. A regional study of Holocene climate change and human occupation in Peruvian Amazonia. Journal of Biogeography 34, 1342–1356.

Buso Junior, A.A., 2010. Dinâmica ambiental holocênica (vegetação, clima e nível relativo marinho) baseada em estudos interdisciplinares de alta resolução, no litoral norte do estado do Espírito Santo. Piracicaba – SP: Universidade de São Paulo, Programa de Pós-Graduação em Ciências, Dissertação de Mestrado, p.190.

Buso Junior, A.A., Pessenda, L.C.R., de Oliveira, P.E., Giannini, P.C.F., Cohen, M.C.L., Volkmer-Ribeiro, C., Oliveira, S.M.B., Favaro, D.I.T., Rossetti, D.F., Lorente, F.L., Borotti Filho, M.A., Schiavo, J.A., Bendassolli,J.A., Franca, M.C., Guimaraes, J.T.F., Siqueira, G.S., 2013 – *in press*. From an estuary to a freshwater lake: a paleo-estuary evolution in the context of Holocene sea-level fluctuations, southeastern Brazil. Radiocarbon.

Cahoon, D.R., Lynch, J.C., 1997. Vertical accretion and shallow subsidence in a mangrove forest of southwestern Florida, U.S.A. Mang. Salt Marsh. 3, 173–186.

Cahoon, D.R., Hensel, P.F., Spencer, T., Reed, D.J., McKee, K.L., Saintilan, N., 2006. Coastal wetland vulnerability to relative sea-level rise: wetland elevation trends and process controls, in: J.T.A Verhoeven, B. Beltman, R. Bobbing, D.F. Whigham (Eds.), Wetlands and Natural Resource Management, Springer-Verlag, Berlin, pp. 271–292.

Camargo, M.G., 1999. SYSGRAN for Windows: Granulometric Analysis System. Pontal do Sul, Paraná, Brazil.

Carvalho, L.M.V., Jones, C., Liebmann, B., 2004. The South Atlantic Convergence Zone: intensity, form, persistence, and relationships with intraseasonal to interanual activity and extreme rainfall. Journal of Climate 17, 88–108.

Castro, D.F., Rossetti, D.F., Pessenda, L.C.R., 2010. Facies, δ^{13}C, δ^{15}N and C/N analyses in a late Quaternary compound estuarine fill, northern Brazil and relation to sea level. Marine Geology 274, 135–150.

Chapman, V.J., 1976. Mangrove vegetation. Velag Von J. Cramer, Leutershausen, Germany, p. 447.

Chappell, J., Shackleton, N.J., 1986. Oxygen isotopes and sea level. Nature 324, 137–140.

Chappell, J., Woodroffe, C.D., 1994. Macrotidal estuaries, in: Carter, R.W.G., Woodroffe, C.D. (Eds.), Coastal Evolution: Late Quaternary Shoreline Morphodynamics. Cambridge Univ. Press, Cambridge, pp. 187–218.

Chivas, A.R., Garcia, A., Van der Kaars, S., Couapel, M.J.J., Holt, S., Reeves, J.M., 2001. Sea-level and environmental changes since the last interglacial in the Gulf of Carpentaria, Australia: An overview. Quaternary International 85, 19–46.

Clark, M.W., McConchie, D.M., Lewis, D.W., Saenger, P., 1998. Redox stratification and heavy metal partitioning in Avicennia-dominated mangrove sediments: a geochemical model. Chemical Geology 149, 147–171.

Cohen, M.C.L., 2003. Past and current mangrove dynamics on the Bragança Península, northern Brazil. Ph.D. Thesis, University of Bremen, Center for Tropical Marine Ecology, Bremen, Germany.

Cohen, M.C.L., Lara, R.J., 2003. Temporal changes of mangrove vegetation boundaries in Amazonia: Application of GIS and remote sensing techniques. Wetlands Ecology and Management 11, 223–231.

Cohen, M.C.L., Behling, H., Lara, R.J., 2005a. Amazonian mangrove dynamics during the last millennium: the relative sea-level and the little Ice Age. Review of Palaeobotany and Palynology 136, 93–108.

Cohen, M.C.L., Souza Filho, P.W., Lara, R.L., Behling, H. Angulo, R., 2005b. A model of Holocene mangrove development and relative sea-level changes on the Bragança Peninsula (northern Brazil). Wetlands Ecology and management 13, 433–443.

Cohen, M.C.L., Lara, R.J., Smith, C.B., Angélica, R.S., Dias, B.S., Pequeno, T., 2008. Wetland dynamics of Marajó Island, northern Brazil, during the last 1000 years. Catena 76, 70–77.

Cohen, M.C.L., Lara, R.J., Smith, C.B., Matos, H.R.S., Vedel, V., 2009. Impact of sea-level and climatic changes on the Amazon coastal wetlands during the late Holocene. Vegetation History and Archaeobotany 18, 425–439.

Cohen, M.C.L., Pessenda, L.C.R., Behling, H., Rossetti, D.F., França, M.C., Guimarães, J.T.F., Friaes, Y., Smith, C.B., 2012. Holocene palaeovironmental history of the Amazonian mangrove belt. Quaternary Science Reviews 55, 50–58.

Colinvaux, P.A., De Oliveira, P.E., Moreno, J.E., Miller, M.C., Bush, M.B., 1996. A long pollen record from lowland Amazonia: forest and cooling in glacial times. Science 247, 85-88.

Colinvaux, P.A.,1998. A new vicariance model for Amazonian endemics. Glob. Ecol. Biogeogr. Lett. 7, 95–96.

Colinvaux, P., De Oliveira, P.E., Patiño, J.E.M., 1999. Amazon Pollen Manual and Atlas. Harwood Academic Publishers, Dordrecht. 332 p.

Colinvaux, P.A., De Oliveira, P.E., Bush, M.B., 2000. Amazonian and neotropical plant communities on glacial time-scales: the failure of the aridity and refuge hypothesis. Quaternary Science Reviews 19, 141–169.

Collinson, J., Mountney, N., Thompson, D., 2006. Sedimentary Structures (Third edition), Terra Publishing, 292 pp.

Cutler, K.B., Edwards, R.L., Taylor, F.W., Cheng, H., Adkins, J., Gallup, C.D., Cutler, P.M., Burr, G.S., Bloom, A.L., 2003. Rapid sea-level fall and deep ocean temperature change since the last interglacial period. Earth and Planetary Science Letters 206, 253–271.

Da Costa E.M., 1778. Historia Naturalis Testaceorum Britanniae. London: Millan, White, Elmsley and Robson XII 254 VIII p., 17 pl.

D'Alpaos, A., Lanzoni, S., Marani, M., Rinaldo, A., 2007. Landscape evolution in tidal embayments: Modeling the interplay of erosion, sedimentation, and vegetation dynamics. Journal of Geophysical Research Earth Surface 112, 1–17.

Dall, W.H., 1881. Reports on the results of dredging, under the supervision of Alexander Agassiz, in the Gulf of Mexico and in the Caribbean Sea (1877-78), by the United States Coast Survey Steamer "Blake", Lieutenant-Commander C.D. Sigsbee, U.S.N., and Commander J.R. Bartlett, U.S.N., commanding. XV. Preliminary report on the Mollusca. Bulletin of the Museum of Comparative Zoölogy at Harvard College 9 (2), 33–144.

Dall, W. H., 1890. Scientific results of explorations by the U. S. Fish Commission Steamer Albatross. No. VII.--Preliminary report on the collection of Mollusca and Brachiopoda obtained in 1887-'88. Proceedings of the United States National Museum 12 (773), 219–362, pls. 5-14.

Dalrymple, R.W., Knight, R.J., Zaitlin, B.A., Middleton, G.V., 1990. Dynamics and facies model ofa macrotidal sand-bar complex, Cobequid Bay-Salmon River estuary (Bay of Fundy). Sedimentology 37, 577–612.

Dalrymple, W. R., Zaitlin, B. A., Boyd, R., 1992. Estuarine facies models: conceptual basis and stratigraphic implications. Journal of Sedimentary Petrology 62 (6), 1130–1146.

Davis, M.B., 2000. Palynology after Y2K—understanding the source area of pollen in sediments. Annual Review Earth Planetary Science 28, 1–18.

Departamento de Hidrografia e Navegação (DHN), Marinha do Brasil, 2003. Rio de Janeiro, Brasil.

Desjardins T., Filho A.C., Mariotti A., Chauvel A., Girardin C., 1996. Changes of the forest savanna boundary in Brazilian Amazonia during the Holocene as revealed by soil organic carbon isotope ratios. Oecologia 108, 749–756.

Deines, P., 1980. The isotopic composition of reduced organic carbon. In: Fritz, P., Fontes, J.C. (Eds.), Handbook of Environmental Isotope Geochemistry. The Terrestrial Environments, Vol. 1, Amsterdam: Elsevier, 329–406.

Dillenburg, S. R., Barboza, E. G., Tomazelli, L.J., Hesp, P. A.; Clerot, L. C. P., Zouain, R. N. A., 2009. The Holocene Coastal Barriers of Rio Grande do Sul. In: Sergio Rebello Dillenburg; Patrick Alan Hesp. (Org.). Geology and Geomorphology of Holocene Coastal Barriers of Brazil. Berlin/Heidelberg: Springer vol. 107, pp. 53–91.

Dominguez, J.M.L., Bittencourt, A.C.S.P., Leão, Z.M.A.N., Azevedo, A.E.G., 1990. Geologia do Quaternário costeiro do estado de Pernambuco. Revista Brasileira de Geociências 20, 208–215.

Dominguez, J.M.L., Bittencourt, A.C.S.P., Martin, L., 1992. Controls on Quarternary coastal evolution of the east-northeastern coast of Brazil: roles of sea-level history, trade winds and climate. Sedimentary Geology 80, 213–232.

Dominguez, J.M.L., 2006. The coastal zone of Brazil – an overview. Journal of Coastal Research 39, 16–20.

Dominguez, J.M.L., 2009. The Coastal Zone of Brazil, in: Dillenburg, S. R., Hesp, P. A. (Eds.), Geology and geomorphology of Holocene Coastal Barriers of Brazil. Springer-Verlag, Berlin, pp. 17–51.

Dominguez, J.M.L., Andrade, A.C.S., Almeida, A.B., Bittencourt, A.C.S.P., 2009. The Holocene Barrier Strandplains of the State of Bahia. In: Dillenburg S., and Hesp, P. (Ed.), Geology and Geomorphology of Holocene Coastal Barriers of Brazil. Springer, Berlin, Germany, pp. 253–288.

Duclos, P.L., 1840. Histoire Naturelle Générale et de Tous les Particulière Genres de Coquilles Marines univalves vivant l'etat et um Fossile, Monografias par Publiee, Columbella Gênero. Didot, Paris, p. 1, 13 pls.

Duke, N.C., Pinzón, Z.S.M., Prada, M.C., 1997. Large-Scale Damage to Mangrove Forests Following Two Large Oil Spills in Panama. Biotropica 29, 2–14.

Eisma D., Augustinus P.G.E.F., Alexander C., 1991. Recent and subrecent changes in the dispersal of Amazon mud. Netherlands Journal of Sea Research 28, 181–192.

Ellison, J.C., 2005. Holocene palynology and sea-level change in two estuaries in Southern Irian Jaya. Palaeogeography, Palaeoclimatology, Palaeoecology 220, 291–309.

Engelhart, S.E., Horton, B.P., Roberts, D.H., Bryant, C.L., Corbett, D.R., 2007. Mangrove pollen of Indonesia and its suitability as a sea-level indicator. Marine Geology 242, 65–81.

Evin, J., Marechal, J., Pachiaudi, C., 1980. Conditions involved in dating terrestrial shells. Radiocarbon 22, 545-555.

Faegri, K., Iversen, J., 1989. Textbook of Pollen Analysis. . 4th ed.Wiley, Chichester, 328 pp.

Fairbanks, R.G., 1989. A 17,000-year glacio-eustatic sea level record: influence of glacial melting dates on the Younger Dryas event and deep-ocean circulation. Nature 342, 637–642.

Fellerhoff, C., Voss, M., Wantzen, K.M., 2003. Stable carbon and nitrogen isotope signatures of decomposing tropical macrophytes. Aquatic Ecology 37, 361–375.

França, M.C. 2010. Mudanças na vegetação do litoral leste da Ilha de Marajó durante o Holoceno superior. Belém: Universidade Federal do Pará, Programa de Pós-Graduação em Geologia e Geoquímica, Dissertação de Mestrado, p.111.

França, M., Francisquini, M.I. ,Cohen, M.C.L. ,Pessenda, L.C.R., Rosseti, D.F., Guimarães, J., Smith, C. B., 2012. The last mangroves of Marajó Island - Eastern Amazon: impact of climate and/or relative sea-level changes. Review of Palaeobotany and Palynology 187, 50–65.

França, M.C., Cohen, M.C.L., Pessenda, L.C.R., Rossetti, D.F., Lorente, F.L., Buso-Junior, A.A., Guimarães, J.T.F., Friaes, Y., 2013a. Mangrove dynamics in response to sea-level changes on Holocene terraces of the Doce River, southeastern Brazil. Catena.

França, M.C., Francisquini, M.I., Cohen, M.C.L., Pessenda, L.C.R., 2013b – *in press.* An inter-proxy approach to assessing the development of the Amazonian mangrove, northern Brazil. Vegetation History and Archaeobotany.

França, C.F., Sousa Filho, P.W.M., 2006. Compartimentação morfológica da margem leste da ilha de Marajó: zona costeira dos municípios de Soure e Salvaterra – Estado do Pará. Revista Brasileira de Geomorfologia 1, 33–42.

French, J.R., Stoddart, D.R., 1992. Hydrodynamics of saltmarsh creek systems: Implications for marsh morphological development and material exchange. Earth Surface Process and Landforms 17, 235–252.

Freitas, H.A., Pessenda, L.C.R., Aravena, R., Gouveia, S.E.M., Ribeiro, A.S., Boulet, R., 2001. Late Quaternary vegetation dynamics in the southern Amazon sasin inferred from carbon isotopes in soil organic matter. Quaternary Research 55, 39–46.

Freitas, R.A.P., Douglas Lindemann, D., Souza, L.S., Faria, H., Santos, M., Elesbon, A., Casagrande, F., 2010. Análise de Séries Temporais de Vazão e Precipitação na Bacia Hidrográfica do Rio São Mateus. In: Anais do XVI Congresso Brasileiro de Meteorologia, Belém, PA.

Fromard, F., Vega, C., Proisy, C., 2004. Half a century of dynamic coastal change affecting mangrove shorelines of French Guiana. A case study based on remote sensing data analyses and field surveys. Marine Geology 208, 265–280.

Fry, B., Scalan, R.S., Parker, P.L., 1977. Stable carbon isotope evidence for two sources of organic matter in coastal sediments: seagrass and plankton. Geochimica et Cosmochimica Acta 41, 1875–1877.

Fu, R., Dickinson, R.E., Chen, M., Wang, H., 2001. How do tropical sea surface temperatures influence the seasonal distribution of precipitation in the equatorial Amazon? Journal of Climate 14, 4003–4026.

Fujimoto, K., Miyagi, T., Kikuchi, T., Kawana, T., 1996. Mangrove habitat formation and response to Holocene sea-level changes on Kosrae Island, Micronesia. Mangrove and Salt Marshes 1, 47–57.

Furukawa, K.,Wolanski, E., 1996. Sedimentation in mangrove forests. Mang. Salt Marsh 1, 3–10.

Giannini, P.C.F., Sawakuchi, A.O., Martinho, C.T., Tatumi, S.H., 2007. Eolian depositional episodes controlled by Late Quaternary relative sea level changes on the Imbituba–Laguna coast (southern Brazil). Marine Geology 237, 143–168.

Gilman, E.L., Ellison, J., Duke, N.C., Field, C., 2008. Threats to mangroves from climate change and adaptation options: A review. Aquatic Botany 89, 237–250.

Goh, K.M., 2006. Removal of contaminants to improve the reliability of Radiocarbon dates of peats. Journal of Soil Science 29, 340–349.

Gonçalves-Alvim, S.J., Vaz dos Santos, M.C.F., Fernandes, G.W., 2001. Leaf gall abundance on *Avicennia germinans* (Avicenniaceae) along an interstitial salinity gradient. Biotropica 33, 69–77.

Goodfriend, G.A., 1987. Radiocarbon age anomalies in shell carbonate of land snails from semi-arid areas. Radiocarbon 29, 159-167.

Goodfriend, G.A., Stipp, J.J., 1983. Limestone and the problem of radiocarbon dating of land-snail shell carbonate. Geology 11, 575-577.

Gornitz, V., 1991. Global coastal hazards from future sea level Rise. Palaeogeography, Palaeoclimatology, Palaeoecology 89, 379–398.

Gouveia, S.E.M., Pessenda, L.C.R., Aravena, R., Boulet, R., Roveratti, R., Gomes, B.M., 1997. Dinâmica de vegetações durante o Quaternário recente no sul do Amazonas

indicada pelos isótopos do carbono (^{12}C, ^{13}C e ^{14}C). Geochimica Brasiliensis 11, 355–367.

Gray, J.E., 1825. A list and descriptions of some species of shells not taken notice of by Lamarck. Annals of Philosophy (new series), 9, 134–140.

Grimm, E.C., 1987. CONISS: a FORTRAN 77 program for stratigraphically constrained cluster analysis by the method of the incremental sum of squares. Computer and Geosciences 13, 13–35.

Grimm, E.C., 1990. TILIA and TILIAGRAPH: PC spreadsheet and graphic software for pollen data. INQUA Subcommission on Data-Handling Methods. Newsletter 4:5–7.

Grimm, E.C., Lozano-Gárcia, S., Behling, H., Markgraf, V., 2001. Holocene vegetation and climate variability in the Americas. Interhemispheric Climate Linkages, chapter 19, 325–370.

Grindrod, J., Moss, P., Van der Kaars, S., 2002. Late Quaternary mangrove pollen records from continental shelf and ocean cores in the North Australian-Indonesian region. In: Kershaw, P., David, B., Tapper, N., Penny, D., Brown, J. (Eds.), Bridging Wallace´s Line: The environmental and cultural history and dynamics of the SE-Asian-Australian region. Catena Verlag GMBH, Reiskirchen.

Guedes, C.C.G., Giannini, P.C.F., Sawakuchi, A.O., De Witt, R., Nascimento Jr., D.R., Aguiara, V.A.P., Rossia, M.G., 2011. Determination of controls on Holocene barrier progradation through application of OSL dating: the Ilha Comprida Barrier example, Southeastern Brazil. Marine Geology 285, 1–16.

Guimarães, J.T.F., Cohen, M.C.L., França, M.C., Lara, R.J., Behling, H., 2010. Model of wetland development of the Amapá coast during the late Holocene. Anais da Academia Brasileira de Ciências 82, 451–465.

Guimarães, J.T.F., Cohen, M.C.L., Pessenda, L.C.R., França, M.C., Smith, C.B., Nogueira, A.C.R., 2012. Mid- and late-Holocene sedimentary process and palaeovegetation changes near the mouth of the Amazon River. The Holocene 22, 359–370.

Guimarães, J.T.F., Cohen, M.C.L., França, M.C., Pessenda, L.C.R., Behling, H., 2013. Morphological and vegetation changes on tidal flats of the Amazon Coast during the last 5000 cal yr BP. The Holocene 23, 528–543.

Harper, C.W., 1984. Improved methods of facies sequence analysis. In: Walker R.G. (Ed.), Facies Models 2ed. Geological Association of Canada, Ontario, Canada, pp. 11–13.

Haines, E.B., 1976. Stable carbon isotope ratios in biota, soils and tidal water of a Georgia salt marsh. Estuarine and Coastal Marine Science 4, 609–616.

Havinga, A.J., 1967. Palynology and pollen preservation. Review of Paleobotany and Palynology 2, 81–98.

Hermanowski, B., Costa, M.L., Behling, H., 2012. Environmental changes in southeastern Amazonia during the last 25,000 yr revealed from a paleoecological record. Quaternary Research 77, 138–148.

Herrera, L.F., Urrego, L.E., 1996. Atlas de polen de plantas útiles y cultivadas de La Amazonia colombiana (Pollen atlas of useful and cultivated plants in the Colombian Amazon region). Estudios en la Amazonia Colombiana, XI. Tropenbos-Colombia, Bogotá . p. 462.

Hesse, P.R., 1961. Some differences between the soils of *Rhizophora* and *Avicennia* mangrove swamp in Sierra Leone. Plant Soil 14, 335–346.

Hesp P.A., Dillenburg S.R., Barboza, E.G., Clerot, L.C.P., Tomazelli L.J., Zouain R.N.A., 2007. Morphology of the Itapeva to Tramandai transgressive dunefield barrier system and midto late Holocene sea level change. Earth Surface Process and Landforms 32, 407–414.

Horton, B.P., Gibbard, P.L., Milne, G.A., Morley, R.J., Purintavaragul, C., Stargardt, J.M., 2005. Holocene sea levels and palaeoenvironments, Malay–Thai Peninsula, Southeast Asia. The Holocene 15, 1199–1213.

Hutchings, P., Saenger, P., 1987. Ecology of Mangroves. Queensland University Press, St. Lucia, Qld., Australia and New York, p. 370.

Imbrie, J., Hays, J.D., Martinson, D.G., McIntyre, A., Mix, A.C., Morley, J.J., Pisias, N.G., Prell, W.L., Shackleton, N.J., 1984. The orbital theory of Pleistocene climate: support from a revised

chronology of the marine δ O18 record. In: Berger, A., Imbrie, J., Hays, J., Kukla, G., Saltzman, B. (Eds.), Milankovitch and Climate. Reidel Publishing Company,Dordrecht, pp. 269–305.

Janssen, C.R., 1966. Recent pollen spectra from the deciduous and coniferous deciduous forests of northeastern Minnesota: a study in pollen dispersal. Ecology 47, 804–25.

Janssen, C.R., 1973. Local and regional pollen deposition. In Quaternary Plant Ecology, Ed. Birks H.J.B., West RG, Oxford, UK: Blackwell, pp. 31–42.

Kirwan, M.L., Murray, A.B., 2007. A coupled geomorphic and ecological model of tidal marsh evolution. Proceedings of the National Academy of Sciences 104, 6118–6122.

Klein, A.G., Seltzer, G.O., Isacks, B.L., 1998. Modern and local glacial maximum snowlines in the central Andes of Peru, Bolivia and Northern Chile. Quaternary Science Reviews 17, 1–21.

Krauss, K.W., Lovelock, C.E., McKee., K.L., López-Hoffman, L., Ewe, S.M.L., Sousa, W.P., 2008. Environmental drivers in mangrove establishment and early development: A review. Aquatic Botany 89, 105–127.

Labeyrie, L.D., Duplessy, J.C., Blanc, P.L., 1987. Variations in mode of formation and temperature of oceanic deep waters over the past 125.000 years. Nature 327, 477–482.

Lacerda, L.D., Ittekkot, V., Patchineelam, S.R., 1995. Biogeochemistry of mangrove soil organic matter: a comparison between *Rhizophora*, *Avicennia* soils in southeastern Brazil. Estuarine, Coastal and Shelf Science 40, 713–720.

Lamb, A.L., Wilson, G.P., Leng, M.J., 2006. A review of coastal palaeoclimate and relative sea-level reconstructions using δ^{13}C and C/N ratios in organic material. Earth-Science Reviews 75, 29–57.

Lambeck, K., 1997. Sea-level change along the French Atlantic and channel coasts since the time of the Last Glacial Maximum. Palaeogeography, Palaeoclimatology, Palaeoecology 129, 1–22.

Lambeck, K., Chappell, J., 2001. Sea level change through the Last Glacial cycle. Science 292, 679–686.

Lambeck, K., Yokoyama, Y., Purcell, T., 2002. Into and out of the Last Glacial Maximum: sea-level change during oxygen isotope stages 3 and 2. Quaternary Science Reviews 21, 343–360.

Lara, R., Szlafsztein, C., Cohen, M.C.L., Berger, U., Marion, G., 2002. Implications of mangrove dynamics for private land use in Bragança, North Brazil: a case study. Journal of Coastal Conservation 8, 97–102.

Lara, J.R., Cohen, M.C.L., 2006. Sediment porewater salinity, inundation frequency and mangrove vegetation height in Bragança, North Brazil: an ecohydrology-based empirical model. Wetlands Ecolgy Management 4, 349–358.

Lara, R.J., Cohen, M.C.L. 2009. Palaeolimnological studies and ancient maps confirm secular climate fluctuations in Amazonia. Climatic Change, 94, 399–408.

Latrubesse, E.M., Franzinelli, E., 2002. The Holocene alluvial plain of the middle Amazon River, Brazil. Geomorphology 44, 241–257.

Ledru, M.-P., Braga, P.I.S., Soubiès, F., Fournier, M., Martin, L., Suguio, K., Turq, B., 1996. The last 50,000 years in the Neotropics (Southern Brazil) evolution of vegetation and climate. Palaeogeography, Palaeoclimatology, Palaeoecology 123, 239–257.

Ledru, M.P., 2001. Late Holocene rainforest disturbance in French Guiana. Review of Palaeobotany and Palynology 115, 161–176.

Ledru, M.-P., Mourguiart, P., 2001. Late glacial vegetation changes in the Americas and climatic implications. In: Markgraf, V. (Ed.), Interhemispheric Climate Linkages. Academic Press, San Diego, USA, pp. 371–390.

Lentz, S.J., 1995. The Amazon River plume during AMASSEDS: Subtidal current variability and the importance of wind forcing. Journal of Geophysical Research 100, 2377–2390.

Liebmann, B., Marengo, J.A., 2001. Interannual variability of the rainy season and rainfall in the Brazilian Amazon Basin. Jounal of Climate 14, 4308–4318.

Lima, A.M.M., Oliveira, L.L., Fontinhas, R.L., Lima, R.J.S., 2005. Ilha de Marajó: revisão histórica, hidroclimatológica, bacias hidrográficas e propostas de gestão. Holos Environment 5, 65–80.

Link, D.H.F. 1807. Beschreibung der Naturalien–Sammlung der Universität zu Rostock. Alders Erben,Rostock, 166 p.

Lugo, A.E., Snedaker, S.C., 1974. The ecology of mangroves. Annual Review of Ecology and Systematics 5, 39–64.

Macko, S.A., Entzeroth, L., Parker, P.L., 1984. Regional differences in nitrogen and carbon isotopes on the continental shelf of the Gulf of Mexico. Naturwissenchaften 71, 374–380.

Marengo, J.A., Druyan, L.M., Hastenrath, S., 1993. Observational and modeling studies of Amazonia interannual climate variability. Climatic Change 23, 267–286.

Marengo, J.A., Liebmann, B., Kousky, V.E., Filizola, N.P., Wainer, I.C., 2001. Onset and end of the rainy season in the Brazilian Amazon Basin. Journal of Climate 14, 833–852.

Markgraf, V., D´Antoni, H.L., 1978. Pollen flora of Argentina. Tucson: University of Arizona Press.

Martin, L., Suguio, K., Flexor, J.M., 1987. Flutuações do nível relativo do mar no Quaternário e seu papel na sedimentação costeira: Exemplos brasileiros. In: Simpósio de Ecossistemas da Costa Sul Sudeste Brasileira, vol. 1. Publicação CIESP, pp. 40–61.

Martin, L., Suguio, K., 1992. Variation of coastal dynamics during the last 7000 years recorded in beach-ridge plains associated with river mouths: example from the central Brazilian coast. Palaeogeography, Palaeoclimatology, Palaeoecology 99, 119–140.

Martin, L., Flexor, J.N., Suguio, K., 1995. Vibrotestemunhador leve: construção, utilização e potencialidades. Revista IG-USP 16, 59–66.

Martin, L., Suguio, K., Flexor, J.M., Achanjo, J.D., 1996. Coastal Quaternary formations of the Southern part of the State of Espírito Santo (Brazil). Anais da Academia Brasileira de Ciências 68 (3), 389–404.

Martin L., Dominguez J.M.L., Bittencourt A.C.S.P., 1998. Climatic control on coastal erosion during a sea-level fall episode. Anais da Academia Brasileira de Ciências 70, 249–266.

Martin, L., Dominguez, J.M.L., Bittencourt, A.C.S.P., 2003. Fluctuating Holocene Sea Levels in Eastern and Southeastern Brazil: Evidence from Multiple Fossil and Geometric Indicators. Journal of Coastal Research 19, 101–124.

Martinelli, L.A., Pessenda, L.C.R., Espinoza, E., Camargo, P.B., Telles, E.C., Cerri, C.C., Victoria, R.L., Aravena, R., Richey, J., Trumbore, S., 1996. Carbon-13 variation with depth in soils of Brazil and climate change during the Quaternary. Oecologia 106, 376–381.

Martinelli, L.A., Victoria, R.L., Camargo, P.B., Piccolo, M.C., Mertes, L., Richey, J.E., Devol, A.H., Forsberg, B.R., 2003. Inland variability of carbon-nitrogen concentrations and δ^{13}C in Amazon floodplain (várzea) vegetation and sediment. Hydrological processes 17, 1419–1430.

Maslin, M.A., Burns, S.J., 2000. Reconstruction of the Amazon Basin effective moisture availability over the past 14,000 years. Science 290, 2285–2287.

Matthijs, S., Tack, J., van Speybroeck, D., Koedam, N., 1999. Mangrove species zonation and soil redox state, sulphide concentration and salinity in Gazi Bay (Kenya), a preliminary study. Mang. Salt Marsh. 3, 243–249.

McKee, K.L., 1995. Seedlings recruitment patterns in a Belizean mangrove forest: effects of establishment ability and physico-chemical factors. Oecologia 101, 448–460.

McKee, K.L., Cahoon, D.R., Feller, I.C., 2007. Caribbean mangroves adjust to rising sea level through biotic controls on change in soil elevation. Global Ecology and Biogeography 16, 545–556.

Menezes, M., Berger, U., Worbes, M., 2003. Annual growth rings and long-term growth patterns of mangrove trees from the Bragança peninsula, North Brazil. Wetlands Ecology Management 1, 33–242.

Meyers, P.A., 1994. Preservation of elemental and isotopic source identification of sedimentary organic matter. Chemical Geology 114, 289–302.

Meyers, P.A., 1997. Organic geochemical proxies of paleoceanographic, paleolimnologic and paleoclimatic processes. Organic Geochemistry 27, 213–250.

Meyers, P.A., 2003. Applications of organic geochemistry to paleolimnological reconstructions: a summary of examples from the Laurentian Great Lakes. Organic Geochemistry 34, 261–289.

Miall, A.D., 1978. Facies types and vertical profile models in braided river deposits: a summary. In: Miall, A.D. (Ed.), Fluvial sedimentology. Canadian Society of Petroleum Geologists, Calgary, pp 597–604.

Middelburg, J.J., Nieuwenhuize, J., 1998. Carbon and nitrogen stable isotopes in suspended matter and sediments from the Schelde Estuary. Marine Chemistry 60, 217–225.

Miranda, M.C.C., Rossetti, D.F., Pessenda, L.C.R., 2009. Quaternary paleoenvironments and relative sea-level changes in Marajó Island (Northern Brazil): Facies, δ^{13}C, δ^{15}N and C/N. Palaeogeography, Palaeoclimatology, Palaeoecology 282, 19–31.

Molodkov, A.N., Bolikhovskaya, N.S., 2002. Eustatic sea-level and climate changes over the last 600 ka as derived from molluskbased ERS-chronostratigraphy and pollen evidence in Northern Eurasia. Sedimentary Geology 150, 185–201.

Monacci, N.M., Meier-Grünhagen, U., Finney, B.P., Behling, H., Wooller, M.J., 2009. Mangrove ecosystem changes during the Holocene at Spanish Lookout Cay, Belize. Palaeogeography, Palaeoclimatology, Palaeoecology 280, 37–46.

Monacci, N.M., Meier-Gruenhagen, U., Finney, B.P., Behling, H., Wooller, M.J., 2011. Paleoecology of mangroves along the Sibun River, Belize. Quaternary Research 76, 220–228.

Mörner, N.A., 1996. Global change and interaction of earth rotation, ocean circulation and paleoclimate. Anais da Academia Brasileira de Ciências 68, 77–94.

Mörner, N.A., 1999. Sea level and climate: rapid regressions at local warm phases. Quaternary International 60, 75–82.

Mourguiart, P., Ledru, M.-P., 2003a. Last Glacial Maximum in an Andean cloud forest environment (eastern Cordillera, Bolivia). Geology 31 (3), 195–198.

Mourguiart, P., Ledru, M.-P., 2003b. Last Glacial Maximum in an Andean cloud forest environment. Geology, 26–27.

Munsell Color, 2009. Munsell Soil Color Charts. New Revised Edition. New Windsor, NY: Macbeth Division of Kollmorgen Instruments.

Nobre, P., Shukla, J., 1996. Variations of sea surface temperature, wind stress, and rainfall over the Tropical Atlantic and South America. Jounal of Climate 9, 2464–2479.

Orbigny A.D., 1841. Paléontologie française. Description zoologique et géologique de tous les animaux mollusques et rayonnés fossiles de France. Tome 1. Terrains Crétacés. Céphalopodes. Paris, Masson, Part II (1841), 121–430.

Orbigny, A.D., 1846. Mollusques. In: Voyage dans l'Amérique Meridionale (le Bresil) execute pendant les annes 1829-1833. P. Bertrand, Paris, v. 5, pt. 3, 758p, 85 pls.

Otvos, E.G., 2000. Beach ridges – definitions and significance. Geomorphology 32, 83–108.

Paduano, G.M., Bush, M.B., Baker, P.A., Fritz, S.L., Seltzer, G.O., 2003. The Late Quaternary vegetation history of Lake Titicaca, Peru/Bolivia. Palaeogeography, Palaeoclimatology, Palaeoecology 194, 259–279.

Parkinson, R.W., Delaune, R.D., White, J.R., 1994. Holocene sea-level rise and the fate of mangrove forests within the wider Caribbean region. Jounal of Coastal Research 10, 1077–1086.

Peixoto, A.L., Gentry, A., 1990. Diversidade e composição florística da mata de tabuleiros na Reserva Florestal de Linhares (Espírito Santo, Brasil). Revista Brasileira de Botânica 13, 19–25.

Peltier, W.R., Fairbanks, R.G., 2006. Global glacial ice volume and Last Glacial Maximum duration from an extended Barbados sea level record. Quaternary Science Reviews 25, 3322–3337.

Pessenda, L.C.R., Camargo, P.B., 1991. Datação radiocarbônica de amostras de interesse arqueológico e geológico por espectrometria de cintilação líquida de baixo nível de radiação de fundo. Química Nova 14, 98–103.

Pessenda, L.C.R., Valencia, E.P.E., Martinelli, L.A., 1996. ^{14}C measurements in tropical soil developed on basic rocks. Radiocarbon 38, 203–208.

Pessenda, L.C.R., Gomes, B.M., Aravena, R., Ribeiro, A.S., Boulet, R., Gouveia, S.E.M., 1998a. The carbon isotope record in soils along a forest-cerrado ecosystem transect: implications for vegetation changes in the Rondonia state, southwestern Brazilian Amazon region. The Holocene 8, 631–635.

Pessenda, L.C.R., Gouveia, S.E.M., Aravena, R., Gomes, B.M., Boulet, R., Ribeiro, A.S., 1998b. ^{14}C dating and stable carbon isotopes of soil organic matter in forest savanna boundary areas in the southern Brazilian Amazon region. Radiocarbon 40, 1013–1022.

Pessenda, L.C.R., Boulet, R., Aravena, R., Rosolen, V., Gouveia, S.E.M., Ribeiro, A.S., Lamotte, M., 2001. Origin and dynamics of soil organic matter and vegetation changes

during the Holocene in a forest-savanna transition zone, Brazilian Amazon region. The Holocene 11, 250–254.

Pessenda, L.C.R., Ribeiro, A.S., Gouveia, S.E.M., Aravena, R., Boulet, R., Bendassoli, J.A., 2004. Vegetation dynamics during the late Pleistocene in the Barreirinhas region, Maranhão State, northeastern Brazil, based on carbon isotopes in soil organic matter. Quaternary Research 62, 183–193.

Pessenda, L.C.R., Gouveia, S.E.M., Ledru, M.P., Aravena, R., Ricardi-Branco, F., Bendassolli, J.A., Ribeiro, A.S., Saia, S.E.M.G., Siffedine, A., Menor, A., Oliveira, S., Cordeiro, R.C., Freitas, A.M.M., Boulet, R., Filizolla, H., 2008. Interdisciplinary paleovegetation study in the Fernando de Noronha Island (Pernambuco State), northeastern Brazil. Anais Academia Brasileira de Ciências 80 (4), 677–691.

Pessenda L.C.R., Gouveia, S.E.M., Ribeiro, A.S., De Oliveira, P.E., Aravena, R., 2010. Late Pleistocene and Holocene vegetation changes in northeastern Brazil determined from carbon isotopes and charcoal records in soils. Palaeogeography, Palaeoclimatology, Palaeoecology 297: 597-608.

Pessenda, L.C.R., Vidotto, E., de Oliveira, P.E., Buso Jr, A.A., Cohen, M.C.L., Rossetti, D.F., Ricardi-Branco, F., Bendassolli, J, A., 2012. Late Quaternary vegetation and coastal environmental changes at Ilha do Cardoso mangrove, southeastern Brazil. Palaeogeography, Palaeoclimatology, Palaeoecology 363 and 364, 57–68.

Peterson, B.J., Howarth, R.W., 1987. Sulfur, carbon, and nitrogen isotopes used to trace organic matter flow in the salt-marsh estuary of Sapelo Island, Georgia. Limnology and Oceanography 32, 1195–1213.

Peterson, B.J., Fry, B., Hullar, M., Saupe, S., Wright, R., 1994. The distribution and stable carbon isotope composition of dissolved organic carbon in estuaries. Estuaries 17, 111–121.

Pezeshki, S.R., DeLaune, R.D., Meeder, J.F., 1997. Carbon assimilation and biomass in *Avicennia germinans* and *Rhizophora mangle* seedlings in response to soil redox conditions. Environmental and Experimental Botany. 37, 161–171.

Philippi, R.A., 1841. Zoologische Bemerkungen. Archiv für Naturgeschichte, Berlin 7 (1), 42–59; pl. 5.

Pigati, J.S., McGeehin, J.P., Muhs, D.R., Bettis, E.A., 2013. Radiocarbon dating late Quaternary loess deposits using small terrestrial gastropod shells. Quaternary Science Reviews. 76, 114-128.

Porter, S.C., 2001. Snowline depression in the tropics during the Last Glaciation. Quaternary Science Reviews 20, 1067–1091.

Posamentier, H.W., Allen, G.P., James, D.P., Tesson, M., 1992. Forced regressions in a sequence stratigraphic framework: Concepts, examples, and exploration significance. The American Association of Petroleum Geologists Bulletin 76, 1687–1709.

Rabineau, M., Berné, S., Aslanian, D., Olivet, J.L., Joseph, P., Guillocheau, F., Bourillet, J.F., Ledrezen, E., Granjeon, D., 2006. Paleo sea levels reconsidered from direct observation of paleoshoreline position during Glacial Maxima (for the last 500,000 yr). Earth and Planetary Science Letters 252, 119–137.

Raymond, P.A., Bauer, J.E., 2001. Use of ^{14}C and ^{13}C natural abundances for evaluating riverine, estuarine, and coastal DOC and POC sources and cycling: A review and synthesis. Organic Geochemistry 32, 469–485.

Reimer, P.J., Baillie, M.G.L., Bard, E., Bayliss, A., Beck, J.W., Bertrand, C., Blackwell, P.G., Buck, C.E., Burr, G., Cutler, K.B., Damon, P.E., Edwards, R.L., Fairbanks, R.G., Friedrich, M., Guilderson, T.P., Hughen, K.A., Kromer, B., McCormac, F.G., Manning, S., Ramsey, C.B., Reimer, R.W., Remmele, S., Southon, J.R., Stuiver,M., Talamo, S., Taylor, F.W., van der Plicht, J., Weyhenmeyer, C.E., 2004. INTCAL04 terrestrial radiocarbon age calibration, 0–26 cal kyr B.P. Radiocarbon 46, 1029–1058.

Reimer, P.J.; Baillie, M.G.L.; Bard, E.; Bayliss, A., Beck, J.W.; Blackwell, P.G.; Bronk Ramsey, C.; Buck, C.E.; Burr, G.S.; Edwards, R.L.; Friedrich, M.; Grootes, P.M.; Guilderson, T.P.; Hajdas, I.; Heaton, T.J.; Hogg, A.G.; Hughen, K.A.; Kaiser, K.F.; Kromer, B.; Mccormac, F.G.; Manning, S.W.; Reimer, R.W.; Richards, D.A.; Southon, J.R.; Talamo, S.; Turney, C.S.M.; Van der Plicht, J.; Weyhenmeyer, C.E., 2009. IntCal09 and Marine09 radiocarbon age calibration curves, 0– 50,000 years cal BP. Radiocarbon 51, 1111–1150.

Reineck, H.E., Singh I.B., 1980. Depositional Sedimentary Environments with Reference to Terrigenous Clastics (Second edition). Berlin: Springer-Verlag, 542 pp.

Reis, A.T., Maia, R.M.C., Silva, C.G., Rabineau, M., Guerra, J.V., Gorini, C., Ayres, A., Arantes-Oliveira, R., Benabdellouahed, M., Simões, I.C.V.P., Tardin, R. 2013. Origin of step-like and

lobate seafloor features along the continental shelf off Rio de Janeiro State, Santos basin-Brazil. Geomorphology V. Special, 1-18.

Rohling, E.J., Fenton, M., Jorissen, F.J., Bertrand, P., Ganssen, G., Caulet, J.P., 1998. Magnitudes of sea level lowstands of past 500,000 years. Nature 394, 162–165.

Rosario, R.P., Bezerra, M.O.M., Vinzon, S.B., 2009. Dynamics of the saline front in the Northern Channel of the Amazon River - influence of fluvial flow and tidal range (Brazil). Journal of Coastal Research 2, 503–514.

Rossetti, D.F., Goes, A.M., Valeriano, M.M., Miranda, M.C.C., 2007. Quaternary tectonics in a passive margin: Marajó Island, northern Brazil. Journal of Quaternary Science 22, 1–15.

Rossetti, D.F., Valeriano, M.M., Goes, A.M., Thales, M., 2008. Palaeodrainage on Marajó Island, northern Brasil, in relation to Holocene relative sea-level dynamics. The Holocene 18, 1–12.

Rossetti, D.F., Bezerra, F. H., Góes, A. M., Valeriano, M. M., Andrades Filho, C. O., Mittani, J.C.R., Tatumi, S.H., Brito-Neves, B.B. 2011. Late Quaternary sedimentation in the Paraíba Basin, Northeastern Brazil: landform, sea level and tectonics in Eastern South America passive margin. Palaeogeography, Palaeoclimatology, Palaeoecology 300, 191-204.

Rossetti, D.F., Souza, L.S.B., Prado, R.,Elis, V.R., 2012. Neotectonics in the northern equatorial Brazilian margin. Journal of South American Earth Sciences 37, 175–190.

Rossetti, D.F., Bezerra, F.H., Dominguez, J.M.L. 2013. Late Oligocene-Miocene transgressions along the equatorial and eastern margins of Brazil. Earth-Science Reviews 123, 87-112.

Roubik, D.W., Moreno, J.E., 1991. Pollen and spores of Barro Colorado Island, vol. 36. Missouri Botanical Garden, St. Louis (268 pp). Rull, V., Vegas-Vilarrùbia, T., Espinoza, N.P., 1999. Palynological record of an early-mid Holocene mangrove in eastern Venezuela. Implications for sea-level rise and disturbance history. Journal of Coastal Research 15, 496–504.

Rubin, M., Likins, R.C., Berry, E.G., 1963. On the validity of radiocarbon dates from snail shells. Journal of Geology 71, 84-89.

Ruddiman, W.F., 2008. Earth`s Climate - Past and Future. W. H. Freeman and Company. New York. 388 p.

Rull, V., Vegas-Vilarrùbia, T., Espinoza, N.P., 1999. Palinological Record na early-mid Holocene mangrove in eastern Venezuela: Implications for sea-level rise and disturbance history. Journal of Coastal Research 15, 496-504.

Salgado-Labouriau, M.L., 1973. Contribuição à palinologia dos cerrados. Rio de Janeiro: Academia Brasileira de Ciências. 273p.

Sallun, A.E.M., Filho, W.S., Suguio, K., Babinski, M., Gioia, S.M.C.L., Harlow, B.A., Duleba, W., Oliveira, P.E., Garcia, V.J., Weber, C.Z., Christofoletti, S.R., Santos, C.S., Medeiros, V.B., Silva, J.B., Santiago-Hussein, M.C., Fernandes, R.S., 2012. Geochemical evidence of the 8.2 ka event and other Holocene environmental changes recorded in paleolagoon sediments southeastern Brazil. Quaternary Research 77, 31–43.

Sanders, C.J.,Smoak, J.M., Naidu, A.S., Sanders, L.M., Patchineelam, S.R., 2010. Organic carbon burial in a mangrove forest, margin and intertidal mud flat. Estuarine, Coastal and Shelf Science 90, 168–172.

Sanders, C.J., Smoak, J.M., Waters, M.N., Sanders, L.M., Bradini, N., Patchineelam, S.R., 2012. Organic matter content and particle size modifications in mangrove sediments as responses to sea-level rise. Marine Environmnetal Research 77, 150–155.

Santos, M.L.S., Medeiros, C., Muniz, K., Feitosa, F.A.N., Schwamborn, R., Macedo, S.J., 2008. Influence of the Amazon and Pará Rivers on water composition and phytoplankton biomass on the Adjacent Shelf. Journal of Coastal Research 24, 585–593.

Sawakuchi, A.O., Kalchgruber, R., Giannini, P.C.F., Nascimento Jr., D.R., Guedes, C.C.F., Umisedo, N.K., 2008. The development of blowouts and foredunes in the Ilha Comprida barrier (Southeastern Brazil): the influence of Late Holocene climate changes on coastal sedimentation. Quaternary Science Reviews 27, 2076–2090.

Say, T., 1822. An account of some of the marine shells of the United States. Jour. Acad. Nat Sci. Phila, vol. 2. p228.

Schaeffer-Novelli, Y., Cintrón, G.M., Adaime, R.R., 1990. Variability of mangroves ecosystems along Brazilian coast. Estuaries 13, 204–218.

Schaeffer-Novelli, Y., Cintrón, G., Soares, M.L.G., Tognella-de-Rosa, M.M.P., 2000. Brazilian mangroves. Aquatic Ecosystem Health and Management 3, 561–570.

Scheel-Ybert, R., 2000. Vegetation stability in the Southeastern Brazilian coastal area from 5500 to 1400 14C yr BP deduced from charcoal analysis. Review of Paleobotany and Palynology 110, 111–138.

Schidlowski, M., Hayes, J.M., Kaplan I.R., 1983. Isotopic inferences of ancient biochemistries: Carbon, sulphur, hydrogen and nitrogen. In: Scholf JW (ed.) Earth's Earliest Biosphere, Its Origin and Evolution. Princeton: Princeton University Press, 149–186.

Schwartz, M.L., 1965. Laboratory study of sea-level rise as a cause of shore erosion. Journal of Geology 73, 528–534.

Schwartz, M.L., 1968. The scale of shore erosion. Journal of Geology 76, 508–517.

Semeniuk, V., 1994. Predicting the effect of sea-level rise on mangroves in northwestern Australia. Journal of Coastal Research 10, 1050–1076.

Shackleton, N.J., 2000. The 100,000-year Ice-Age cycle identified and found to lag temperature, carbon dioxide, and orbital eccentricity. Science 289, 1897–1902.

Siddall, M., Almogi-Labin, R.E.J.A., Hemleben, C., Meischner, D., Schmelzer, I., Smeed, D.A., 2003. Sea-level fluctuations during the last glacial cycle. Nature 423, 853–858.

Sifeddine A., Bertrand P., Fournier M., Martin L., Servant M., Soubiès F., Suguio K., Turcq B., 1994. La sédimentation organique lacustre en milieu tropical humide (Carajás, Amazonie orientale, Brésil): relation avec les changements climatiques au cours des 60,000 dernières années. Bulletin de La Société Geologique de France 165, 613–621.

Sifeddine, A., Marint, L., Turcq, B., Volkmer-Ribeiro, C., Soubiès, F., Cordeiro, R.C., Suguio, K., 2001. Variations of the Amazonian rainforest environment: a sedimentological record covering 30,000 years. Palaeogeography, Palaeoclimatology, Palaeoecology 168, 221–235.

Skene, K.I., Piper, D.J.W., Aksu, A.E., Syvitski, J.P.M., 1998. Evaluation of the global oxygen isotope curve as a proxy for Quaternary sea level by modeling of delta progradation. Journal of Sedimentary Research 68, 1077–1092.

Smith, C.B., Cohen, M.C.L., Pessenda, L.C.R., França, M., Guimarães, J.T.F., Rossetti, D.F., 2011. Holocene coastal vegetation changes at the mouth of the Amazon River. Review of Palaeobotany and Palynology 168, 21–30.

Smith, C.B., Cohen, M.C.L., Pessenda, L.C.R., França, M.C., Guimarães, J.T.F., 2012. Holocenic proxies of sedimentary organic matter and the evolution of Lake Arari-Northern Brazil. Catena 90, 26–38.

Snedaker, S.C., 1978. Mangroves: Their value and perpetuation. Natural Resources 16, 179–188.

Snedaker, S.C., 1982. Mangrove species zonation: why? In: Sen, D.N., Rajpurohit, K.S. (Eds.), Contributions to the Ecology of Halophytes, Tasks for Vegetation Science, Vol. 2. W. Junk, The Hague, New York, NY, pp. 111–125.

Soares, M.L.G., Estrada, G.C.D., Fernandez, V., Tognella, M.M.P., 2012. Southern limit of the Western South Atlantic mangroves: Assessment of the potential effects of global warming from a biogeographical perspective. Estuarine, Coastal and Shelf Science 101, 44–53.

Solomon, A.M., Blasing, T.J., Solomon, J.A. 1982. Interpretation of floodplain pollen in alluvial sediments from an arid region. Quaternary Research 18, 52–71.

Souza, M.C., Angulo, R.J., Pessenda, L.C.R., 2001. Evolução paleogeográfica da planície costeira de Itapoá, litoral norte de Santa Catarina. Revista Brasileira de Geociências 31, 223–230.

Souza Filho, P.W.M., Martins, E.S.F., Costa, F.R., 2006. Using mangroves as a geological indicator of coastal changes in the Bragança macrotidal flat, Brazilian Amazon: A remote sensing data approach. Ocean and Coastal Management 49, 462–475.

Spenceley, A.P., 1982. Sedimentation patterns in a mangal on Magnetic Island near Townsville, North Queensland, Australia. Singap. J. Trop. Geogr. 3, 100–107.

Stevens, P.W., Fox., S.L., Montague, C.L., 2006. The interplay between mangroves and saltmarshes at the transition between temperate and subtropical climate in Florida. Wetlands Ecology Management 14, 435–444.

Stockmarr, J., 1971. Tablets spores used in absolute pollen analysis. Pollen et Spores 13 (4), 615–621.

Stuart, S.A., Choat, B., Martin, K.C., Holbrook, N.M., Ball, M.C., 2007. The role of freezing in setting the latitudinal limits of mangrove forests. New Phytologist 173, 576–583.

Stuiver, M., Reimer, P., Braziunas, T.F., 1998. High precision radiocarbon age calibration for terrestrial and marine samples. Radiocarbon 40, 1127–1151.

Stute, M., Forster, M., Frischkorn, H., Serejo, A., Clark, J.F., Schlosser, P., Broecker, W.S., Bonani, G., 1995. Cooling of tropical Brazil (5°C) during the last glacial maximum. Science 269, 379– 383.

Sugita, S., 1994. Pollen representation of vegetation in quaternary sediments: theory and method in patchy vegetation. Journal of Ecology 82, 881–97.

Suguio, K., Martin, L., Dominguez, J.M.L., 1982. Evolução da planície costeira do Rio Doce (ES) durante o Quaternário: influência das flutuações do nível do mar. Atas do IV Simpósio do Quaternário no Brasil: 93–116.

Suguio, K., Martin, L., Bittencourt, A.C.S.P., Dominguez, J.M.L., Flexor, J.M., Azevedo, A.E.G., 1985. Flutuações do Nível do Mar durante o Quaternário Superior ao longo do Litoral Brasileiro e suas Implicações na Sedimentação Costeira. Revista Brasileira de Geociências 15, 273–286.

Sukigara, C., Saino, T., 2005. Temporal variations of δ^{13}C and δ^{15}N in organic particles collected by a sediment trap at time-series station off the Tokyo Bay. Continental Shelf Research 25, 1749–1767.

Sun, X., Li, X., 1999. A pollen record of the last 37 ka in deep sea core 17940 from the northern slope of the South China Sea. Marine Geology 156, 227–244.

Suter, J.R., 1994. Deltaic coasts, in: R.W.G. Carter and C.D. Woodroffe (Eds.), Coastal Evolution: Late Quaternary Shoreline Morphodynamics. Cambridge University Press, Cambridge, pp. 87–120.

Swift, D.J.P., 1975. Barrier island genesis: evidence from the central Atlantic Shelf, eastern USA. Sedimentary Geology 14, 1–43.

Thornton, S.F., McManus, J., 1994. Applications of organic carbon and nitrogen stable isotope and C/N ratios as source indicators of organic matter provenance in estuarine systems: Evidence from the Tay Estuary, Scotland. Estuarine, Coastal and Shelf Science 38, 219–233.

Toledo, M.B., Bush, M.B., 2007. A mid-Holocene environmental change in Amazonian savannas. Journal of Biogeography 34, 1313–1326.

Toledo, M.B., Bush, M., 2008. Vegetation and hydrology changes in Eastern Amazonia inferred from pollen record. Anais da Academia Brasileira de Ciências 80, 191–203.

Tomazelli L.J., 1990. Contribuicão ao Estudo dos Sistemas Deposicionais Holocênicos do Nordeste da Província Costeira do Rio Grande do Sul, com Ênfase no Sistema Eólico, Ph.D Thesis (Tese de Doutorado). Porto Alegre, Universidade Federal do Rio Grande do Sul, 270 p.

Toscano, M.A., Lundberg, J., 1999. Submerged Late Pleistocene reefs on the tectonically stable SE Florida margin: high precision geochronology, stratigraphy, resolution of Substage 5a sea-level elevation, and orbital forcing. Quaternary Science Reviews 18, 753–767.

Tyson, R.V., 1995. Sedimentary Organic Matter: Organic Facies and Palynofacies. London: Chapman and Hall, 15pp.

Urrego, D.H., Silman, M.R., Bush, M.B., 2005. The last glacial maximum: stability and change in a western Amazonian cloud forest. Journal of Quaternary Science 20, 693–701.

Van der Hammen, T., 1974. The Pleistocene changes of vegetation and climate in tropical South America. Journal of Biogeography 1, 3–26.

Van Meerbeeck, C.J., Renssen, H., Roche, D.M., 2008. How did Marine Isotope Stage 3 and Last Glacial Maximum climates differ? Perspectives from equilibrium simulations. Climate of the Past Discussions 4, 1115–1158.

Vannucci, M., 2001. What is so special about mangroves? Brazilian Journal of Biology 61 (4), 599–603.

Vedel, V., Behling, H., Cohen, M.C.L., Lara, R.J., 2006. Holocene mangrove dynamics and sea-level changes in Taperebal, northeastern Pará State, northern Brazil. Vegetation History and Archaeobotany 15, 115–123.

Versteegh, G.J.M., Schefuß, E., Dupont, L., Marret, F., Damsté, J.S.S., Jansen, J.H.F., 2004. Taraxerol and *Rhizophora* pollen as proxies for tracking past mangrove ecosystems. Geochimica et Cosmochimica Acta 68, 411–422.

Vinzon, B.S., Vilela, C.P.X., Pereira, L.C.C. 2008. Processos físicos na Plataforma Continental Amazônica. Relatório-Técnico, Potenciais Impactos Ambientais do Transporte de Petróleo e Derivados na Zona Costeira Amazônico. Petrobrás, Brasil, 31 pp.

Wada, E., 1980. Nitrogen isotope fractionation and its significance in biogeochemical process occurring in marine environments, p. 375–398. *In:* Isotope marine chemistry. Uchida Rokakuho.

Waelbroeck, C., Labeyrie, L.D., Michel, E., Duplessy, J.-C., McManus, J., Lambeck, K., Balbon, E., Labracherie, M., 2002. Sea level and deep water changes derived from benthic Foraminifera isotopic record. Quaternary Science Reviews 21, 295–305.

Walker R.G., 1992. Facies, facies models and modern stratigrahic concepts. In: Walker R.G,. James N.P. (Eds.), Facies Models - Response to Sea Level Change. Geological Association of Canada, Ontario, Canara, pp. 1–14.

Walsh, G.E., 1974. Mangroves, a review. In: Reimold, R.J., Queens,W.H. (Eds.), Ecology of Halophytes. Academic Press, New York, NY, pp. 51–174.

Weng C., Bush M.B., Athens J.S., 2002. Two histories of climate change and hydrarch succession in Ecuadorian Amazonia. Review of Palynology and Paleobotany 120, 73–90.

Weng, C., Bush, M.B., Silman, M.R., 2004. An elevation transect of modern pollen spectra from Amazonia to the high Andes, Peru. J. Trop. Ecol. 20, 113–124.

Wentworth, C.K., 1922. A scale of grade and class terms for clastic sediments. Journal of Geology 30, 377–392.

Whitney, B.S., Mayle, F.E., Punyasena, S.W., Fitzpatrick, K.A., Burn, M.J.,Guillen, R., Chavez, E., Mann, D., Pennington, R.T., Metcalfe, S.E., 2011. A 45 kyr palaeoclimate record from the lowland interior of tropical South America. Palaeogeography Palaeoclimatology Palaeoecology 307, 177–192.

Wilson, G.P., Lamb, A.L., Leng, M.J., Gonzales, S., Huddart, D., 2005. Variability of organic $\delta^{13}C$ and C/N in the Mersey Estuary, U.K. and its implications for sea-level reconstruction studies. Estuarine, Coastal and Shelf Science 64, 685–698.

Wolanski, E., Mazda, Y., King, B., Gay, S., 1990. Dynamics, flushing and trapping in Hinchinbrook channel, a giant mangrove swamp, Australia. Estuarine, Coastal and Shelf Science 31, 555–579.

Woodroffe, C.D., 1981. Mangrove swamp stratigraphy and Holocene transgression, Grand Cayman Island, West India. Marine Geology 41, 271–294.

Woodroffe, C.D., 1982. Geomorphology and Development of Mangrove Swamps, Grand Cayman Island, West Indies. Bulletin Marine Science 32 (2), 381–398.

Woodroffe, C.D., Chappell, J.M.A., Thom, B.G., Wallensky, E., 1989. Depositional model of a macrotidal estuary and flood plain, South Alligator River, Northern Australia. Sedimentology 36, 737–756.

Woodroffe, C.D., 1995. Response of tide-dominated mangrove shorelines in northern Australia to anticipated sea-level rise. Earth Surface Processes and Landforms 20, 65–85.

Woodroffe, C.D., 2002. Coasts: form, process and evolution. Cambridge University Press, Cambridge.

Wright, H.E., Seltzer, G.O., Hansen, B.C.S., 1989. Glacial and climatic history of the central Peruvian Andes. National Geographic Research 5, 439–445.

Xu, Q., Tian, F., Bunting, M.J., Li, Y.,Ding, W., Cao, X., He, Z. 2012. Pollen source areas of lakes with inflowing rivers: Modern pollen influx data from Lake Baiyangdian, China. Quaternary Science Reviews 37, 81–91.

Youssef, T., Saenger, P., 1999. Mangrove zonation in Mobbs Bay-Australia. Estuarine Coastal and Shelf Science 49, 43–50.

Yulianto, E., Sukapti, W.S., Rahardjo, A.T., Noeradi, D., Siregar, D.A., Suparan, P., Hirakawa, K., 2004. Mangrove shoreline responses to Holocene environmental change, Makassar Strait Indonesia. Review of Palaeobotany and Palynology 131, 251–268.

Yulianto, E., Rahardjo, A.T., Noeradi, D., Siregar, D.A., Hirakawa, K., 2005. A Holocene pollen record of vegetation and coastal environmental changes in the coastal swamp

forest at Batulicin, South Kalimantan, Indonesia. Journal of Asian Earth Sciences 25, 1–8.

Zular, A., Sawakuchi, A.O., Guedes, C.C.F., Mendes, V.R., Nascimento Jr, D.R., Giannini, P.C.F., Aguiar, V.A.P., DeWitt, R., 2013. Late Holocene intensification of colds fronts in southern Brazil as indicated by dune development and provenance changes in the São Francisco do Sul coastal barrier. Marine Geology 335, 64–77.

UNIVERSIDADE FEDERAL DO PARÁ
INSTITUTO DE GEOCIÊNCIAS
PROGRAMA DE PÓS-GRADUAÇÃO EM GEOLOGIA E GEOQUÍMICA

PARECER

Sobre a Defesa Pública da Tese de Doutorado de
MARLON CARLOS FRANÇA

A banca examinadora da Tese de Doutorado de **MARLON CARLOS FRANÇA,** intitulada **"DESENVOLVIMENTO DA VEGETAÇÃO E MORFOLOGIA DA FOZ DO AMAZONAS-PA E RIO DOCE-ES DURANTE O QUATERNÁRIO TARDIO",** composta pelos Professores Doutores **Marcelo Cancela L. Cohen** (Orientador-UFPA), **Susy Eli Marques Gouveia** (UFPA), **Maria Inês F. Ramos** (MPEG), **Paulo César F. Giannini (USP)** e **Mário Luiz Gomes Soares** (UERJ), após a apresentação oral e arguição do candidato, emite o seguinte parecer:

O candidato apresentou contribuição importante ao conhecimento sobre a dinâmica e desenvolvimento da foz dos rios Amazonas e Doce, no que se refere a sua geomorfologia e vegetação, de acordo com as mudanças climáticas e de nível do mar ocorridas no Quaternário tardio. O candidato mostrou segurança durante a exposição de seu trabalho, com uma apresentação clara, didática, bem estruturada e de conteúdo relevante, demonstrando conhecimento da literatura e dos dados palinológicos, isotópicos e sedimentológicos apresentados. Na arguição, o candidato defendeu muito bem sua Tese, respondendo a várias questões gerais e específicas. O documento está bem redigido e bem estruturado, na forma de quatro artigos, sendo três já publicados e um quarto em revisão. Destaca-se o fato do candidato ter defendido sua Tese em 36 meses, portanto antes do prazo estipulado de 48 meses.

Com base no exposto, a banca examinadora decidiu, por unanimidade, aprovar a Tese de Doutorado, "COM DISTINÇÃO".

Belém, 5 de novembro de 2013.

Prof. Dr. Marcelo Cancela L. Cohen
(Orientador-UFPA)

Prof.ª Dr.ª Susy Eli Marques Gouveia
(Membro-UFPA)
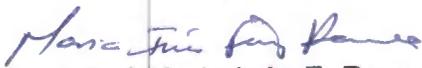
Prof.ª Dr.ª Maria Inês F. Ramos
(Membro-MPEG)
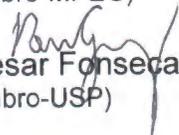
Prof. Dr. Paulo César Fonseca Giannini
(Membro-USP)

Prof. Dr. Mário Luiz Gomes Soares
(Membro-UERJ)